[redacted]

UNCLASSIFIED

C72 72006

COPY NO. 46

CLASSIFICATION CHANGE

NASA CR-112094

To UNCLASSIFIED

EDS, EO 11652 7/22/79

Scientific and Technical Information Facility, NASA

(NASA-CR-112094) AIR AUGMENTED CONVERTIBLE SCRAMJET ENGINE STUDY (THE DUPONT JET ENGINE) (Du Pont Aerospace Co., Inc., Torrance) 112 p

N79-76864

Unclas 00/07 19209

AIR AUGMENTED CONVERTIBLE SCRAMJET ENGINE STUDY (U)

(The duPont Jet Engine)

by

Anthony A. duPont
Albert E. Gaede
Franklin A. Weisman

Prepared under Contract No. NAS1-11467 by

duPont Aerospace Company, Inc.
Torrance, California

April 15, 1972

for

the Langley Research Center

NATIONAL AERONAUTICS AND SPACE ADMINISTRATION

FOR U.S. GOVERNMENT AGENCIES AND THEIR CONTRACTORS ONLY

[redacted]

"This material contains information affecting the National defense of the United States within the meaning of the Espionage Laws, Title 18, U.S. Code, Sections 793 and 794, the transmission or revelation of which in any manner to an unauthorized person is prohibited by law".

[redacted]

[redacted]

[redacted] 72003

COPY NO. 45

NASA CR-112094

N79 76864

AIR AUGMENTED CONVERTIBLE SCRAMJET ENGINE STUDY (U)

(The duPont Jet Engine)

by

Anthony A. duPont
Albert E. Gaede
Franklin A. Weisman

CLASSIFIED BY _____
SUBJECT TO GENERAL DECLASSIFICATION SCHEDULE OF EXECUTIVE ORDER 11652. AUTOMATICALLY DOWNGRADED AT TWO-YEAR INTERVALS AND DECLASSIFIED ON DECEMBER 31, 1972.

Prepared under Contract No. NAS1-11467 by

duPont Aerospace Company, Inc.
Torrance, California

April 15, 1972

for

the Langley Research Center

NATIONAL AERONAUTICS AND SPACE ADMINISTRATION

[redacted]

[redacted]

[redacted]

[redacted]

[redacted]

112

PFD

ABSTRACT

An engine cycle which provides static and acceleration thrust for a high Mach number ramjet without compromising the ramjet geometry has been analyzed to determine engine performance and engine weight. Its weight and performance have been compared to other engine cycles and found to offer large potential improvements in aircraft performance. The performance analysis is based on a detailed computer study using equilibrium chemistry of hydrogen-air reactants. The analytical model used to predict compression performance gives results which agree closely with experimental data. The weight analysis is based on the structural design, design criteria and actual weights of the Hypersonic Research Engine (HRE) which has been extensively tested in the NASA hot structures tunnel.

Pages i and ii are blank.

CONTENTS

CONTENTS (continued)

CONTENTS (concluded)

ILLUSTRATIONS

ILLUSTRATIONS (concluded)

TABLES

SYMBOLS

Symbol	Description	Units
A	area	$in.^2$
a_{ij}	formula numbers (number of atoms of ith element in jth species)	gm-atoms/mole
b_i^0	specific formula numbers (total number of gm-atoms/gm of element i in the chemical system)	gm-atoms/gm
C^*	characteristic velocity	ft/sec
C_d	drag coefficient	--
C_f	friction coefficient	--
C_p	specific heat at constant pressure	$Btu/lb_m/°R$
C_v	specific heat at constant volume	$Btu/lb_m/°R$
C_v	nozzle velocity coefficient	--
C_v'	primary nozzle velocity coefficient	--
CR	contraction ratio (A_c/A_2)	--
D_h	hydraulic diameter	in.

SYMBOLS (continued)

Symbol	Description	Units
F	stream thrust	lb_f
G	Gibbs free energy	--
g	functional - Equation 7	--
g	acceleration of gravity	$(lb_m/lb_f)(ft/sec^2)$
H	enthalpy	cal/mole
HP	assigned enthalpy-pressure problem	
Ivac	vacuum specific impulse	$(lb_f/lb_m)sec$
j	energy conversion factor	lb_f-ft/Btu
M	Mach number	--
MFR	mass flow ratio (A_0/A_c)	--
N_f	number of fuels	--
N_o	number of oxidants	--
n	reciprocal of molecular weight	lb_m-moles/lb_m
n_j^α	composition variables (number of moles of species j in the phase α)	--

SYMBOLS (continued)

Symbol	Description	Units
O/F	oxidant-to-fuel ratio	--
p	pressure	psia
Q	heat transferred into or out of engine	Btu/sec
q	dynamic pressure	$lb_f/in.^2$
R	gas constant (1.987165)	Btu/mole/°R
R_c	inlet cowl radius	in.
r	condensation ratio	--
S	entropy	$Btu/lb_m/°R$
SP	assigned entropy-pressure problem	--
T	temperature	°R
TP	assigned temperature-pressure problem	--
V	velocity	ft/sec
W	mass flow	lb_m/sec
W_{ft}	total fuel flow	lb_m/sec

SYMBOLS (continued)

Symbol	Description	Units
WF	weight fraction	--
X_c	distance from spike tip to cowl lip	in.
β_f	fuel injection angle	degrees
β'	primary stream injection angle	degrees
γ	ratio of specific heats $= C_p/C_v$	--
γ_s	isentropic exponent	--
δ	angle of attack	degrees
δ	denotes variation of	--
ϵ	heat exchanger effectiveness	--
ϵ	tolerance	%
η_c	chemical or mixing efficiency	--
λ_i	Lagrangian multiplier for element i	cal/gm-atom
μ	ejector air entrainment ratio	--

SYMBOLS (continued)

Symbol	Description	Units
μ_t	total entrainment ratio	--
μ_j^{α}	chemical potential	cal/mole
ρ	density	--
σ	shock angle	degrees
τ	skin friction per unit area	$lb_f/in.^2$
ϕ	equivalence ratio	--
ϕ_t	over-all equivalence ratio	--
ϕ^*	stoichiometric mixture ratio	--

B

SYMBOLS (continued)

Subscript	Description
a	denotes conditions relating to air
c	denotes conditions relating to cowl station
f	denotes conditions relating to fuels
f	denotes force units
f,f'	fictitious stations in diffuser where dissipative terms are applied
i	denotes conditions at primary injection station
m	denotes mass units
o	denotes conditions relating to oxidants
t	denotes total conditions
z	frozen composition
0	denotes conditions in pressure field
1	denotes conditions at end of accommodation region
2	denotes conditions at inlet throat
3	denotes conditions in diffuser
4	denotes conditions in combustor

SYMBOLS (concluded)

Subscript	Description
5	denotes conditions at nozzle throat
6	denotes conditions at nozzle exit
∞	denotes conditions in freestream
*	denotes sonic conditions

Superscript

(n)	nth iteration
(1)	initial estimate
'	primary stream
"	secondary stream
*	denotes sonic conditions

INTRODUCTION

One of the most difficult problems in designing a practical hypersonic airplane has been integrating a static and low-speed thrust engine with the ramjet propulsion system required for high-speed acceleration and cruise. The static and low-speed acceleration engine which has been selected in the past as being most suitable is a turbojet. A propulsion system would, however, be significantly lighter and minimize the penalties to performance in the ramjet mode of flight, if the necessity for a completely separate engine were eliminated and the ramjet duct used for producing thrust at all flight speeds. The duPont Jet Engine is such an engine.

A single ramjet duct is used for developing propulsion thrust at all flight Mach numbers from sea-level static conditions to the highest attainable flight speeds. At low speeds, jets of high-pressure, high-temperature air are injected ahead of the inlet throat to mix with the propulsive airstream and produce a total pressure rise as the flow passes through the inlet. The rise in total pressures produces thrust. Combustion in the ramjet duct will augment this thrust. The engine cycle is similar to a duct-burning turbofan with the air injection process replacing the fan stage. The pressure rise due to air injection is similar to the pressure rise obtainable from a single fan stage.

The efficient new aircraft made possible by this type of engine are quite promising. The difference between the weight of this engine and the engines previously considered most attractive for hypersonic aircraft would be equal to or greater than the anticipated payload of a single-stage-to-orbit aerospaceplane or equal to from 140 to 200 passengers in a typical high-speed transport application. In the case of the aerospaceplane the difference in engine weight is the difference between attaining orbit with a reasonable payload and running out of fuel before reaching orbital velocity. In the case of the high-speed transport the difference in engine weight produces a substantial increase in payload and therefore reduction in unit operating cost. The lighter engines can be located on the trailing edge of the wing, if necessary, without unbalancing the aircraft. This location has several advantages including reduction in boattail drag at high subsonic speeds, enabling the engines to be placed in the wing shock pressure field even at very high flight Mach numbers, directional stability at high Mach numbers, and elimination of pitch trim changes and aerodynamic heating due to exhaust nozzle expansion against the aft portions of the aircraft.

The advantages offered by this new type of engine are great enough to make it worthwhile to perform a detailed analysis of its performance and weight so that its impact on aircraft design can be accurately assessed. This report presents the results of that analysis, which had three major elements: a detailed computer simulation of the engine aerothermochemistry providing accurate calculations of performance at all flight conditions and power settings, a comparison of the values calculated using the analytical model of the injection and mixing

process with available experimental data, and a detailed analysis of the engine weight as a function of size and maximum internal pressures in the engine. The report, after presenting a description of the engine and its method of operation, gives a detailed description and results of the analyses performed in these three major areas, and presents the results of a comparison with four engines selected by NASA as being typical of the engines previously proposed for this application.

DESCRIPTION OF DUPONT JET ENGINE

The duPont Jet Engine provides static and acceleration thrust from a hydrogen-fueled ramjet. Thrust is produced by the rise in total pressure in the ramjet duct obtained by injecting a heated primary airstream. The refrigeration capacity of the hydrogen fuel is used to liquefy the primary air. A high pressure is attained with very little compression work by pumping the primary air in the liquid state. Some of the hydrogen fuel is introduced into an air preheater and the primary air is heated by combustion. The hot high-pressure air is then directed to a number of small convergent-divergent nozzles and injected supersonically in a downstream direction. The high-velocity primary airstream mixes with the secondary engine airstream in the favorable pressure gradient ahead of the inlet throat, inducing flow through the ramjet duct. The rise in total pressure provides a pressure ratio for nozzle expansion and therefore thrust when the engine is operating without forward motion of the aircraft. When the aircraft is flying, the total pressure rise due to air injection supplements the static rise due to the aircraft's forward motion.

The pressure rise obtained by injecting a primary airstream is due to the exchange of momentum between the fast moving primary and the slower moving secondary airstreams. As the streams mix, the slower stream is accelerated and the faster stream slowed down until, at a distance of 8 to 15 mixing tube diameters downstream from the injection point, an essentially uniform velocity is achieved. The mixed velocity is greater than the initial velocity of the secondary stream, and since the mixing takes place at constant or nearly constant pressure this increased velocity is reflected in increased total pressure of the mixed airstream. The mixing process is a very inefficient method of compression compared to expanding the primary stream through a turbine and using the turbine work to drive a compressor. However, the pressure ratio attainable from mixing, although lower than that attainable from a gas turbine system, is adequate for an acceleration engine. When the thrust per pound of airflow or fuel of the duPont Jet Engine is compared with a stoichiometric turbojet cycle or duct-burning fan cycle, the thrust efficiency although lower is still reasonable. The duPont Jet Engine trades cycle efficiency for engine simplicity.

Cycle

The duPont Jet Engine operation is shown in Figure 1. The free-stream air at station 1 is diffused to the conditions at the injection station 2 by the secondary inlet. At supersonic speeds the primary and secondary airflows pass through a normal shock ahead of the inlet cowls. A high-pressure, high-temperature, primary airstream (station 9) is injected ahead of the inlet throat. Between the injection point and station 3, the primary and secondary airflows

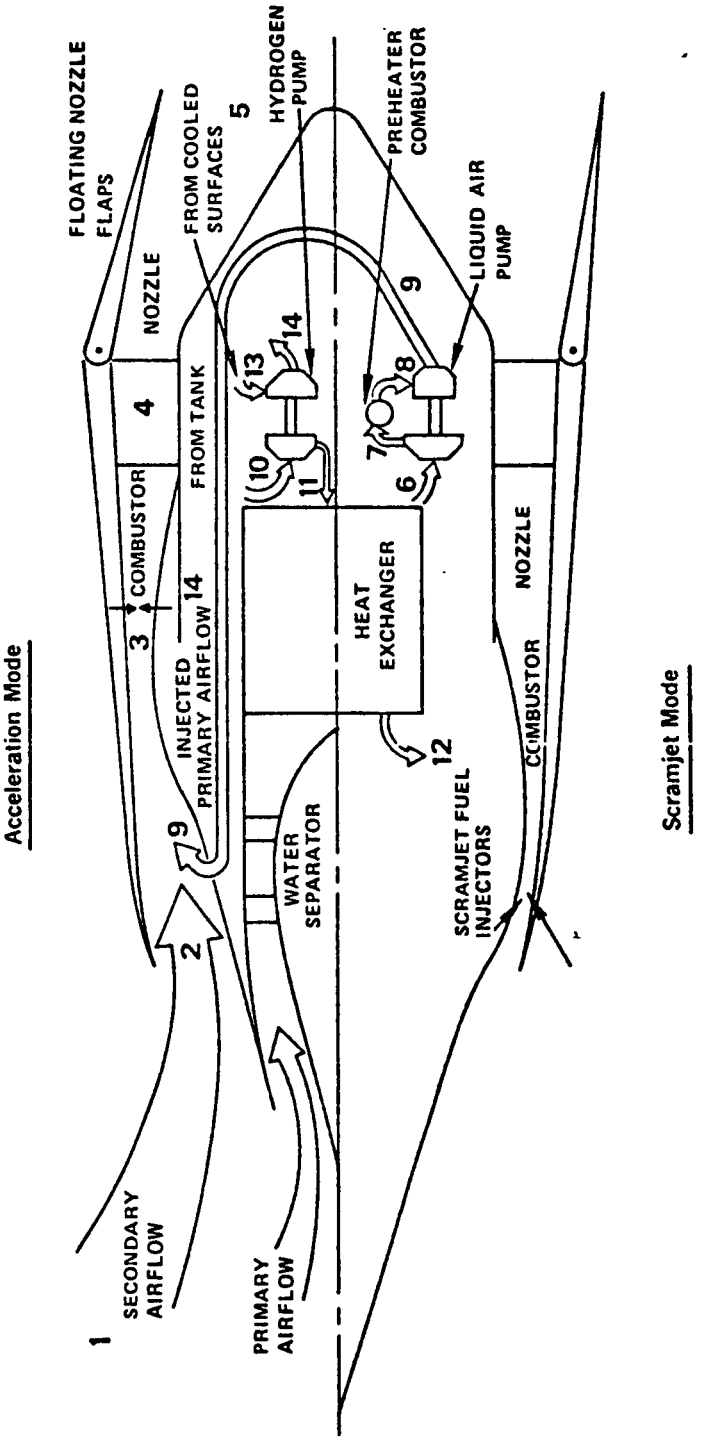

Figure 1. - duPont Jet Engine operation

mix causing a rise in total pressure over that of the secondary airflow. The pressurized stream is diffused downstream of station 3 and enters the combustor where the hydrogen fuel is injected and burned. Flow goes through a sonic throat at station 4 and expands in the nozzle to station 5. Floating nozzle flaps are used to vary the exit area during low-speed operation. The primary airstream enters the primary inlet obtained by retracting the tip of the axisymmetric spike. The airflow then goes through a series of vanes which swirl the air to centrifuge out liquid or solid water. The airstream is then diffused to the heat exchanger face and enters the air-to-hydrogen heat exchanger. The air leaves the heat exchanger at station 6 as a liquid and enters the liquid air pump impeller. The primary air leaves the pump impeller at a high pressure (on the order of 1000 psia) and enters the preheater combustor where a small amount of hydrogen is burned to raise its temperature to 1800°R. The high-pressure gas then goes through the pump turbine and is ducted to the manifold that supplies the primary airflow injection nozzles at station 9.

The hydrogen fuel enters the hydrogen pump at station 10. The fuel leaves the pump at high pressure at station 11 and enters the air-to-hydrogen heat exchanger. At takeoff conditions it leaves the heat exchanger at a temperature of about 270°R at station 12. The temperature of the hydrogen at the exit of the heat exchanger increases with free-stream total temperature. After leaving the heat exchanger, the hydrogen temperature is further increased by cooling the walls of the combustor and nozzle. It then enters the pump turbine at station 13 and is expanded to drive the pump impeller. After leaving the pump turbine at station 14 the fuel is injected into the combustion chamber and burned.

When the inlet can be started (approximately Mach 3), the duPont Jet Engine is converted to a conventional subsonic combustion ramjet by closing off the primary airflow inlet. At Mach 6 the engine may be operated either as a subsonic or a supersonic combustion ramjet. The scramjet mode used above Mach 6 is illustrated by the lower half of Figure 1. In this case the fuel leaving the pump at station 11 is bypassed to the cooled surfaces which must include the inlet as well as the combustor and nozzle. After leaving the pump turbine at station 14, the hydrogen is directed to the forward set of scramjet fuel injectors, injected into the inlet airflow and burned in the inlet throat. The region of minimum inlet throat area serves as the combustor, and the entire aft portion of the engine serves as the nozzle.

The duPont Jet Engine obtains superior performance over other ejector ramjet schemes because the primary flow can be injected at conditions which produce the highest possible pressure ratios at the end of mixing. The translating axisymmetric spike permits the inlet throat area to be adjusted to that value which gives the best performance. Combustion takes place after mixing and diffusion to reduce combustor total pressure loss.

In order to get the maximum flow through the fixed nozzle throat, a mixture ratio higher than stoichiometric may be used. During low-speed operation a rich mixture increases the amount of primary air liquefied in direct proportion to the fuel flow, but the exhaust nozzle limits the total flow in a manner which increases the relative fraction of primary airflow and therefore the engine pressure ratio. It has a slight secondary effect of cooling the exhaust

products which also reduces the throat area required to pass a given flow. Otherwise the fixed nozzle will limit the airflow in the engine at any fuel-to-air ratio in the conventional manner. At constant fuel flow, the duPont Jet Engine compression process has a characteristic similar to a conventional rotating compressor. The pressure ratio will rise at reduced total mass flow due to a relatively larger fraction of primary airflow. This characteristic enables the engine to handle inlet distortion and to be throttled smoothly with a fixed nozzle throat area.

Performance of the engine can be calculated by conventional ramjet methods once the conditions at the inlet throat are known. Conditions at the inlet throat are computed from the conditions at the injection station. Conditions at the injection station are a function of freestream and primary flow conditions. Conditions in the primary stream are determined by the total fuel flow, the mass of air that can be liquefied per unit mass of fuel, the temperature reached by the primary air as a result of preheater combustion, and the total pressure required to pass the primary flow through the throat areas of the primary injection nozzles. A one-dimensional mixing analysis has been used to calculate the flow conditions at the inlet throat.

The over-all cycle is very similar to a duct-burning fan with the injector mixing replacing the fan compression part of the cycle. The achievable pressure ratios are of the same order as those achieved by a single stage fan.

Component Description

The ramjet duct comprises the inlet, diffuser, combustor and nozzle. The combustor and nozzle must always be regeneratively cooled by the hydrogen fuel. At higher speeds the inlet must be regeneratively cooled as well in order to protect the structure against the severe aerodynamic heating encountered in high-speed flight. The energy to run the hydrogen fuel pump is obtained by using hot hydrogen from the regenerative cooling system and expanding it through a turbine which drives the pump impeller. If necessary this type of turbine can be used to generate electric and hydraulic power for the aircraft subsystems. Except for the energy that may be delivered to the aircraft subsystems in the form of electrical or hydraulic energy, all heat absorbed by the fuel in the regenerative cooling system is returned to the cycle as the fuel is injected into the ramjet duct. The energy transferred to the liquid air during the pumping process is returned to the cycle as the air is injected. The aerodynamic functions and the design requirements of the different sections of the ramjet duct are described below.

Inlet. - The ramjet inlet must diffuse the air from free-stream conditions to the inlet throat at conditions which are compatible with the combustor and nozzle operation. If the ramjet is designed for operation at supersonic or hypersonic speeds, the inlet will have an appreciable contraction ratio. This contraction ratio, or diminishing of the stream tube area as the flow approaches the throat, diffuses the supersonic airstream to a lower supersonic

Mach number. Experimental and analytical results indicate that the pressure recovery of such a supersonic inlet increases linearly with contraction ratio, so for greatest efficiency a subsonic combustion ramjet requires the highest attainable contraction ratio and a variable exit nozzle throat to match it. In supersonic combustion, which is the most efficient mode of operation at and above Mach 8, higher contraction ratios give better performance until either the inlet or combustor reaches the choking limit or, in the case of very high Mach numbers, dissociation losses overcome the benefits of increased compression.

For compatibility with duPont Jet Engine operation at sea-level-static and at low flight speeds, it is desirable to have some internal contraction to approximate a bell mouth inlet with low Mach numbers at the entrance. The low Mach numbers limit pressure losses due to a sharp lip. High-pressure recoveries can be achieved under these conditions with an internal contraction ratio between 2 and 3. The same type of internal contraction is also necessary to obtain a high over-all contraction at high Mach numbers without excessive external turning. The inlet that meets these requirements and gives good engine performance is one with an over-all geometric contraction, A_C/A_2, of 10 to 20 or more with an internal contraction ratio of approximately 3. Inlet turning must be gentle to keep the strength of each successive compression wave low enough to prevent boundary layer separation. A practical design constraint for engines that fly faster than approximately Mach 4 is that the inlet be closed off when the engine is not in use to protect the internal surfaces from aerodynamic heating. To obtain more thrust at low speeds, it is desirable to open the inlet throat as much as possible to maximize the engine airflow. The physical contraction ratio, A_C/A_2, may be reduced to approximately 4 at low speeds to improve thrust.

Complete mixing between the primary and secondary streams requires a mixing length of 8 to 15 hydraulic diameters. The normal shock train after supersonic diffusion also requires 8 or more hydraulic diameters for best pressure recovery. Therefore the hydraulic diameter of the throat should be as small as possible to minimize engine length. Minimizing hydraulic diameter may be accomplished by increasing the lateral dimension of the throat as in an axisymmetric spike inlet which permits wall injection, or by means of struts which inject the primary stream at many points in the center of the secondary stream.

There should be some smoothly curved, forward facing surface on the external cowl where spillage drag can be recovered at subsonic and transonic speeds. The initial inlet cone or wedge angle should be as small as possible to minimize spillage drag when the inlet is started and spilling supersonically.

An inlet that meets all of these design requirements is an axisymmetric mixed-compression inlet with a drooped cowl and a translating spike such as that shown in Figure 1. Spike translation permits complete closure of the inlet and a variable contraction ratio. Translation also permits starting the inlet. Figure 2 shows a typical curve of geometric contraction, A_C/A_2, versus spike translation. A three-dimensional fixed geometry inlet with multistrut injection will meet many of the requirements such as a reasonable internal contraction and self-starting with fixed geometry. The problems of fixed geometry that will have to be overcome to use this type of inlet efficiently are closure of the inlet when the engine is not operating to protect the engine should fuel

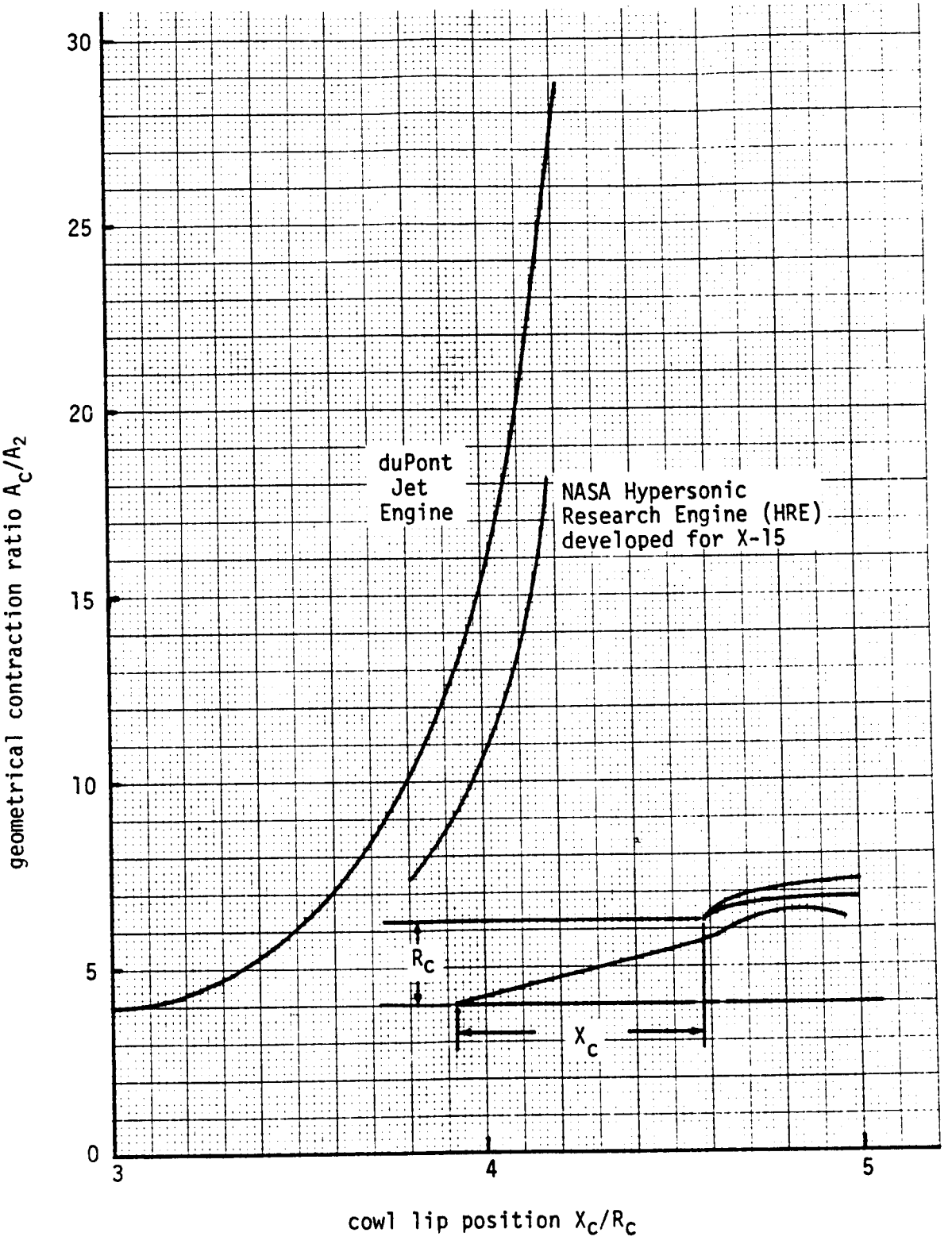

Figure 2. - Contraction ratio vs spike position

flow be interrupted at high speed and the desirability of increasing the throat area to achieve more thrust at low speeds. Closure doors and variable geometry struts might make both forms of inlet functionally equivalent. Swept-back struts will give some decrease in low-speed contraction ratio even with fixed geometry.

Diffuser. - During subsonic combustion the diffuser section slows the air from the throat condition to conditions for combustion. The diffusion process requires a diverging stream tube area. During supersonic combustion the diffuser section can also serve as the beginning of the nozzle since ideally supersonic combustion should take place in a constant area duct at the area of maximum contraction. At lower flight speeds, when constant area combustion would choke the inlet throat combustor, a diverging area or even staged combustion is necessary.

The diffuser section to meet these requirements should begin with constant area or nearly constant area followed by a gentle divergence such as would be produced by a six-degree half-angle conical surface. The length should be sufficient to contain the normal shock train and to provide a suitable length for supersonic combustion. Between 8 and 12 hydraulic diameters are necessary to do this.

Combustor. - The combustor section must be long enough to complete the combustion process for subsonic combustion and large enough in cross section to permit a low combustor entrance Mach number to reduce Rayleigh losses and permit completion of combustion at a reasonable subsonic Mach number. A step must be provided as a flame holder during low-speed operation. The blunt end of the inlet spike skirt is adequate for this purpose.

Nozzle throat. - A sonic nozzle throat must be provided for the subsonic combustion mode of operation. The area reduction must be large enough to choke the flow during subsonic combustion, but not so large as to seriously degrade nozzle performance in the supersonic combustion mode. The larger the ratio of combustor to nozzle throat area the greater will be local supersonic diffusion in the nozzle throat and the greater will be the loss in nozzle efficiency in the supersonic combustion mode. In this mode both the combustor and the nozzle can be considered the engine nozzle.

Expansion nozzle. - Downstream of the throat the stream tube diverges to form the expansion section of the convergent-divergent nozzle. At high Mach numbers this area should be as large as possible to maximize internal performance. In axisymmetric pod installations a trade-off is made between internal performance and external drag that will determine the ratio of nozzle exit area to cowl area. This trade-off usually produces an area ratio between 1.5 and 2.0. At subsonic and transonic speeds the ideal nozzle exit area is very close to the choked area in the throat. Therefore, some means must be employed at low speeds to decrease the exit area. The standard solution to this problem on axisymmetric engines consists of hinged nozzle flaps to balance the external and internal pressures and to optimize the losses between external boattail drag and internal overexpansion losses. Typically the exit area must be reduced to the order of the cowl area to get the overexpansion losses down to a reasonable value.

Primary Air System

The primary air system consists of a primary air inlet that can be closed off when not in use, a diffuser for the incoming air with provisions for separating out liquid water, a precooler heat exchanger, a condenser, a liquid air pump, a preheater combustor, and air injection manifolds and nozzles.

Inlet. - The inlet for the primary air system must match the characteristics of the secondary airflow and be capable of smooth closure when the primary air system is not in use. Pressure recovery of the primary inlet is only important as it affects flow characteristics. A normal shock inlet appears to be satisfactory. One example of a primary air inlet could be that formed when the tip section of the inlet spike of an axisymmetric inlet is partially retracted into the downstream section as shown in Figure 1. Another could be a separate two-dimensional inlet located in the adjacent airframe in the case of a two-dimensional engine installation.

Diffuser. - The inlet diffuser must slow the incoming air to the velocity at the heat exchanger face. The desired velocity at the heat exchanger face is on the order of Mach 0.03 to Mach 0.07. It is desirable to introduce swirl into the flow and then deswirl it before it enters the diffuser section to remove liquid or solid water in the primary airstream and reduce heat exchanger fouling.

Precooler. - The precooler portion of the heat exchanger cools the air to the temperature where air condenses. The maximum hydrogen temperature on the cold side of the heat exchanger is approximately 270°R during operation at conditions where there is a large atmospheric moisture content, so that moisture will tend to be solidified before contact with the heat exchanger core. Two possible core configurations--tubular matrix, and plate-and-offset-fin--appear satisfactory at this time. The tubular matrix is better for anti-fouling but requires more volume. A solution to fouling is to use several cores so that at least one is redundant. Each core may be taken out of service and heated periodically to clear it. This method is standard practice in portable liquid oxygen plants. The plate-fin heat exchanger's compactness makes this solution possible, and, therefore, the plate-fin configuration was selected as the most practical. Preliminary sizing studies indicate that it is possible to package the heat exchanger system within the spike of an axisymmetric inlet.

Condenser. - The condenser is either a tubular or plate-fin heat exchanger with catalysts in the headers to reduce the time required to convert the parahydrogen coming from the pump to an equilibrium mixture of orthohydrogen and parahydrogen at the condenser exit conditions. The terms ortho- and para- reflect the direction of spin of the atoms in a hydrogen molecule. Energy is required to change the spin from the para to the ortho condition, and this change increases the heat absorbed by the hydrogen and thereby its capacity to liquefy air. Liquid hydrogen must be stored in the para condition to prevent boiloff due to heat released in converting from the ortho to the para condition.

Liquid air pump. - The liquid air pump consists of a single-stage impeller driven by the heated primary air just prior to injection. The air turbine is preferred over a hydrogen turbine from a safety point of view since a catastrophic reaction would not occur if the induced and driving fluids came into contact with each other. Use of preheated air to drive the turbine increases the heat sink available in the hydrogen fuel over a system that uses a hydrogen expansion turbine.

Combustor. - A preheater combustor is used to burn some of the hydrogen fuel with the liquid air. Because the air is under such high pressure, the combustor is very small. The temperature leaving the combustor is on the order of 1800°R. This temperature is similar to the maximum fuel temperatures in the regeneratively cooled surfaces, and is close to the optimum temperature for maximum engine pressure ratio. Although the velocity of the primary stream and therefore the mixed velocity may be increased by additional temperature, the entropy production due to equalizing the temperatures in the primary and secondary streams during mixing increases with the temperature difference so that the engine pressure ratio as a function of primary stream total temperature declines at higher temperatures.

Injection nozzles. - The vitiated air from the preheater combustor enters a manifold which distributes it to a series of small convergent-divergent nozzles located on the wall or walls of the ramjet duct approximately 8 to 15 hydraulic diameters ahead of the minimum inlet throat area station. These nozzles inject the flow downstream at a slight angle outward so that the primary flow can penetrate and mix with the secondary airstream. The dimension of each nozzle is small compared to the dimension of the ramjet inlet throat, so that the nozzles are very similar to the fuel injection nozzles used for supersonic combustion.

Engine Subsystems

The engine, in addition to the ramjet duct and the primary air system, contains the following ramjet subsystems:

Inlet spike actuation system. - The inlet spike is positioned by multiple hydraulic cylinders in the case of an axisymmetric installation. Hydraulic actuation is preferred over pneumatic or electric because of its resistance to oscillation and its capability of handling large loads with rapid and precise positioning. The forward portion of the spike uses a single cylinder.

Fuel pump. - The fuel pump is a bootstrap turbopump with a single-stage centrifugal impeller driven by a single-stage axial turbine. The turbine is driven by hot hydrogen from the regenerative cooling system, giving the system its designation as bootstrap. A safety advantage of this kind of system is that almost any conceivable failure or leak in the fuel system tends to deny fuel to the turbine and to shut the engine down by slowing the delivery of fuel. Pump rotation is started simply by letting fuel trickle into the cooling system. The boiling hydrogen will start turning the fuel pump turbine, which

will pump fuel into the heat exchanger and primary and engine combustors. The engine walls are heated from combustion, increasing the temperature of the fuel delivered to the pump, which in turn increases its pumping ability until the engine has bootstrapped itself to full power operation.

Fuel valves. - The fuel system has several valves which meter the fuel to the various injector stations and engine cooling circuits. These valves are of the fail-safe type. The power which actuates the valve, whether it is hydraulic, pneumatic or electrical, is necessary to force the valve away from the safe position. Therefore, the fuel valves will return to the safe positions if the actuating power is lost for any reason. Valves are actuated in response to commands from the fuel control computer.

Fuel control. - The fuel control digital processor computes the correct fuel valve setting for each position of the power lever and flight condition. The full forward position of the power lever corresponds to maximum thrust available at that flight condition, and full aft corresponds to the minimum thrust available. Intermediate positions correspond to a fraction of maximum thrust equal to the fraction of the distance between the full aft and full forward positions. The digital processor computes the fuel flow required through each valve and outputs the required signals to control the valve positions. An electronic digital computer is preferred for the fuel control because of its flexibility and the level of computational complexity involved in the fuel control calculations. Another reason for selecting a digital computer is the relative ease with which a digital engine simulation can be used to develop and check out the control program used in the engine.

EJECTOR ANALYSIS VERSUS EXPERIMENT

The ejector analytical model described in the Appendix and used in the performance computer program was compared to the available experimental data on ejectors. A literature search comprising 250 references in microfiche produced only three (References 1 through 3) which contained experimental data in the general range of the duPont Jet Engine and in sufficient detail to permit simulation in the analytical model. The ejector geometry was illegible in the microfiche of Reference 2, and the hard copy was received too late to include with this study.

The experimental conditions of References 1 and 3 were simulated in the analytical model using reasonable values of skin friction coefficient, C_f, and primary nozzle velocity coefficient, C_v, in the momentum equation to account for the effects of wall skin friction and irreversibilities in the primary nozzle expansion process, respectively. Excellent agreement was obtained for those experiments which incorporated large ratios of the area at the end of mixing, A_2, to the primary nozzle throat area, A_*. In simulating those experiments with smaller area ratios, it was necessary to include a blockage factor (fraction reduction in effective flow area at the end of mixing) in order to obtain agreement with the experimental data. However, the analytical model was unable to predict the maximum bypass ratios (secondary flow/primary flow) observed in any of the experiments.

The maximum theoretical values of bypass ratio were obtained by adjusting the secondary Mach number to maximize the flow at the end of the accommodation region where primary flow expands to match static pressure with secondary flow and where it was assumed that no mixing had occurred between the primary and secondary streams. This implied that the flow was choked. However, the same criterion for choking applies both to striated flow and to the flow of a single stream. That is, both types of flow must pass through a minimum area in order to reach sonic conditions. Therefore, it is postulated that the maximum values of bypass ratio predicted by ejector theory cannot be attained unless the flow area ahead of the mixing duct passes through a minimum. This theory has been partially verified in that the maximum theoretical values of bypass ratio could not be attained judging by the results of ejector experiments reported in the literature. However, since none of these experiments incorporated a minimum area ahead of the mixing duct, it has not been determined whether the maximum theoretical bypass ratio could be attained in any circumstance.

The comparison between the analytical model and the data from constant area mixing experiments reported in Reference 1 is shown in Figure 3. The ordinate represents the ratio of measured to calculated static pressure when applied to the experimental data and the ratio of calculated static pressure with losses to the calculated static pressure without losses when applied to the calculated data. The same representation applies to the 'measured bypass ratio' in the

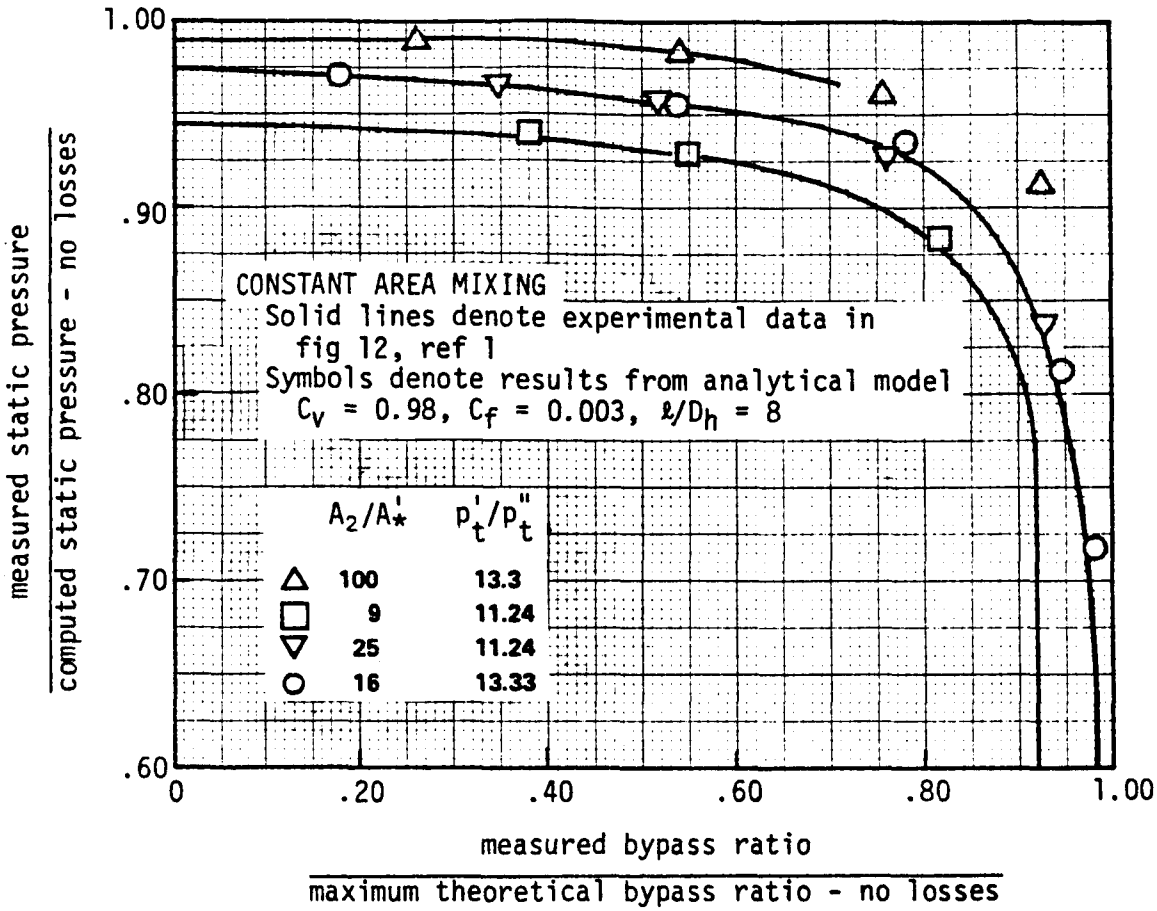

Figure 3. - Comparison of ejector analytical model with Reference 1

notation of the abscissa. The upper curve in Figure 3 represents a ratio of mixed area to primary nozzle throat area of 100 which has nearly the same geometry as the ejector used in the duPont Jet Engine. The analytical model was able to duplicate this curve with the loss coefficients C_v = 0.98, C_f = 0.003 and a nominal mixing length of 8 hydraulic diameters. The other curves in Figure 3 could be duplicated out to a bypass ratio equal to 0.7 of the maximum theoretical bypass ratio. Beyond this point, increasing values of blockage had to be used to duplicate the experimental data. Excellent agreement was obtained with the experimental data until the slopes of the experimental curves became infinite after which the analytical model continued to calculate bypass ratios out to the theoretical maximum (see discussion in preceding paragraph).

The simulation of the experimental data in Figure 3 was accomplished by first determining the values of nozzle velocity and skin friction coefficients required to match the left-hand portions of the curves with a constant mixing length of 8 hydraulic diameters. Then, holding the values of the coefficients

constant, the right-hand portions of the curves were matched by determining the required area blockage. In all cases, values of C_f = 0.003 and C_v = 0.98 produced the best correlation while the blockage varied between 8 and 12 percent. The blockage accounted for the increase in boundary layer thickness.

The conditions of Test 18 - Run 102 in Reference 3 were simulated in the ejector analytical model as closely as possible. Vitiated air was used in the primary stream in the analytical model instead of the heated air used in the experiment. As a result, it was necessary to increase the primary nozzle throat area from 1.69 x 10^{-4} ft^2 used in the experiment to 1.7225 x 10^{-4} ft^2 in the analytical model in order to duplicate the measured primary mass flow.

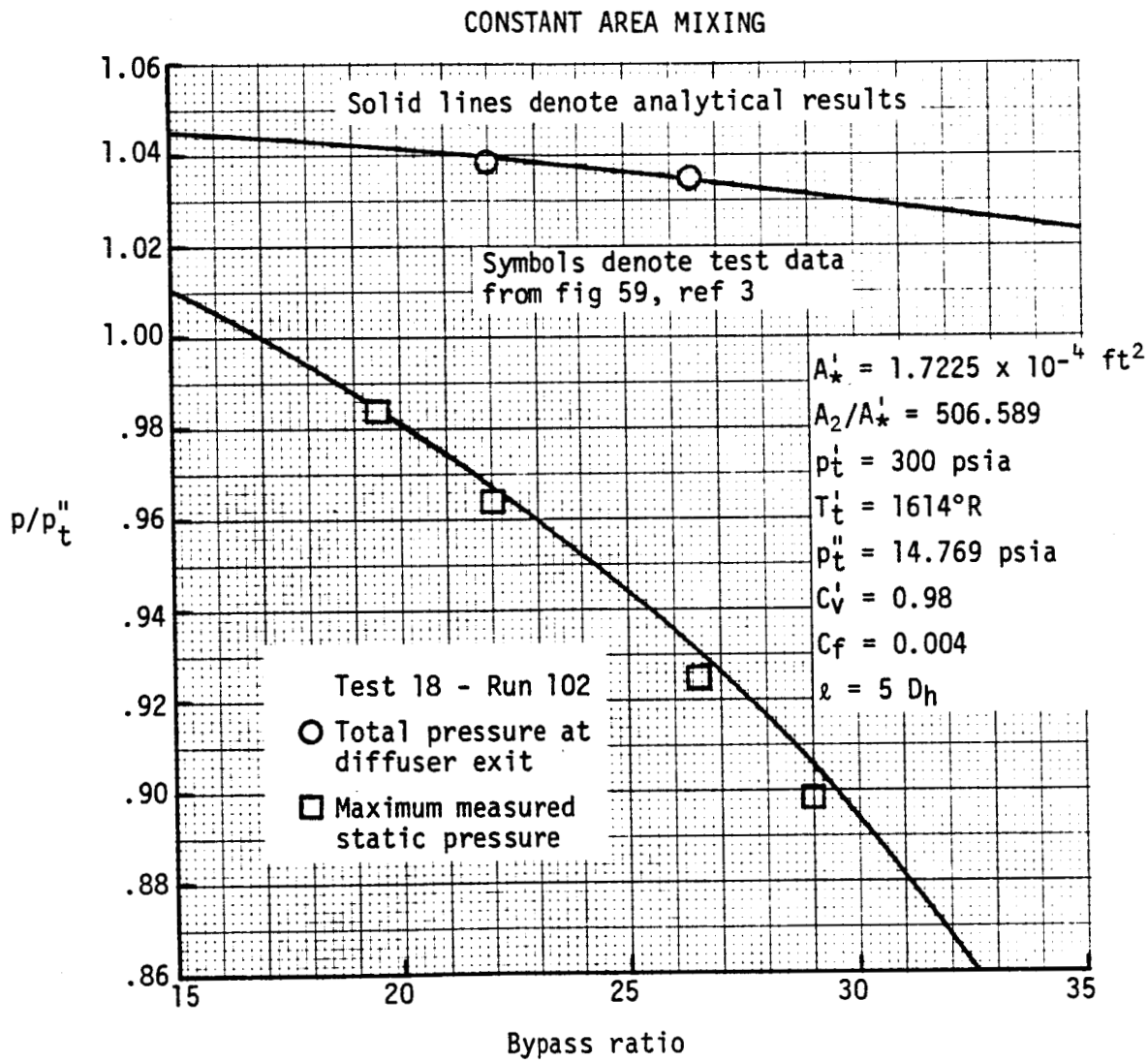

Figure 4. - Comparison of ejector analytical model with Reference 3

Comparison between the analytical model and the data from a constant area mixing experiment (Test 18 - Run 102) reported in Reference 3† is presented in Figure 4. The ordinate in Figure 4 denotes the ratio of either measured or calculated static or total pressure to the total pressure in the secondary flow. The abscissa denotes the bypass ratio.

The total pressure measurements taken at the diffuser exit were matched very closely using a $C_V' = 0.98$, a $C_f = 0.004$ and the actual length of the mixing duct. These same values of the loss coefficients gave satisfactory agreement with the measured static pressures. It was not necessary to use an area blockage factor at the end of the mixing duct because of the large area ratio incorporated in the test ejector.

†Figure 59, p. 187.

ENERGY BALANCE

Energy was conserved throughout the analysis of the engine cycle. In this cycle all the energy in the fluids is eventually returned to the ramjet duct so that over-all energy is conserved. In practice the only energy that could be removed from the engine cycle would be that energy that is tapped off for electrical and hydraulic power for the aircraft. On the other hand, if the hydrogen fuel is used as a heat sink for airframe cooling, energy will be added to the engine cycle. If we ignore these two effects, however, energy is conserved within the over-all cycle.

Within the cycle itself, work is expended to pump the liquid air, and the work is obtained by the expansion of the heated primary airstream through a turbine which drives the pump. Similarly hydrogen pumping is accomplished in a bootstrap system where the energy to drive the hydrogen pump impeller is obtained by expanding hot hydrogen through a turbine. The hot hydrogen is obtained by routing the hydrogen fuel along the walls of the combustor and nozzle to cool the engine structure. In the regenerative cooling process all the heat that the fuel absorbs from the combustor walls is returned to the propulsive airstream as the fuel is injected and mixed. The work extracted from the hydrogen during the expansion in the pump turbine is added to the hydrogen through the impeller so that energy is conserved in the total hydrogen fuel loop.

Liquid Air Cycle

The energy transfer in the engine cycle between the primary airstream and the hydrogen fuel during the air liquefaction process determines the ratio of secondary to primary flow. The heat removed from the primary airstream during its liquefaction is absorbed by the hydrogen fuel. The amount of air that can be liquefied per unit fuel flow is determined by the heat exchanger pinch effect illustrated in Figure 5. The air enters the heat exchanger at a temperature nearly equal to the free stream total and is precooled to that temperature at which oxygen will liquefy. As the air passes through the condenser the oxygen is liquefied at constant temperature. The temperature is then reduced to the point where nitrogen will liquefy, and heat is removed at constant temperature until all the air leaves the heat exchanger in the liquid state. Flow through the heat exchanger is induced by the volume change of the air as it is liquefied and by the subsequent removal of the liquid air.

The hydrogen enters the condenser at pump exit conditions and its temperature is increased as it passes through the condenser and absorbs the heat of condensation of the oxygen and nitrogen. It then continues to increase in temperature as it cools the air in the precooler portion of the heat exchanger ahead

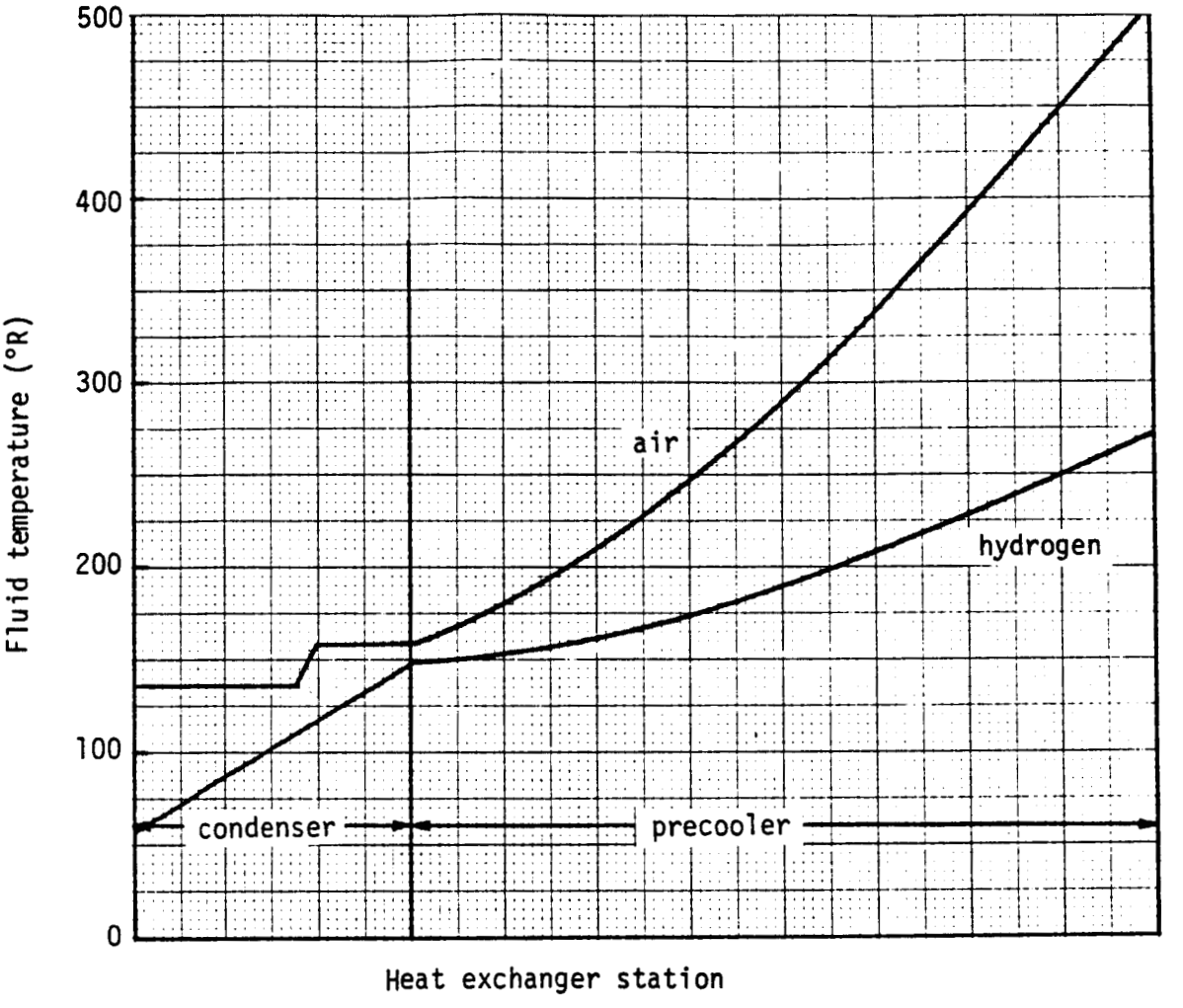

Figure 5. - Heat exchanger "pinch" effect

of the condenser. Examination of Figure 5 shows that the difference between the temperature of the hydrogen and the air is at a minimum at the pinch point where condensation of oxygen begins. Since the ability to transfer heat is a function of the temperature difference between the fluids, more heat may be transferred per unit surface area at the entrance of the heat exchanger and the exit of the condenser than in the region at and near the pinch point.

The surface area of the heat exchanger is related to the temperature difference between air and hydrogen at the pinch point. For zero temperature difference at the pinch point, an infinite heat exchanger would be required. The greater the temperature difference the smaller the heat exchanger. The air-side single-phase precooler effectiveness is defined as

$$\varepsilon = [T_a(\text{precooler-in}) - T_a(\text{precooler-out})] / [T_a(\text{precooler-in}) - T_{H_2}(\text{condenser-out})]$$

so that the temperature difference at the pinch point (ΔT_{pp}) is

$$\Delta T_{pp} = \frac{1-\epsilon_a}{\epsilon_a}\left[T_a(\text{precooler-in}) - T_a(\text{precooler-out})\right]$$

As the temperature of the air entering the precooler increases in a heat exchanger having a constant air-side precooler effectiveness, the temperature difference at the pinch point increases. Therefore, the effect of increasing the free stream total temperature is to reduce the quantity of air liquefied per unit hydrogen flow.

For the purpose of this study an air-side single-phase precooler effectiveness of 0.97 was used in a cross-counterflow heat exchanger. The amount of air that can be liquefied per pound of hydrogen (condensation ratio, r) as a function of static pressure in the condenser and free stream total temperature is shown in Figure 6. To simplify the duPont Jet Engine analytical performance model, the

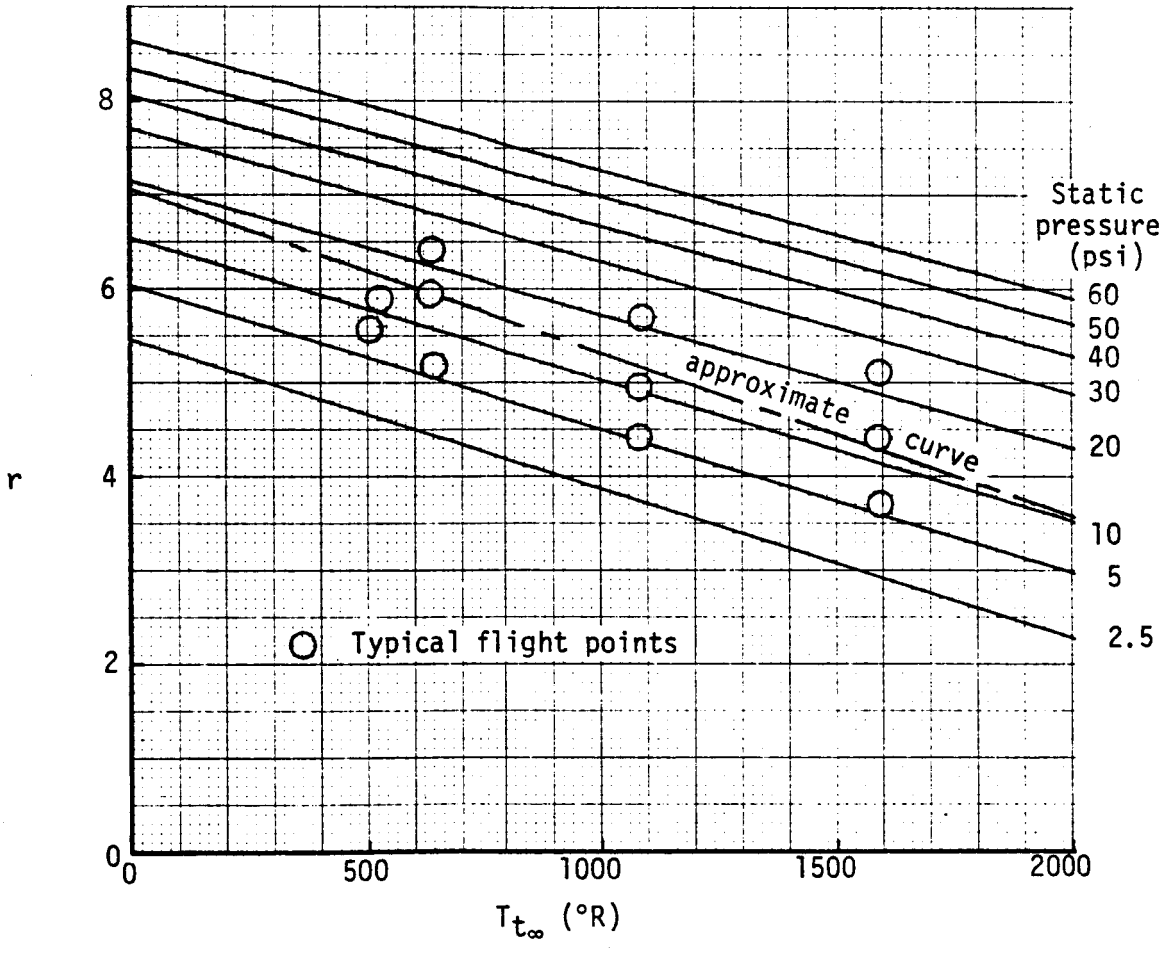

Figure 6. - Condensation ratio versus free stream total temperature

pressure dependence was eliminated and a single line representing the number of pounds of air that can be liquefied per pound of fuel was used. This line has been superimposed on Figure 6. This approximation gave slightly optimistic condensation ratios at sea-level-static and conservative ratios with increasing free stream Mach numbers.

In the calculation of engine performance, it was assumed that the hydrogen would change from parahydrogen in the tank to an equilibrium mixture of parahydrogen and orthohydrogen at the pinch point. It is necessary to run the hydrogen through a catalyst in order to accelerate the conversion from parahydrogen to equilibrium. This conversion has been demonstrated in the laboratory with amounts of catalyst that are realistic for flight applications. It was demonstrated in Reference 5 that 75% conversion from parahydrogen to the equilibrium mixture of orthohydrogen and parahydrogen could be obtained with five pounds of catalyst per pound per second of hydrogen flow. The catalyst used was ruthenium on a bed of silicon dioxide and zirconium oxide. Although this laboratory demonstration indicates that flight weight catalytic conversion is possible, a flight weight heat exchanger with catalytic conversion has not yet been demonstrated. If there is no conversion at all and the additional heat sink from the para-ortho conversion is not realized, the condensation ratio shown in the lower line in Figure 7 will be realized, compared to that

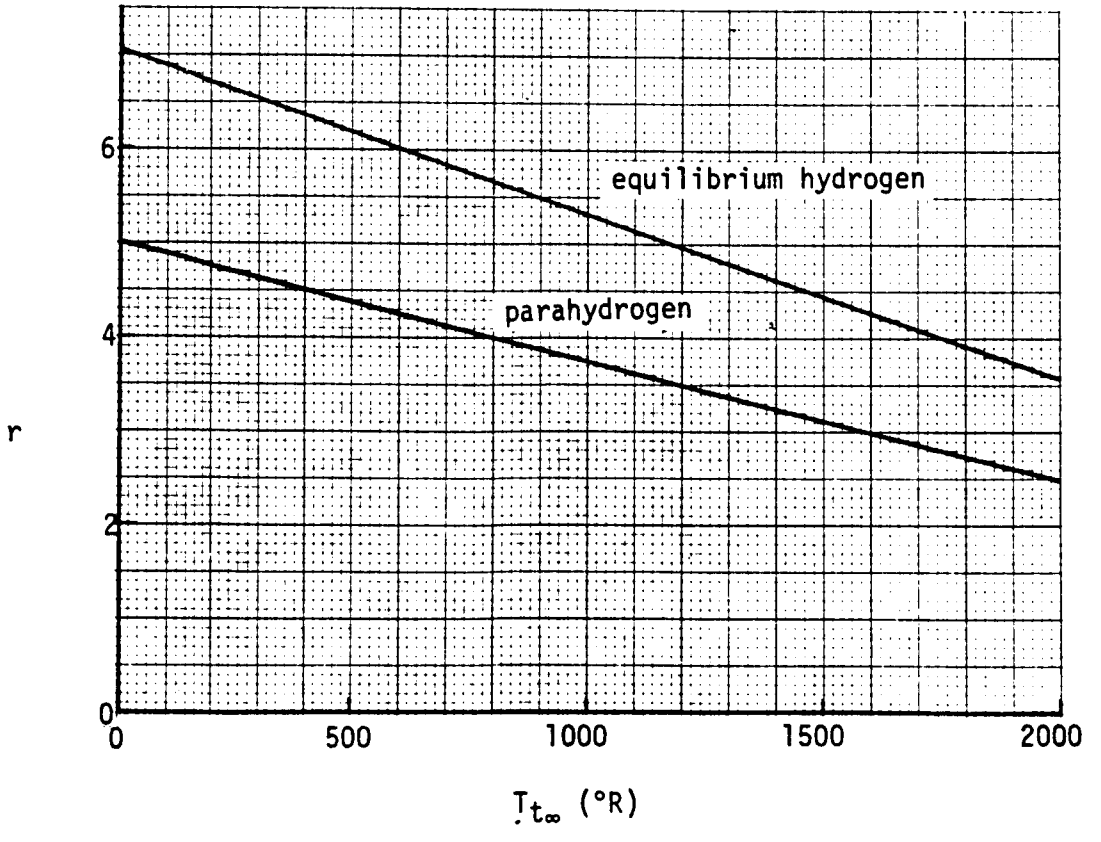

Figure 7. - Effect of parahydrogen to orthohydrogen conversion

attainable with complete conversion shown on the upper line. The effect of not achieving conversion is to require more fuel flow for the same engine pressure ratio and thrust, or lower pressure ratio and thrust for the same fuel flow.

In this analysis no consideration was given to schemes that might augment the heat sink capability of the hydrogen. For example, if slush hydrogen is used in the tank, the fuel flow for air liquefaction can be made independent of the fuel consumed during combustion, the excess being returned to the tank giving a much better performance than in the case where all the fuel used for air liquefaction must be burned. Other schemes advanced by the Marquardt Corporation under the generic name of SUPERLACE, which involve expansion turbines and reliquefaction of some of the hydrogen, can also potentially augment the fuel heat sink available.

Engine Cooling

A comparison with the Hypersonic Research Engine (HRE) at Mach 8 shows that the 90-inch diameter duPont Jet Engine can be cooled with 63% of the available heat sink in the hydrogen fuel used for stoichiometric combustion. The comparison was made by using Figure 5.1-25 of Reference 6 as a reference. This figure shows heating rate versus engine station at a free stream number of Mach 8 and a local Mach number of 6.5 corresponding to flight under a wing at approximately 7 degrees angle of attack. The heating rate for a 90-inch diameter duPont Jet Engine was obtained by multiplying the heating rate of the HRE by the reciprocal of the local Reynolds number to the one-fifth power times the ratio of the local airflow per unit area of the duPont Jet Engine to that of the HRE.

The resulting curves of heating rate are plotted versus nondimensional engine station in Figure 8. The heating rate was then integrated over the engine surface to obtain the heat load on the engine. This heat load was then compared to the heat sink available in raising the fuel flow from the pump outlet temperature to the maximum permitted temperature of 1600°R. The comparison showed that 63% of the available heat sink is required to absorb the engine heat load.

The differences in basic aerodynamic heating parameters that affect the results for the 90-inch engine with respect to the HRE are a larger Reynolds number due to increasing the scale by a factor of 5, a 50% reduction in airflow per unit area in the region that is used for subsonic combustion between approximately station 6 and station 7 due to increasing the subsonic combustor area to achieve greater low-speed thrust, an 8% reduction in wetted perimeter in the subsonic combustor due to increasing the combustor area, and a shortening of the engine internal length indicated in Figure 8.

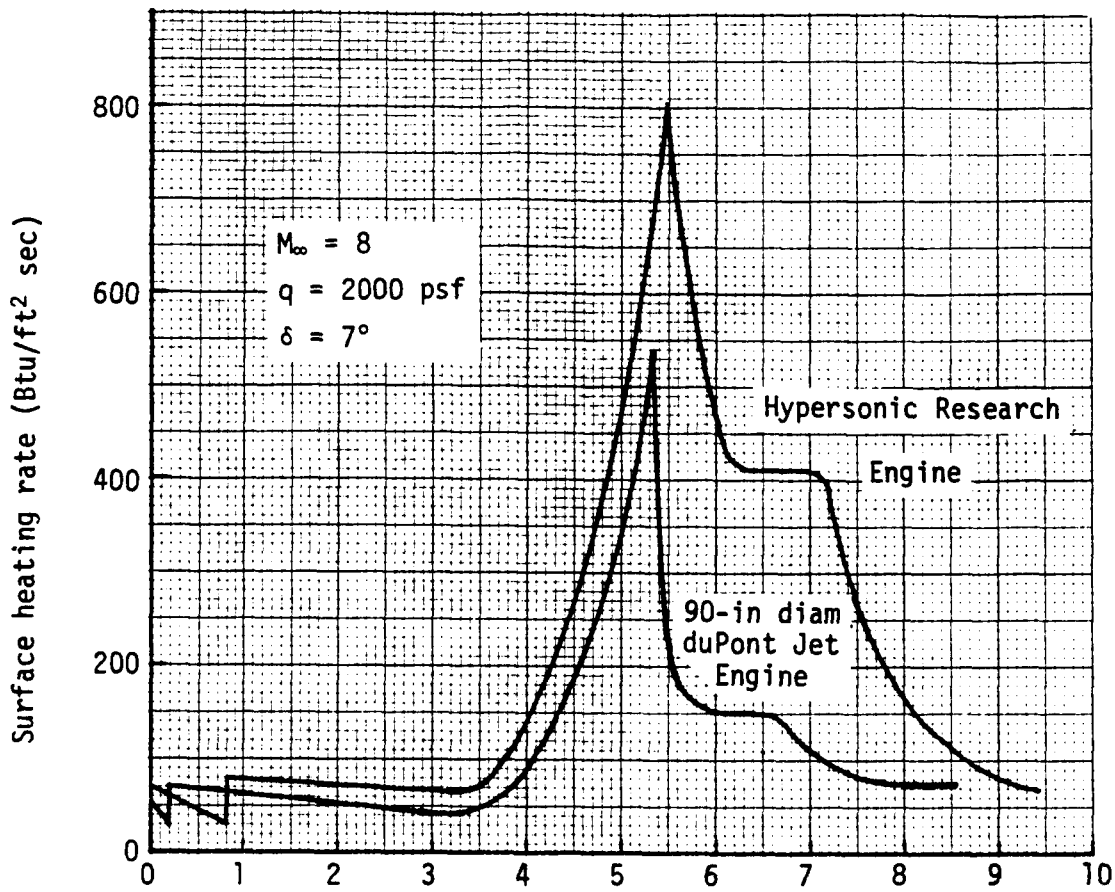

Figure 8. - Comparison of heating rates

ENGINE WEIGHT

The weight of the duPont Jet Engine as a function of inlet cowl diameter was obtained by establishing an acceptable design from an aerodynamic and thermodynamic standpoint using the Hypersonic Research Engine (HRE) as a guideline. The design criteria for the HRE were used throughout. Two layouts of the engine were drawn: one with a 90-inch inlet cowl diameter, the other with an 18-inch inlet cowl diameter. A detailed weight breakdown of the two layouts is included in Tables I and II. Figure 9 shows the structural subassemblies considered in the weight analysis. In the case of the 18-inch engine, all of the cooled skin and heat transfer surfaces are similar to those of the HRE except for the outer cowl which was cooled with an ablative material on the HRE and is regeneratively cooled on the duPont Jet Engine. In the case of the 90-inch engine the structural inner skins were adjusted for hoop stress.

After the detailed weight analyses for the two engine sizes were completed, the weight per wetted area of each major structural subassembly was derived. The wetted areas for three intermediate-sized engines were then determined by scaling all dimensions proportionately to inlet cowl diameter, with the exception of the combustor length which was held constant. The weight per wetted area of the shell subassemblies was determined for each intermediate size by adjusting the inner skin thicknesses. The weight of the auxiliary structure and the subsystems was interpolated as a square function of the inlet cowl diameter ratio. The weights of the five engine sizes are shown in Table III. The weight of the duPont Jet Engine as a function of inlet cowl diameter, shown in Figure 10, is based on these five engine sizes and weights. The engine weight increases as a function of maximum combustor pressure for the subsonic and supersonic combustion modes were determined by calculating weight increases to satisfy hoop stress requirements in the critical areas of the combustor for that mode in the five engine sizes. The weight increases for the subsonic and supersonic combustion modes are shown in Figures 11 and 12, respectively.

Most of the shell is the same on the duPont Jet Engine as the HRE for equivalent engine sizes, i.e., fins and skins for internal wetted area and basic structural skin thicknesses. All of the weights of the subsystem valves and controls are the same as the actual weights from the HRE reports for common parts and engine size. The weight of these items accounts for approximately half of the calculated engine weight; therefore the 15% development margin, which is 15% of the total weight, really amounts to approximately 30% of the new design areas. Substantial weight savings are realized on the duPont Jet Engine compared to the HRE in the spike actuation and support system and in the fuel injection and coolant manifolds. New areas of design are in the heat exchanger, the liquid air pump and the variable exhaust nozzle. An additional 10% margin is included in the weight of these components. A comparison between the 18" diameter duPont Jet Engine and the HRE is contained in Table IV.

TABLE I. - DUPONT JET ENGINE WEIGHT SUMMARY
FOR 90-INCH INLET COWL DIAMETER

Item	Wetted area (ft^2)	Assembly weight (lbs)	Shell only (lbs)	Auxiliary structure (lbs)
Spike, forward	28	120	81	39
Spike, aft	257	1325	884	441
Inner shell	153	505	420	85
Innerbody nozzle	95	210	174	36
Outer cowl	299	1865	1735	292
Variable nozzle	177	1070	859	211
Struts	30	325	103	222
Total	1039	5420	4256	1326

Subsystems:		
Hydraulic actuation		620
Heat exchangers		930
Liquid hydrogen pump		340
Liquid air pump (includes combustor)		150
Miscellaneous controls		150
Miscellaneous plumbing		180
Total subsystems weight		2370

Shell weight	4256
Auxiliary structure weight	1326
Subsystems weight	2370
Development margin 15%	1193
GRAND TOTAL	9145

TABLE II.- DUPONT JET ENGINE WEIGHT SUMMARY
FOR 18-INCH INLET COWL DIAMETER

Item	Wetted area (ft^2)	Assembly weight (lbs)	Shell only (lbs)	Auxiliary Structure (lbs)
Spike, forward	1.1	6	4	2
Spike, aft	11.2	70	41	29
Inner shell	7.1	30	20	10
Innerbody nozzle	3.8	14	8	6
Outer cowl	13.5	95	67	28
Variable nozzle	7.1	53	37	16
Struts	1.2	24	6	18
Total	45.0	292	183	109

Subsystems:		
Ignition system		16
Hydraulic actuation		65
Heat exchanger		57
Liquid hydrogen pump		30
Liquid air pump (includes combustor)		25
Miscellaneous controls		84
Miscellaneous plumbing		40
Total subsystems weight		317
Shell weight	183	
Auxiliary structure weight	109	
Subsystems weight	317	
Development margin 15%	91	
GRAND TOTAL	700	

1 Forward spike
2 Aft spike
3 Inner shell
4 Innerbody nozzle
5 Outer cowl
6 Variable exhaust nozzle
7 Struts

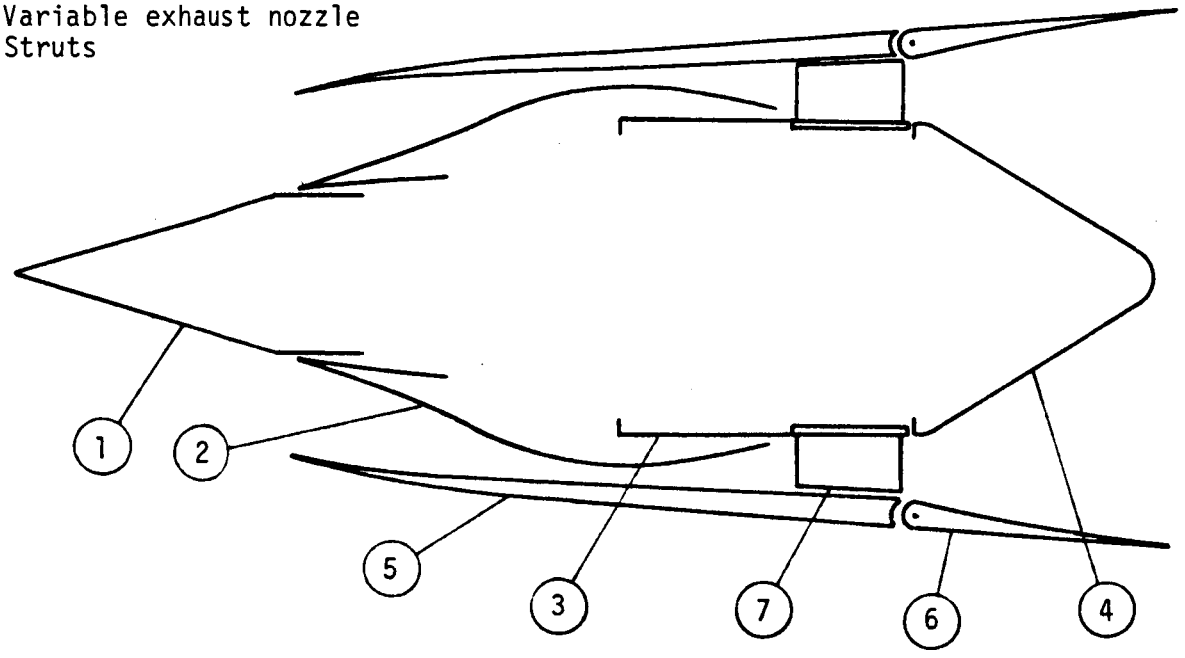

Figure 9. - Structural subassemblies of the duPont Jet Engine

Inlet Spike Actuation and Support System

The largest weight savings in the duPont Jet Engine compared to the HRE are in the spike actuation and support system. The hydraulic actuator used in the HRE was replaced with separate actuators each attached to a strut and directly attached to the base of a manifold ring on the spike as shown in Figure 13. A single actuator moves the spike tip. This shortened the load path and removed the heavy mounting legs used on the HRE. Support for the engine unstart load was moved to the largest possible diameter since the support weight required to resist bending moment is inversely proportional to the square of the radius of gyration. This further reduced the weight required for keeping the spike concentric with the inner shell during an asymmetric unstart and eliminated the bellows required on the HRE. The HRE spike actuator was a modified off-the-shelf unit which was required to have greater force than that required for the duPont Jet Engine. The duPont Jet Engine spike design allows pressure balancing by necking down the trailing edge of the spike thereby reducing forward actuation forces which further reduces actuation system weight.

TABLE III. - DUPONT JET ENGINE WEIGHT SUMMARY
VARIOUS COWL DIAMETERS

Item	18-inch diameter engine		36-inch diameter engine		54-inch diameter engine		72-inch diameter engine		90-inch diameter engine	
	wetted area (ft^2)	weight (lbs)	wetted area (ft^2)	weight (lbs)	wetted area (ft^2)	weight (lbs)	wetted area (ft^2)	weight (lbs)	wetted area (ft^2)	weight (lbs)
Spike, forward†	1.1	6	4	21	10	44	18	72	28	120
Spike, aft†	11.2	70	43	242	94	503	165	860	257	1325
Inner shell†	7.1	30	26	95	58	201	102	343	153	505
Innerbody nozzle†	3.8	14	15	44	34	85	61	140	95	210
Outer cowl†	13.5	95	50	335	110	728	193	1293	299	2027
Variable nozzle†	7.1	53	28	197	64	418	114	712	177	1070
Struts†	1.2	24	5	71	11	138	19	224	30	325
Subsystems	---	317	---	574	---	1000	---	1599	---	2370
Development margin 15%	---	91	---	236	---	467	---	786	---	1193
ENGINE TOTAL	45.0	700	171	1815	381	3584	672	6029	1039	9145
Engine wt/wetted area	15.56		10.61		9.36		8.86		8.62	

†see Figure 9

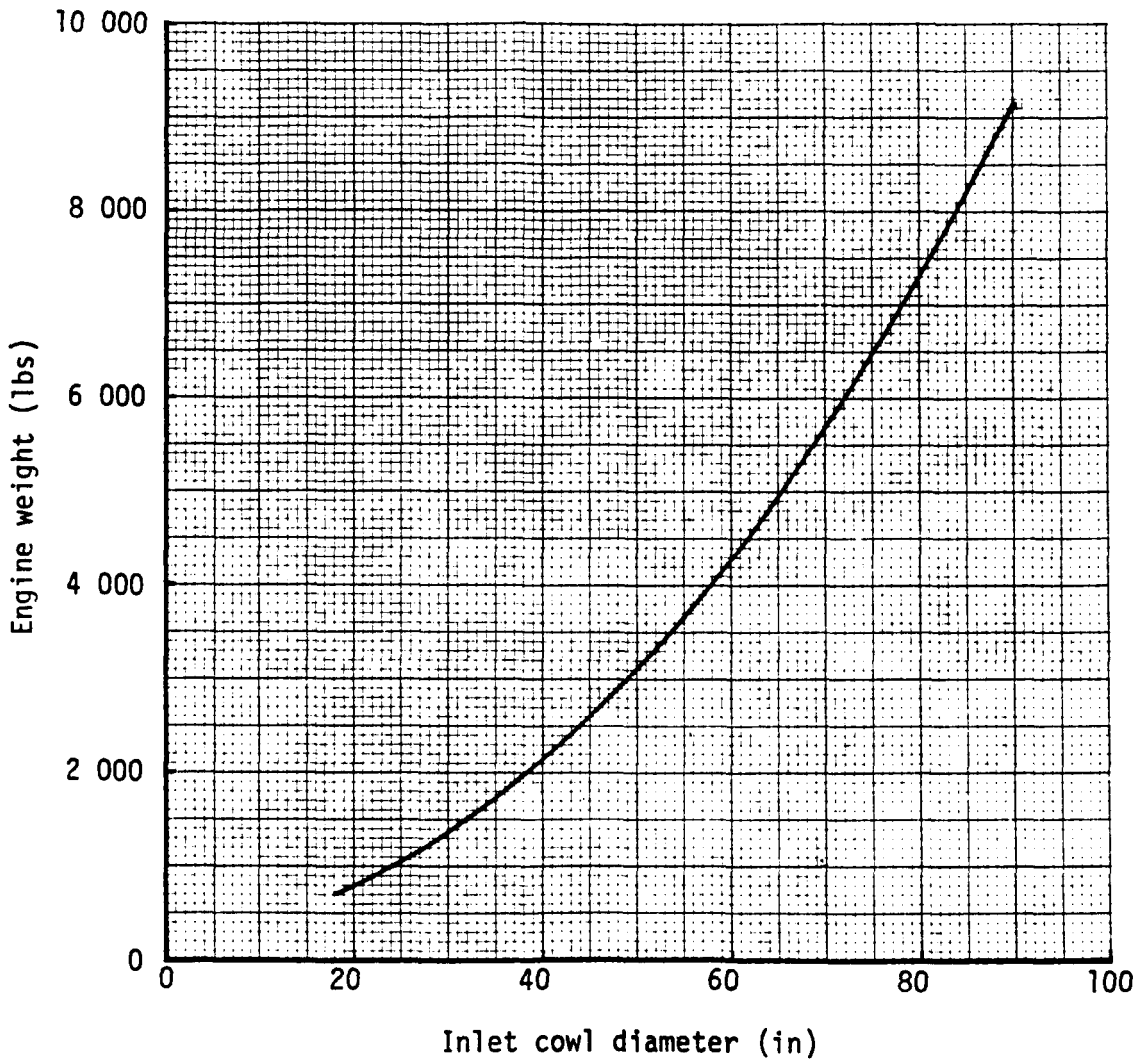

Figure 10. - Weight of duPont Jet Engine

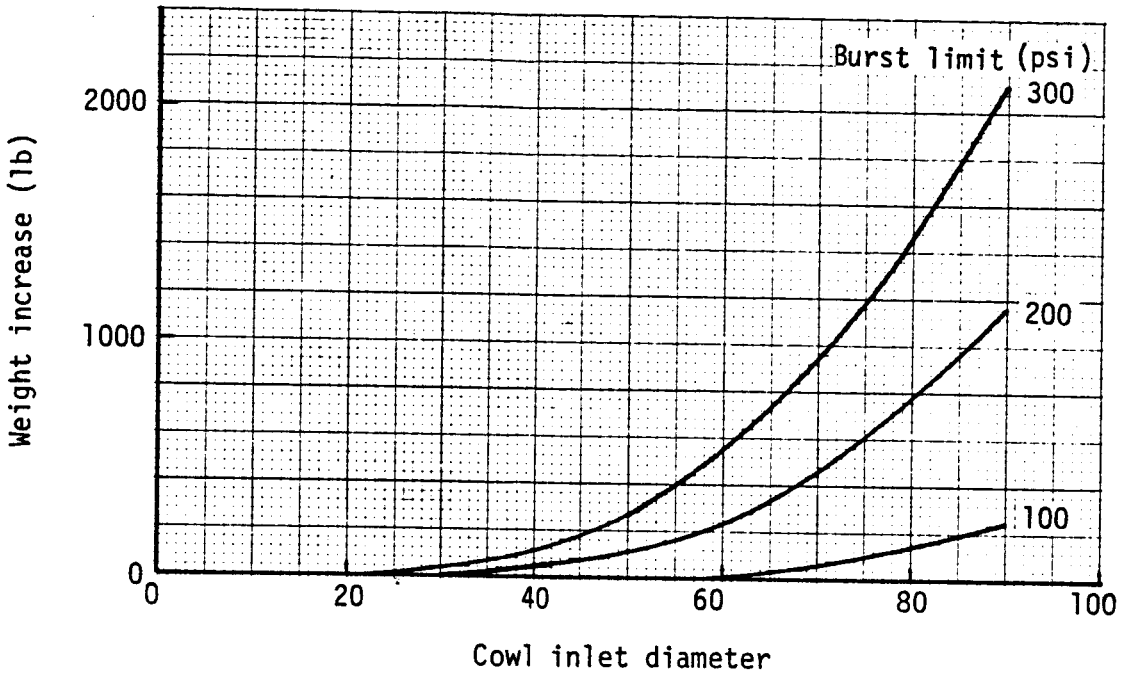

Figure 11. - Weight increase versus maximum combustor pressure - subsonic combustion mode

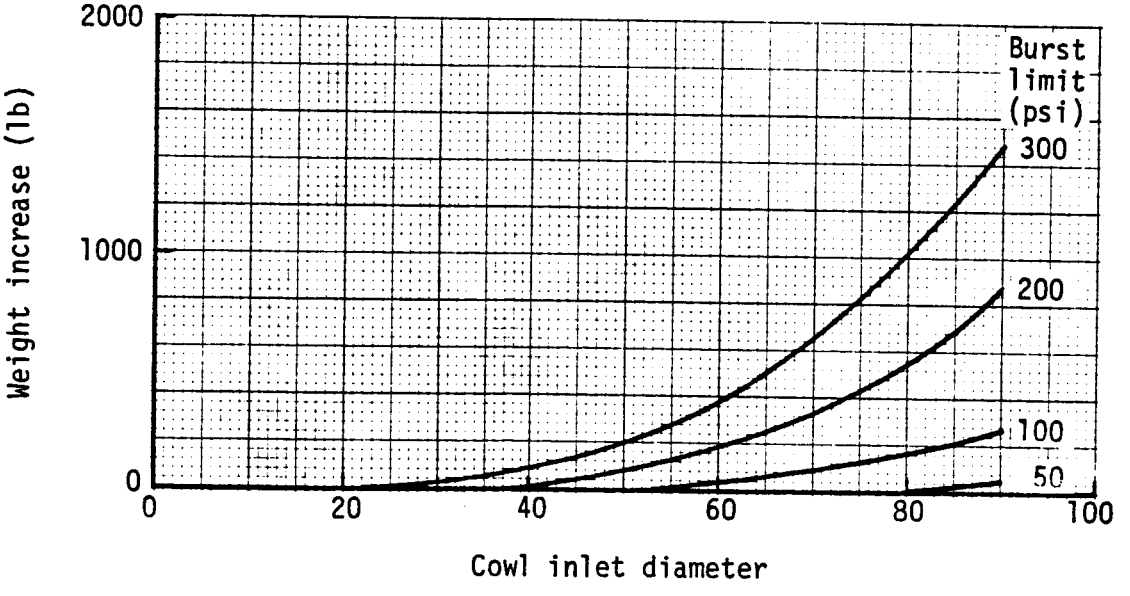

Figure 12. - Weight increase versus maximum combustor pressure - supersonic combustion mode

TABLE IV. - WEIGHT COMPARISON HYPERSONIC RESEARCH ENGINE VERSUS 18-INCH DIAMETER DUPONT JET ENGINE

Subassemblies	Hypersonic Research Engine				duPont Jet Engine			
	wetted area (ft^2)	subassembly weight (lbs)	shell only (lbs)	auxiliary structure (lbs)	wetted area (ft^2)	subassembly weight (lbs)	shell only (lbs)	auxiliary structure (lbs)
Spike, forward and aft	13.75	116	51	65	12.3	76	45	31
Inner shell	6.30	67	24	43	7.1	30	20	10
Innerbody nozzle	5.35	29	11	18	3.8	14	8	6
Outer cowl	24.19	212	94	118	13.5	95	67	28
Variable nozzle	---	---	---	---	7.1	53	37	16
Struts	1.05	22	5	17	1.2	24	6	18
SUBTOTAL, STRUCTURE	50.64	446	185	261	45.0	292	183	109
Ignition system		16				16		
Hydraulic actuation system		193				65		
Heat exchanger system		---				57		
Liquid hydrogen pump		30				30		
Liquid air pump		---				25		
Miscellaneous controls		84				84		
Miscellaneous plumbing		15				40		
SUBTOTAL, SYSTEMS		338				317		
Development margin 15%		---				91		
ENGINE TOTAL (FLIGHT WEIGHT)		784				700		
Research instrumentation		113						
Equipment aboard X15 and pylon		130						
Ablative cowl		66						
X15 INSTALLATION TOTAL		1093†						

†per AiResearch 7/17/68

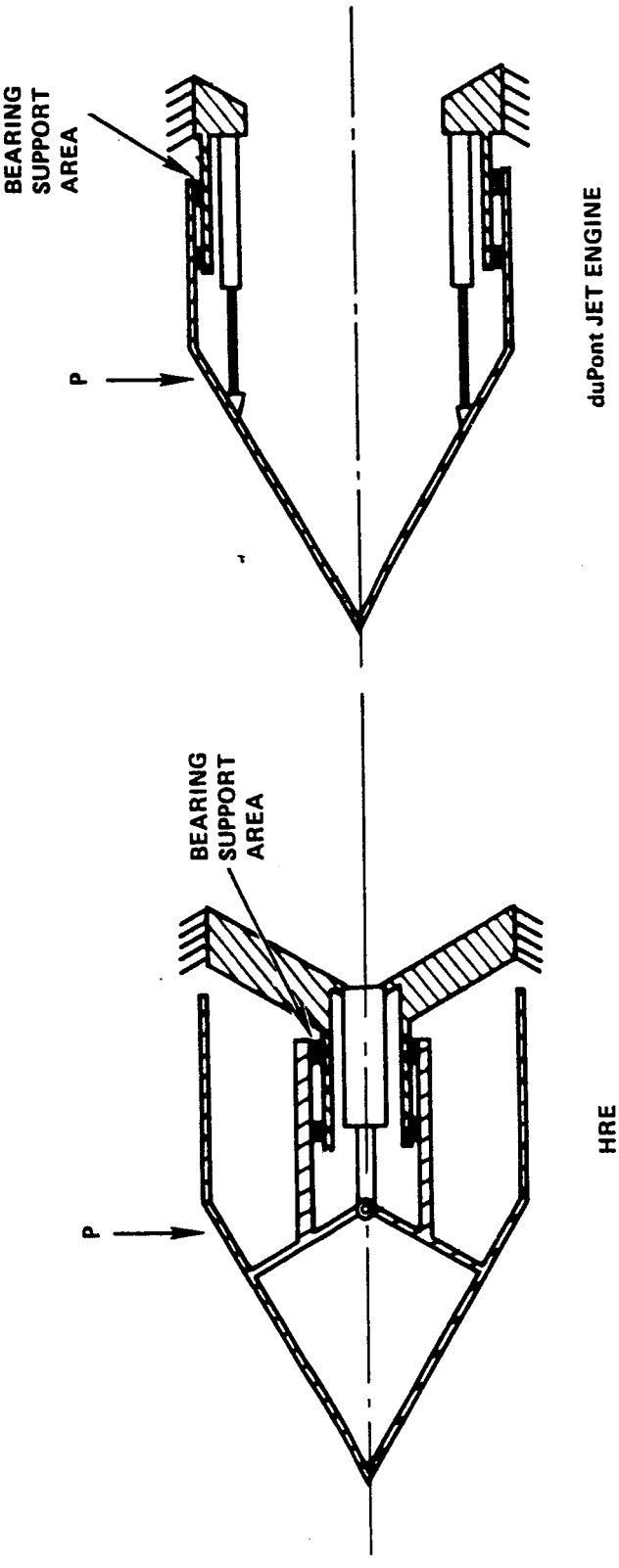

Figure 13. - Comparison of spike actuation systems - Hypersonic Research Engine and the duPont Jet Engine

Coolant and Fuel Manifolds

Most of the coolant and fuel manifolds on the HRE were designed to be integral with mating flanges and were half-round or quarter-round in cross-section. The duPont Jet Engine manifold rings are designed to take advantage of hoop stress by using circular cross-sections (only a few of the HRE manifolds were built in this manner). The cross-sectional shape of the HRE manifold ring requires larger thicknesses to resist flat plate bending that is four times the thickness requirement of the duPont Jet Engine manifold ring of equivalent cross-sectional area. In addition the perimeter of the manifold is larger on the HRE. In the areas where manifold rings were integral with mating flanges, weight penalties were incurred on the HRE because of leakage protection for bolts and lugs and difficulty in machining out between internal bosses and manifold walls. Separating the mating flanges from the manifolds in the duPont Jet Engine design not only allows lightweight flanges, shorter bolts and lightweight nuts, but also increases frequency of internal rings which act as stiffener rings for the shells in compression. Folded flow is used to route coolant to the joint where the flanges meet and to protect the flanges from aerodynamic heating. For the 18-inch diameter duPont Jet Engine the outer shell manifolds are designed to satisfy minimum height of the cowl. Fins and strips are used similar in design to the shell wall with the exception of larger fin heights and spacing. For the 90-inch diameter duPont Jet Engine, ganged manifolds with round cross-sections are used. The weight change per unit area of cowl follows a similar trend as the 18-inch to 90-inch engine weight per wetted area of subassemblies, therefore no significant weight change can be attributed to alternate cowl manifold configurations.

Heat Exchanger

The heat exchanger is unique to the duPont Jet Engine and is not comparable to the HRE. It is a rectangular plate and offset fin unit sized with 15% shutdown volume for de-icing and includes a 10% design margin. A sizing study produced a 14-inch length for the plate-fin heat exchanger core with the height and width both equal to 1.1 times the inlet cowl radius, R_C. The liquid air pump weight is derived from the J-2 rocket engine LOX pump weight. The water separator and the variable exhaust nozzle, which are not comparable to the HRE, include a 10% design margin and account for less than 17% of the engine weight.

The air in the heat exchanger makes a single pass from front to rear while the hydrogen makes several passes back and forth as it travels from the rear to the front using a mitered fin arrangement to make the turns inside the plate fin core. A half-round manifold is used to introduce the hydrogen to the core at the rear and to collect it at the front. Valves can shut off hydrogen to a section of the heat exchanger for de-icing the core. A second set of valves permits the air flowing through the section being de-iced to flow overboard.

DUPONT JET ENGINE PERFORMANCE

The purpose of this phase of the study was to define an engine by optimizing certain key parameters and areas in the range of flight conditions varying between sea level static and a free stream Mach number of 4 and then to obtain off-design performance over the same range. Three computer programs were developed for the performance study. The first computer program implemented the ejector analytical model in both the design-point and off-design modes. The second and third computer programs implemented the engine analytical performance model in the design-point and off-design modes, respectively. The engine was defined from a sizing study using the design-point performance programs. Then the performance of the engine was determined using the off-design performance program.

Sizing Studies

The effect of total temperature, T_t', and pressure, p_t', in the primary air system on the ratio of inlet throat to secondary stream total pressures, p_{t2}/p_t'', was determined by varying either the temperature or pressure while holding the other constant. The total engine fuel flow and equivalence ratio were held constant at W_{ft} = 1 lbm/sec and ϕ_t = 1 for this study so that the geometry of the mixing duct was completely variable. The effect of primary total temperature on the mixed pressure ratio is shown in Figure 14 over the range of free stream conditions and at a ratio of primary to secondary total pressures equal to 40. At sea-level-static conditions, the mixed pressure ratio was maximum for a primary total temperature of approximately 1800°R. The maximum permissible temperature in the regeneratively-cooled engine structures was also 1800°R. The effect of primary total pressure ratio on mixed pressure ratio at a primary total temperature equal to 1800°R is presented in Figure 15. The mixed pressure ratio continually increased over the range of primary total pressure ratios from 10 to 80 so that the selection of the optimum primary total pressure ratio resulted from other considerations. A primary total pressure ratio of 40 was chosen as a compromise between ejector performance, primary air system weight and part-power off-design performance with a fixed primary nozzle throat area.

Using a primary stream total temperature of 1800°R and a primary pressure 40 times the secondary total pressure, design-point performance was obtained for equivalence ratios of 0.5, 1.0, 1.5 and 2.0 over the desired range of free stream conditions. No skin friction or primary injection nozzle losses were included in order to make the trends more apparent. The analysis always obtained maximum theoretical (i.e. minimum area) flow at the injection station and used constant pressure mixing. The inlet throat area was assumed equal to

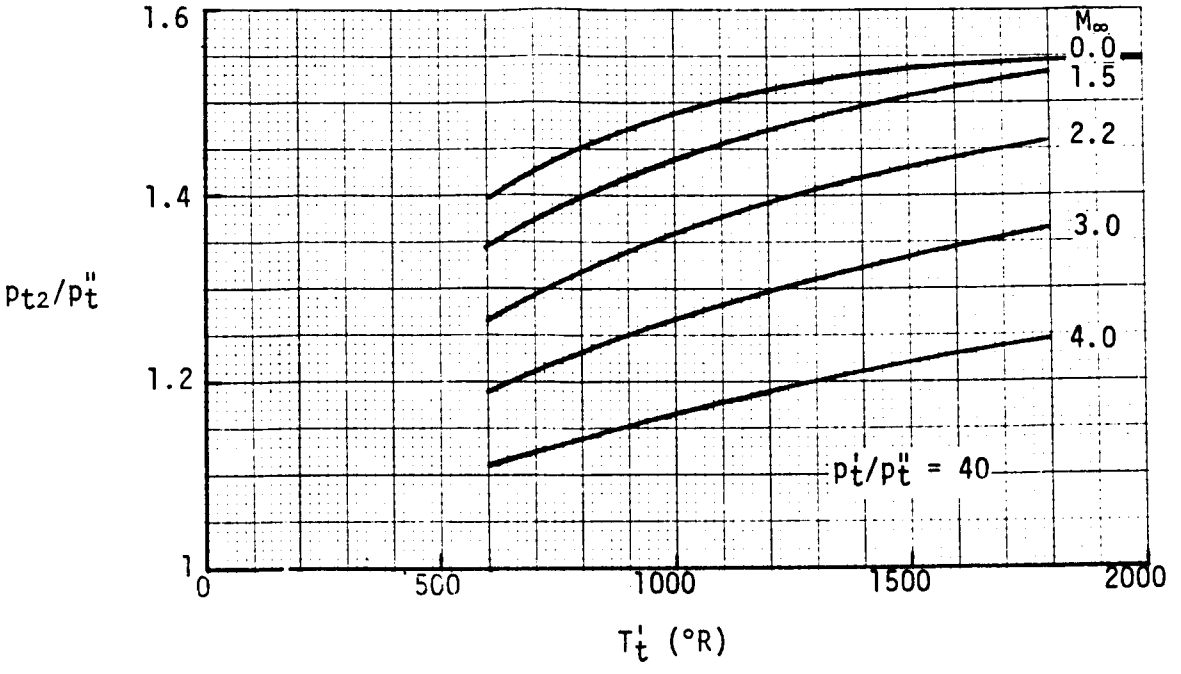

Figure 14. - Effect of primary total temperature on mixed total pressure

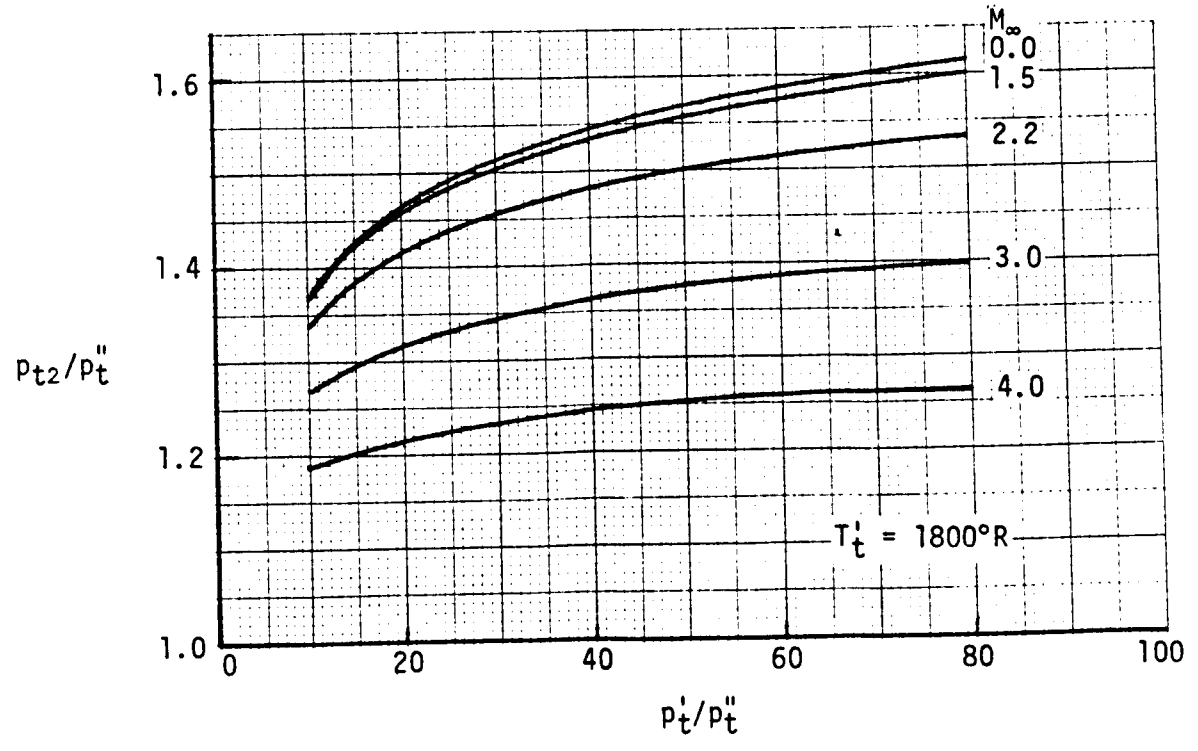

Figure 15. - Effect of primary total pressure on mixed total pressure

the Kantrowitz area in each case so that the velocity at the inlet throat was always sonic. The combustor and exit nozzle throat areas were continually adjusted to match the inlet flow. The ratio of choked inlet throat area to choked exit nozzle area was determined for each case as shown in Figure 16 where the curves illustrate the problem of matching a fixed nozzle throat area.

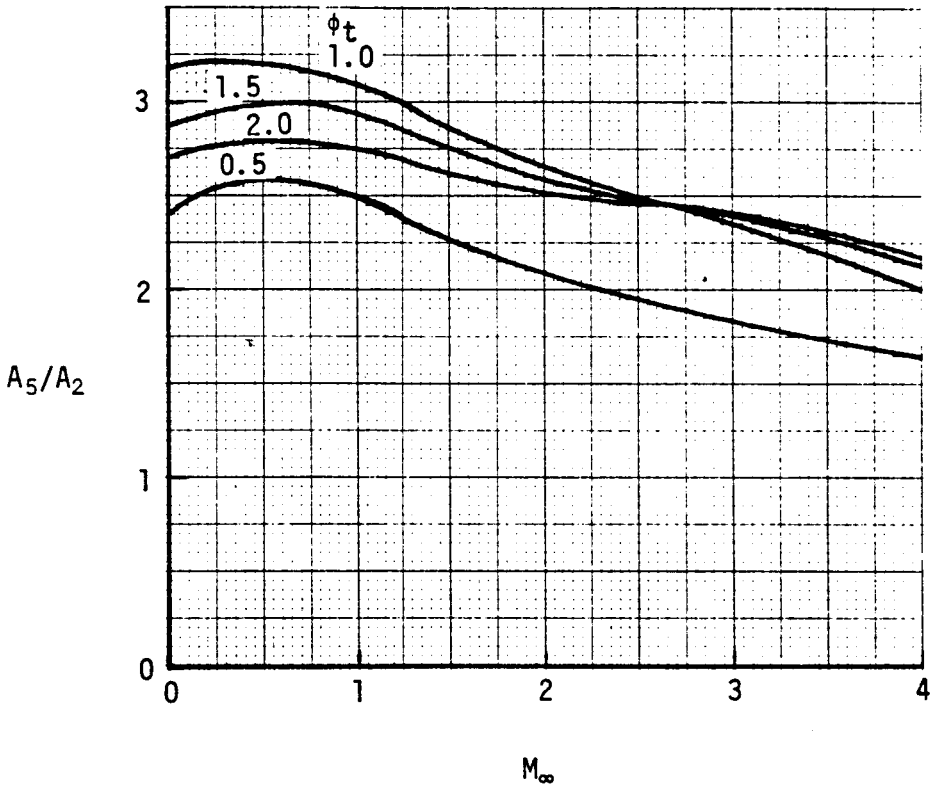

Figure 16. - Ratio of nozzle to inlet throat areas versus M_∞ and ϕ_t

At low speeds a fixed nozzle that will not pass all the flow supplied by the inlet requires the flow to be limited either by reducing the inlet throat area or by reducing the throat Mach number. The former will maintain the engine pressure ratio; the latter, which is the only possibility in a completely fixed geometry engine, will reduce the mixed pressure ratio as illustrated by Figure 17. At the high Mach numbers the fixed nozzle throat will require a loss in total pressure between the inlet and nozzle throat greater than the normal combustor loss. This loss is accomplished by a choked inlet throat and acceleration to supersonic speeds in the diffuser followed by a normal shock.

Since the mismatch between a fixed nozzle throat and a fixed inlet throat is caused by a difference in inlet total temperature with flight Mach number, an examination was made into the possibility of varying the primary stream total temperature to achieve a match. As Figures 18 and 19 illustrate, this method

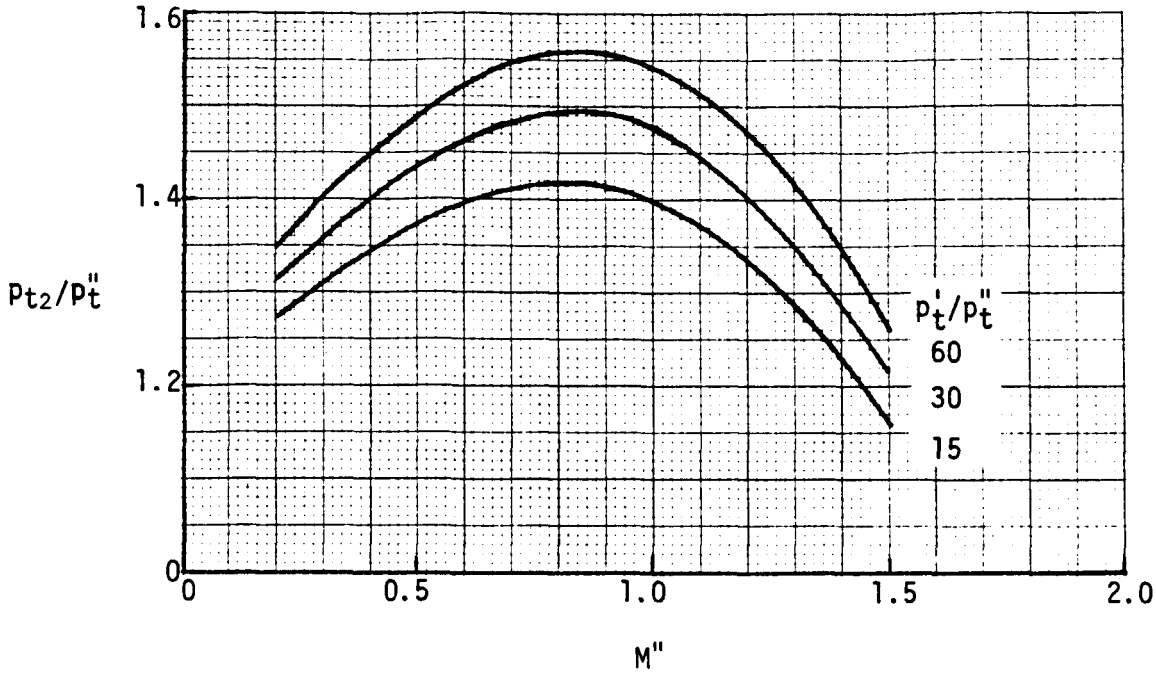

Figure 17. - Mixed pressure ratio versus secondary stream Mach number

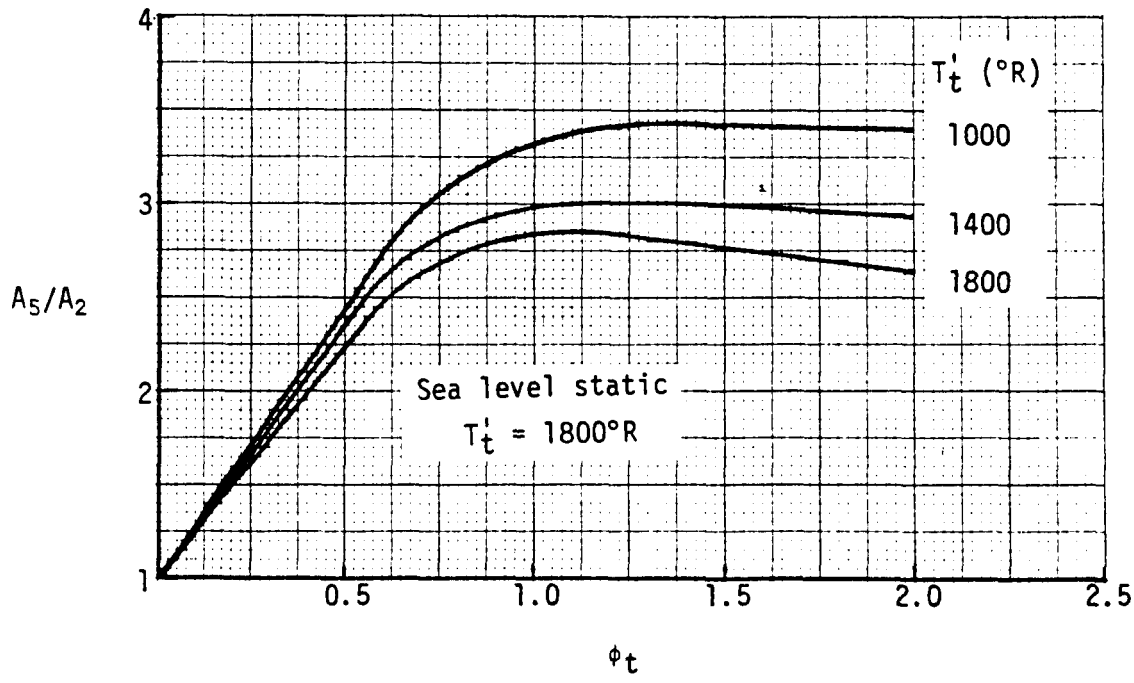

Figure 18. - Ratio of nozzle to inlet throat area - M_∞ = 1.5

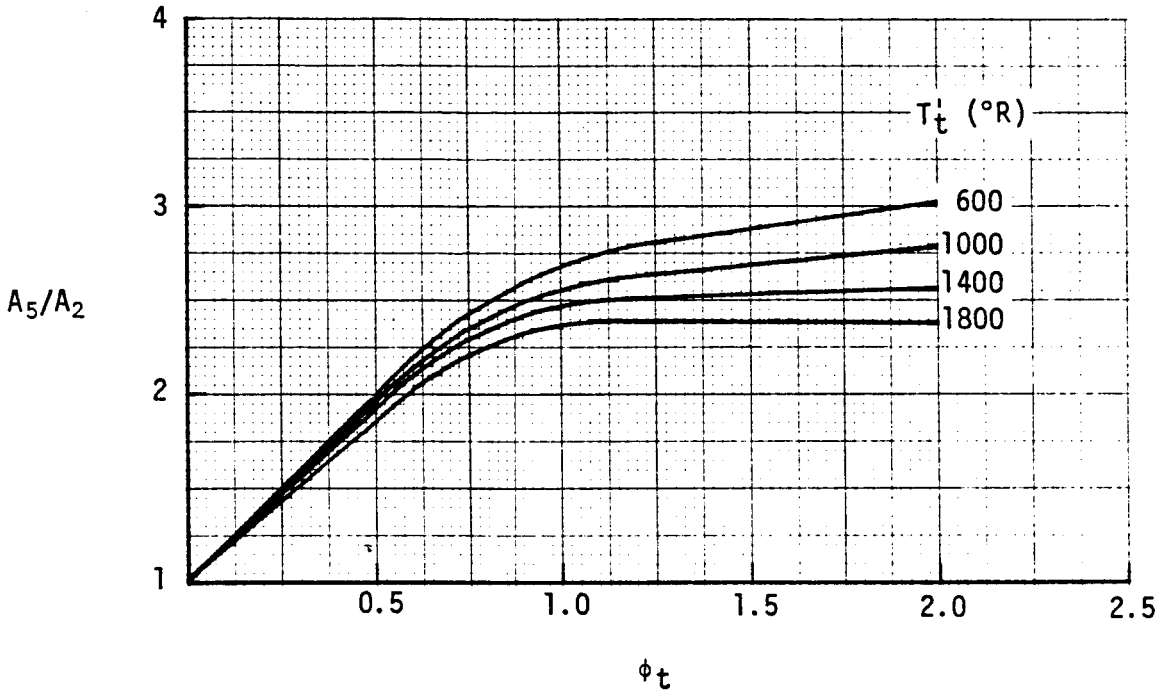

Figure 19. - Ratio of nozzle to inlet throat area - M_∞ = 3.0

was not too successful in that the 1800°R limit on T_t' would not reduce the area ratio required at M_∞ = 1.5 to that required at M_∞ = 3 even with T_t' as low as 600°R, and there was still a large variation with equivalence ratio to be dealt with. The variable inlet throat area mode of operation was selected as the most practical solution. A variable geometry inlet is already included in the axisymmetric engine used as a baseline for the weight analysis. The variation in geometry permits attaining the optimum contraction ratios for supersonic combustion ramjet operation, low-speed operation and inlet starting, and enables inlet closure.

The minimum ratio of nozzle to inlet throat area selected for off-design study is 2.3 corresponding to $A_{2max} = 0.25A_C$ and $A_5 = 0.575A_C$. This value is close to that used on the HRE and will permit subsonic combustion operation to nearly Mach 6 at which point the normal shock will be positioned at the exit of the diffuser so that a transition to supersonic combustion is necessary for operation at higher speeds. A larger value of the nozzle throat area would increase low-speed thrust, but would also decrease the transitional Mach number for supersonic combustion and cause higher losses in the region between Mach 2 and the transition. Optimization of the fixed throat area involves a very detailed analysis of the effect of engine changes on aircraft performance and is considered beyond the scope of this contract. The maximum potential increase in low-speed thrust made possible with a variable nozzle throat is shown in Figure 20. The thrust is proportional to nozzle throat area up to the maximum shown in Figure 20.

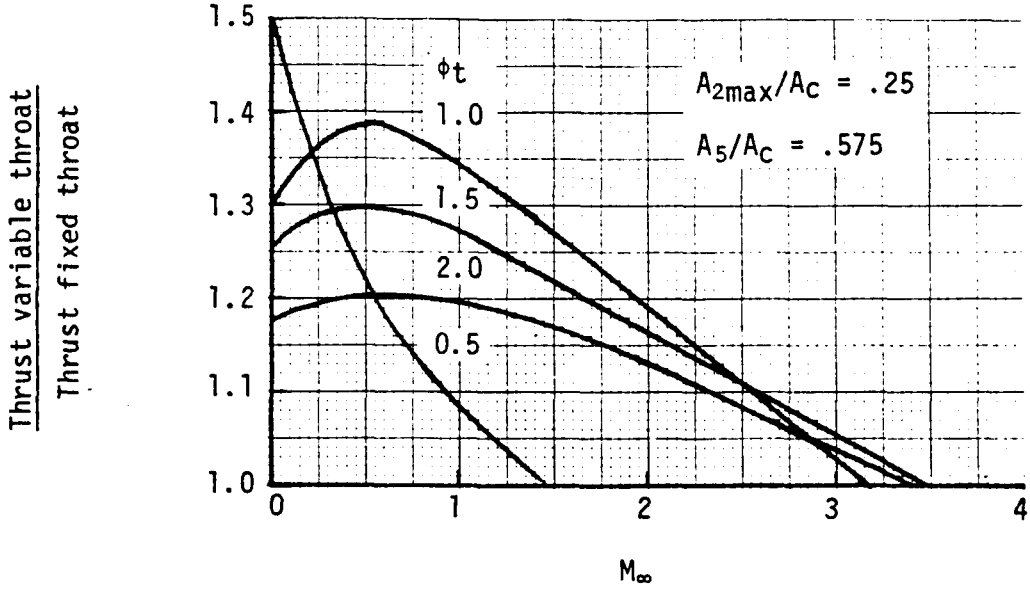

Figure 20. - Effect of variable exit nozzle throat area

Off-Design Performance

All of the off-design performance is based on the assumption that the engine is completely submerged in a pressure field resulting from that angle of attack which corresponds to a 2.5 degree wedge. The pressure recovery of the unstarted inlet is based on conditions downstream of a normal shock ahead of the inlet cowl as shown in the lower curve in Figure 21. A schedule of inlet throat areas slightly larger than those generated by the sizing study was used in order to reduce the subsonic diffusion losses. The friction loss between any two engine stations is obtained from the skin friction coefficient, the wall surface area and the arithmetic average of the dynamic pressures at the stations. The dynamic pressure at the end of the accommodation region is obtained by mass averaging the dynamic pressures in the primary and secondary streams. The nozzle exit area is variable so that the flow always expands (or diffuses) to the static pressure in the pressure field. The engine specifications for the off-design study are tabulated in Table V.

The engine specific impulse as a function of free stream Mach number and equivalence ratio is presented in Figure 22. The decrease in specific impulse demonstrates the effect of increased losses from the normal shock inlet pressure recovery past about Mach 2, however, the abrupt decrease in performance at the lower equivalence ratio is due to losses from shock in the diffuser. With a started inlet, the specific impulse would level off or increase to Mach 4. The almost constant specific impulse independent of equivalence ratio at sea-level-static conditions is the result of increasing engine pressure ratio with

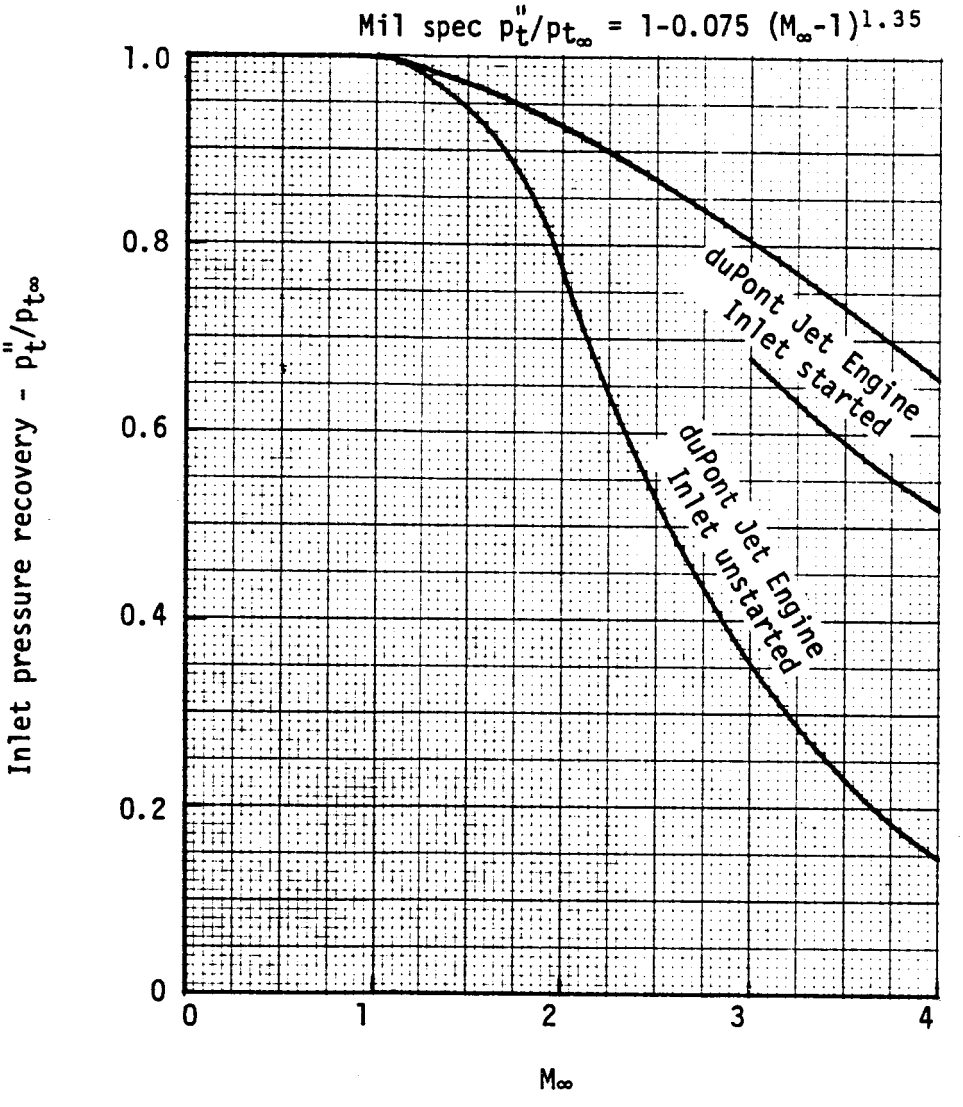

Figure 21. - Inlet pressure recovery

TABLE V

ENGINE SPECIFICATIONS†

Engine area	Value	Engine parameter	Value
A_0/A_c	variable	$C_{f_{12}}$	0.003
A_*'/A_c	0.00185	$C_{f_{23}}$	0.003
A_2/A_c	0.25 (max)	$C_{f_{34}}$	0.003
A_2/A_1	0.925	C_v'	0.980
A_3/A_c	0.69	C_v	0.984
A_4/A_c	0.69	T_t'	1800°R
A_5/A_c	0.575	δ	2.5°
A_6/A_c	variable	β'	20°
A_{w12}/A_c	5.507	η'	0.950
A_{w23}/A_c	4.0	η_4	0.950
A_{w34}/A_c	4.0		

†Double numerical subscripts denote that area or parameter was applied between the stations designated by the numerals.

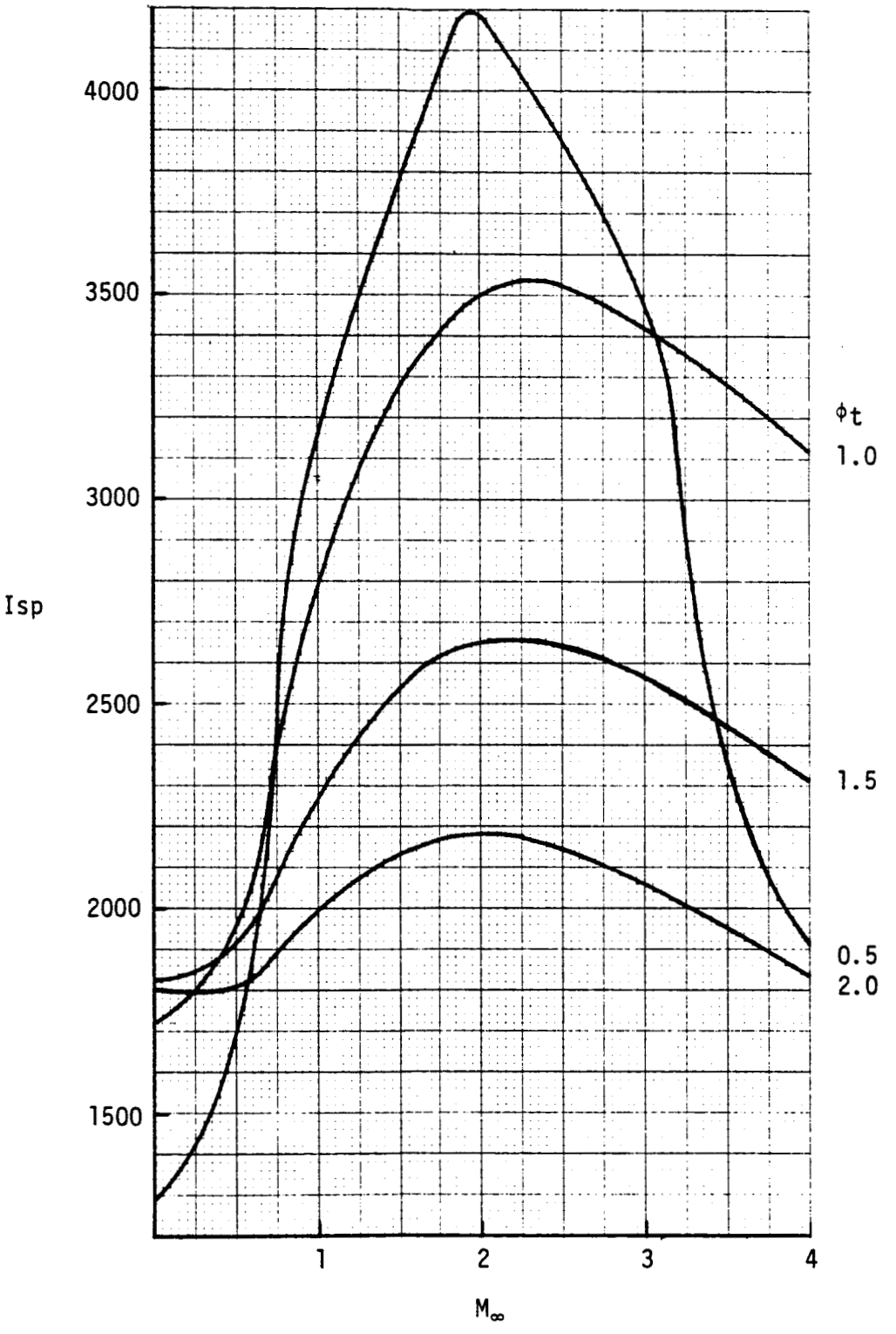

Figure 22. - Specific impulse versus flight Mach number

equivalence ratio which tends to offset that portion of the fuel that is not contributing to combustion during fuel-rich operation. At higher Mach numbers where the ram static pressure rise is added to the total pressure rise due to injection of the primary stream, performance demonstrates a more typical spread with equivalence ratio, although fuel-rich performance still is relatively superior due to increased engine pressure ratio. Above Mach 3 engine performance is degraded slightly from design-point values because a normal shock in the subsonic diffuser has to be used to match the fixed exit nozzle throat. At an equivalence ratio of 0.5, the normal shock required for matching starts to degrade performance near Mach 2 and is responsible for the lean specific impulse becoming lower than the stoichiometric and fuel-rich values between Mach 3 and 4.

The engine thrust coefficient as a function of free stream Mach number and equivalence ratio is shown in Figure 23. The large increases in thrust with increasing equivalence ratio results from increased engine airflow due to a higher engine pressure ratio. The improvement in thrust from equivalence ratios greater than unity is also due to the secondary effects of additional fuel mass flow and lower molecular weight of the exhaust gases. The change in thrust coefficient with equivalence ratio demonstrates how fuel-rich operation increases effective specific impulse even though the basic engine specific impulse is reduced. The increase in transonic thrust is impressive: however, at higher free stream Mach numbers the increase in thrust with equivalence ratio is less pronounced. The sea-level-static thrust is presented separately in Figure 24 since the thrust coefficient becomes infinite at zero forward speed. The increase of thrust with increasing equivalence ratio is evident. The value of equivalence ratio selected for takeoff thrust on an engine sizing basis coincides closely with the value that gives optimum specific impulse. The engine mass flow and expansion nozzle area curves in Figures 25 and 26, respectively, are presented so that installed performance can be computed using experimental data on spillage and boattail drag. The necessity for variable nozzle exit area is apparent from examination of Figure 26.

The potential advantage of the duPont Jet Engine cycle is that it provides takeoff and static thrust to a ramjet without adding too much weight and without compromising the ramjet geometry and therefore the high Mach number fuel consumption. Fuel consumption statically and at low Mach numbers is greater than some turbine engine cycles, but the increased thrust and lower engine weight can potentially compensate for this greater fuel consumption. The typical hypersonic aircraft is more sensitive to the engine fuel consumption at high Mach numbers than to static and low-speed fuel consumption.

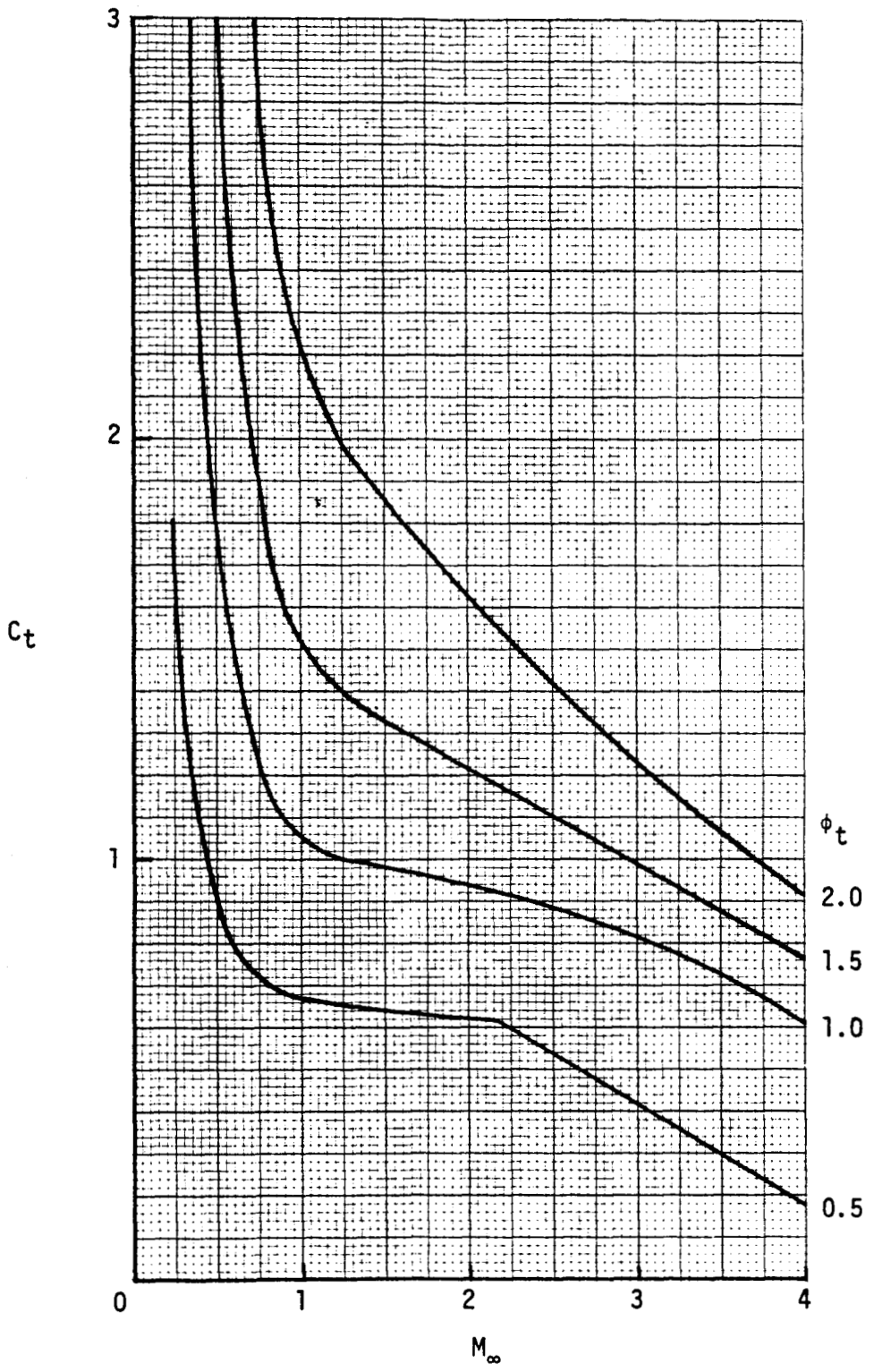

Figure 23. - Thrust coefficient versus flight Mach number

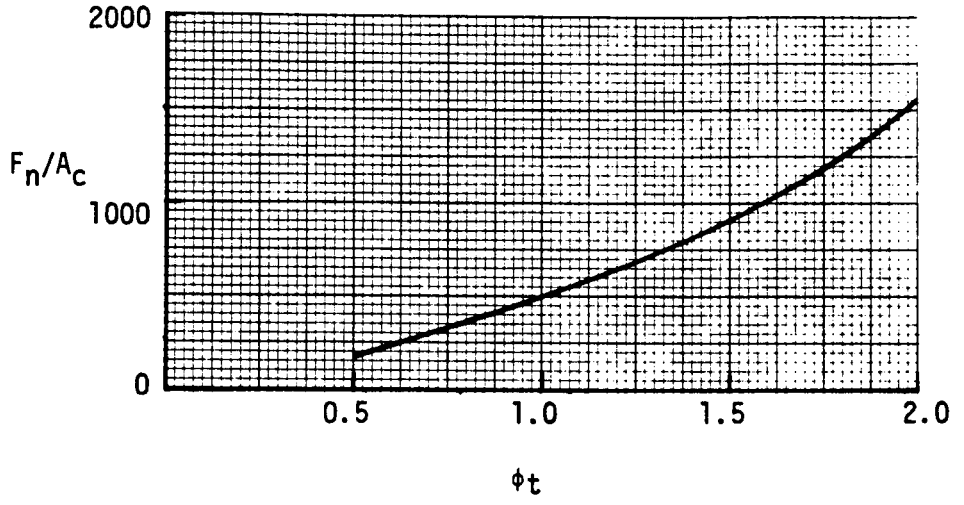

Figure 24. - Takeoff thrust versus equivalence ratio

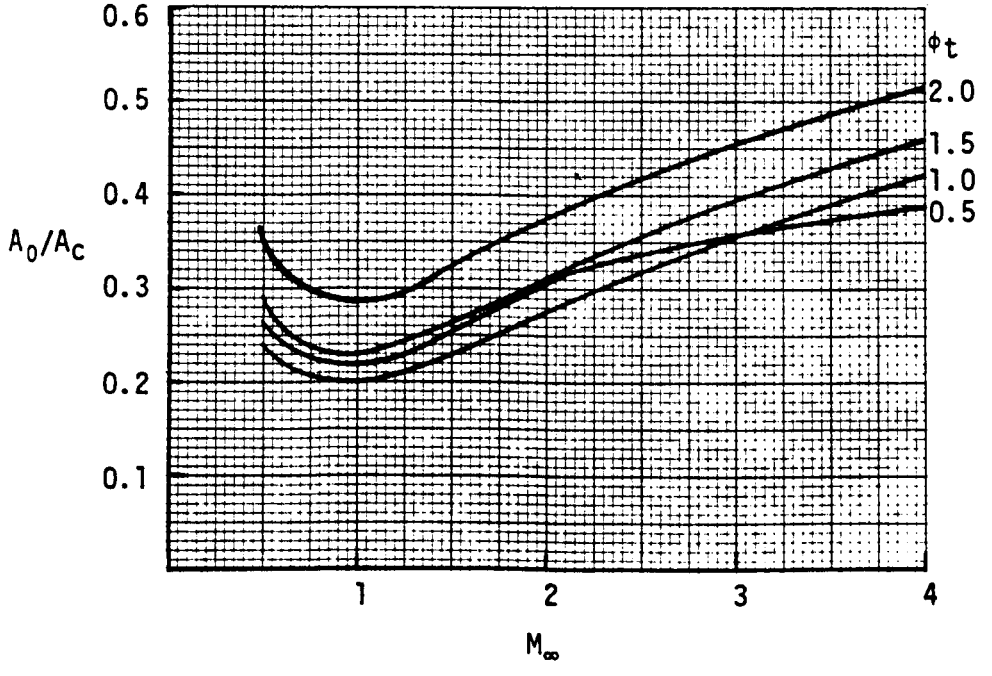

Figure 25. - Inlet mass flow ratio versus flight Mach number

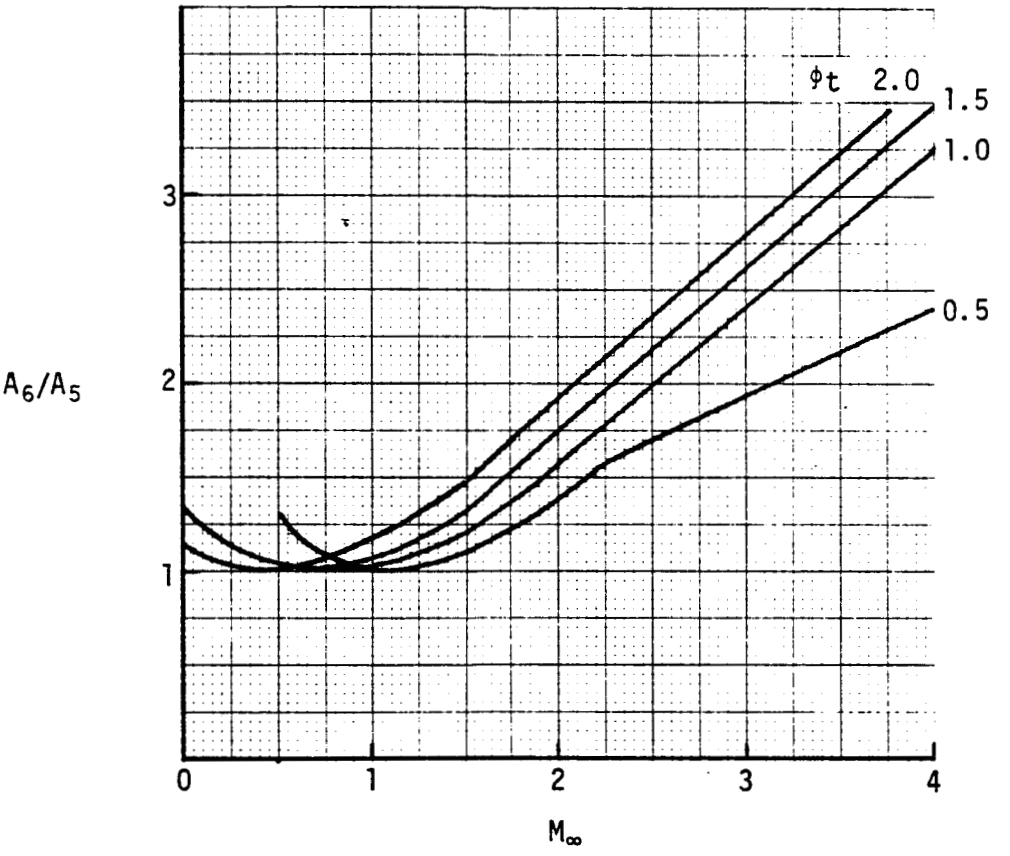

Figure 26. - Nozzle exit area/nozzle throat area versus flight Mach number

ENGINE COMPARISON

The duPont Jet Engine was compared to four other engines: a stoichiometric turbojet, a wraparound or combined turbojet-ramjet, the Supercharged Ejector Ramjet (SERJ) and the SCRAMLACE engine. In addition, the axisymmetric embodiment of the duPont Jet Engine was compared to two other possible configurations: a two-dimensional engine with variable inlet ramps and a fixed geometry configuration such as the Langley three-dimensional engine. The comparisons show the duPont Jet Engine to be greatly superior to all the other engines with respect to weight, and superior or competitive with respect to fuel consumed between sea-level-static conditions and Mach 4 flight. In the configuration comparison, the installed ramjet performance for acceleration is best for the variable ramp two-dimensional inlet, intermediate for the axisymmetric pod, and worst for a fixed geometry integrated engine. On the other hand for design-point cruise fuel consumption, the two-dimensional variable geometry inlet and the fixed geometry engine are potentially better than the axisymmetric pod because these configurations can eliminate the pod drag and use the vehicle surface for additional nozzle expansion. With respect to weight, the axisymmetric pod is the lightest and the two-dimensional variable geometry engine is the heaviest. When the trade-off of weight, pod drag and performance are considered in typical airplane applications, the podded engine is superior or competitive in every case.

Engine and Airplane Data

Engine data were obtained primarily from Reference 7. Data on the stoichiometric turbojet and wraparound turboramjet are proprietary to Pratt & Whitney Aircraft so that the weights and performance of these engines had to be approximated. A common basis for comparison was obtained by scaling the SERJ and SCRAMLACE engines to 44.2 square feet of cowl area equivalent to a 90-inch cowl diameter duPont Jet Engine. The turboramjet was sized to 44.2 square feet of cowl area and 50 000 pounds of sea-level-static thrust so that it is exactly the same at takeoff and during ramjet operation as the 90-inch cowl diameter duPont Jet Engine at these conditions. For weight purposes the stoichiometric turbojet and the wraparound turboramjet are considered to be the same engine. For performance purposes the stoichiometric turbojet is operated alone and the wraparound turboramjet employs both turbojet and ramjet operation.

The engine fuel consumption during climb and acceleration to Mach 4 was evaluated by computing effective specific impulse, [(thrust - drag)/fuel flow]. The drag was obtained from the wind tunnel tests of the NASA HT-4 configuration reported in Reference 8. The drag was corrected for full-scale skin friction using the method of Reference 9. An increment of engine drag obtained from

Reference 7 was added to the basic airplane drag. This increment included spillage drag, cowl drag, and inlet bleed drag. Four basic engines were installed for a total of 177 square feet of reference cowl area. The airplane was 330 feet in length and had a takeoff weight of 700 000 pounds. The airplane was flown over the trajectory shown in Figure 27. The airplane

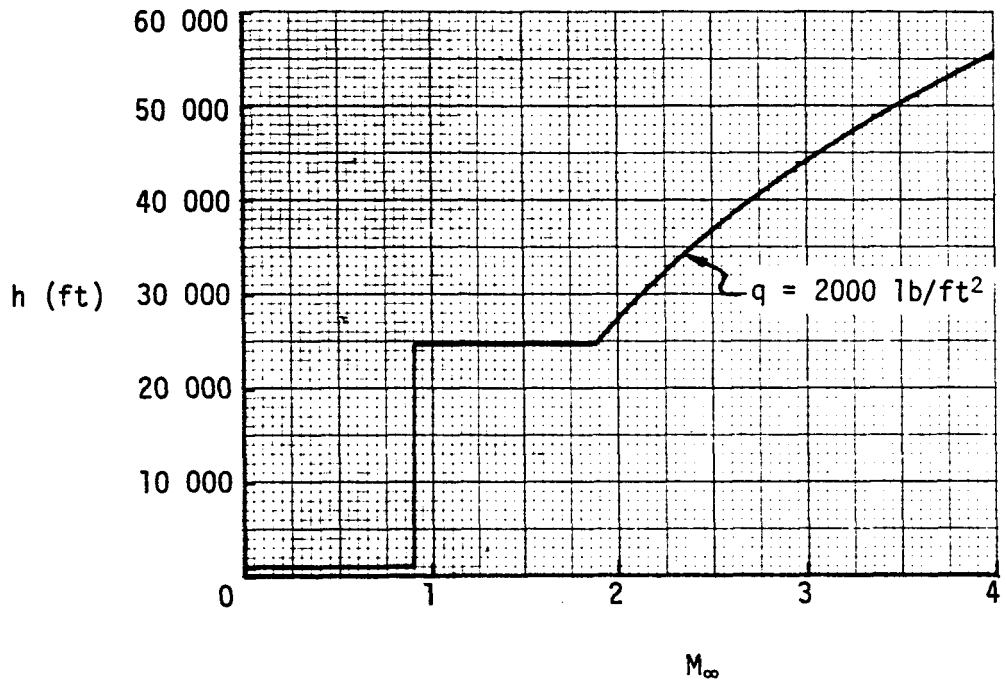

Figure 27. - Acceleration flight path

accelerated at sea level to Mach 0.9, climbed at Mach 0.9 to 25 000 feet, accelerated in level flight to Mach 1.9 and followed a dynamic pressure trajectory of 2000 pounds per square foot to Mach 4 at an altitude of 56 500 feet. The reference drag levels of the HT-4 with and without the Marquardt two-dimensional engine with variable inlet geometry and bleed were obtained from References 7 and 8. These reference drag levels are presented in Figure 28.

Performance

The thrust of the five basic engines is compared to the reference drag level in Figure 28 over the trajectory defined in Figure 27. The results of this comparison between SERJ, SCRAMLACE and the duPont Jet Engine are shown in Figure 29. The SERJ engine converts from the ejector to the fan-ramjet mode at the points on the reference trajectory where the effective specific impulse

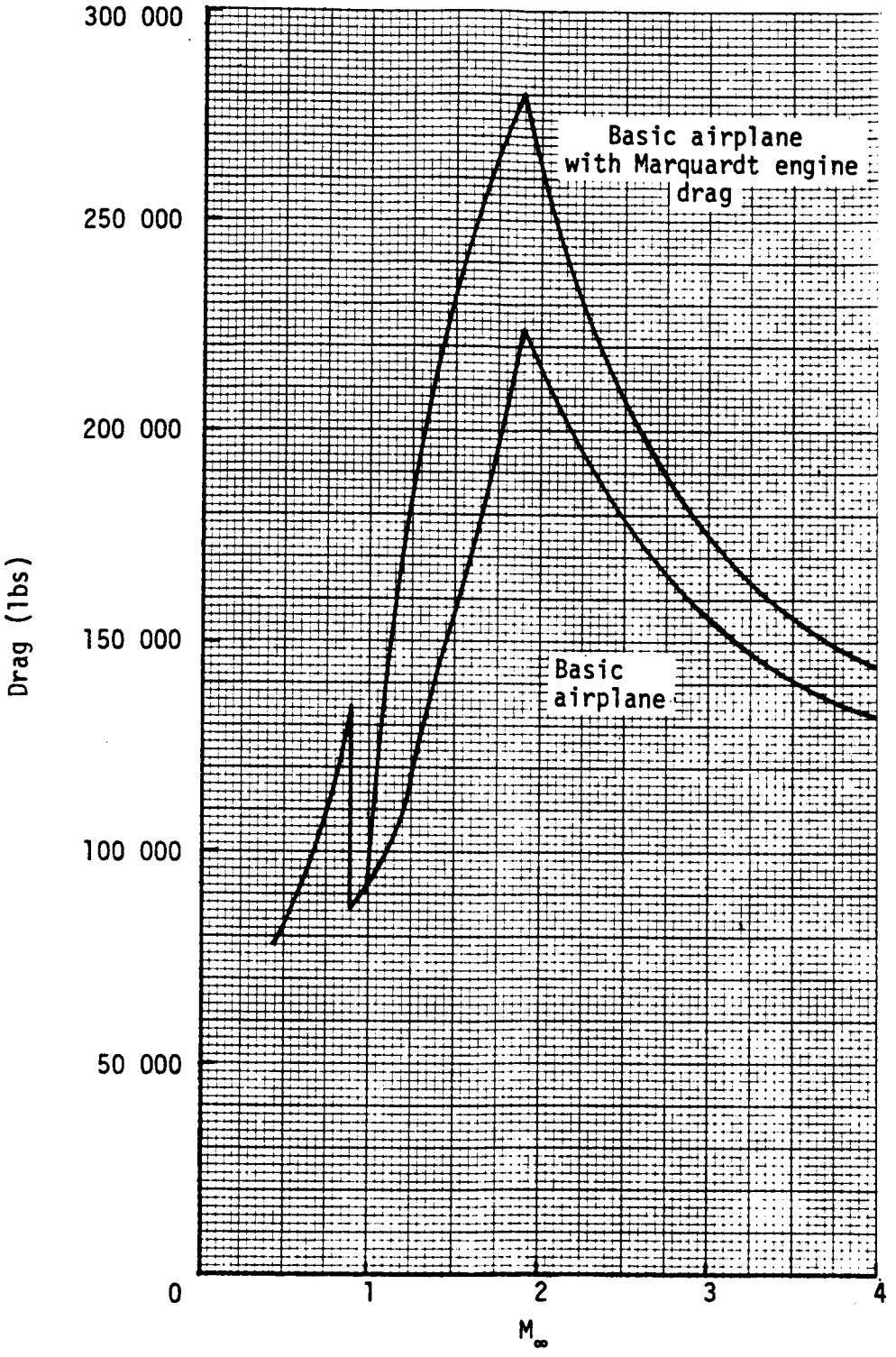

Figure 28. - Drag of HT-4 airplane

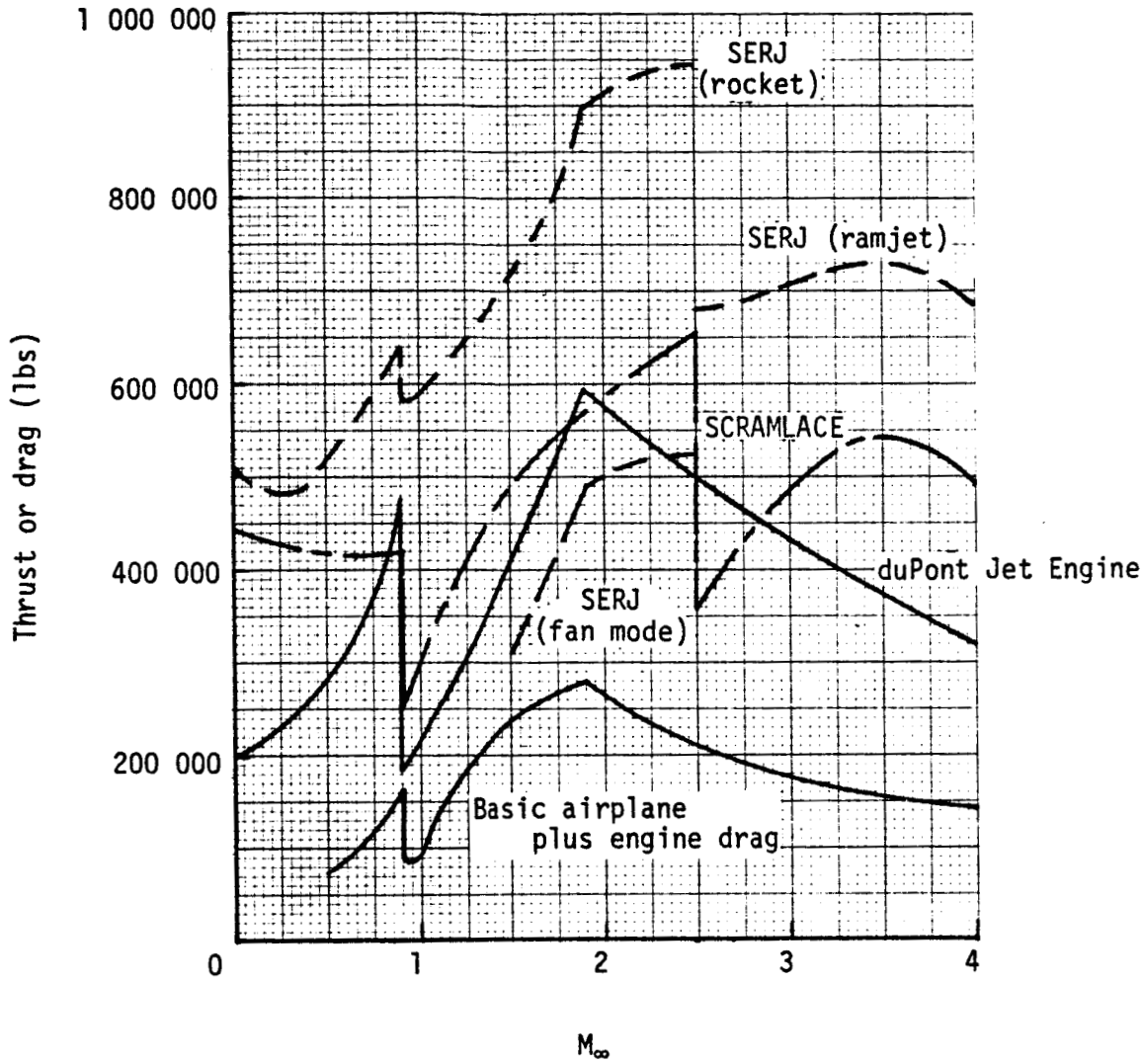

Figure 29. - Thrust of SERJ, SCRAMLACE and duPont Jet Engine

of the two modes is equal. The transition of both the SERJ engine from the fan-ramjet to the pure ramjet mode and the SCRAMLACE from the ejector to the ramjet mode is based on the same criterion. The SERJ and SCRAMLACE demonstrate a much higher takeoff thrust than the duPont Jet Engine under the sizing rules adopted. Transonically, the SCRAMLACE thrust is comparable to the duPont Jet Engine. The SERJ has more thrust in the low specific impulse rocket mode and less in the high specific impulse fan-ramjet mode. When the inlet of the duPont Jet Engine is started, its thrust is similar to that of the other two engines. The results of the comparison between a turbojet, a wrap-around turboramjet and the duPont Jet Engine are shown in Figure 30. It is evident from this comparison that the turbojet produces insufficient thrust to overcome the reference drag levels beyond the transonic range and that the

thrust of the duPont Jet Engine exceeds that of either of the other two engines over the critical transonic speed range.

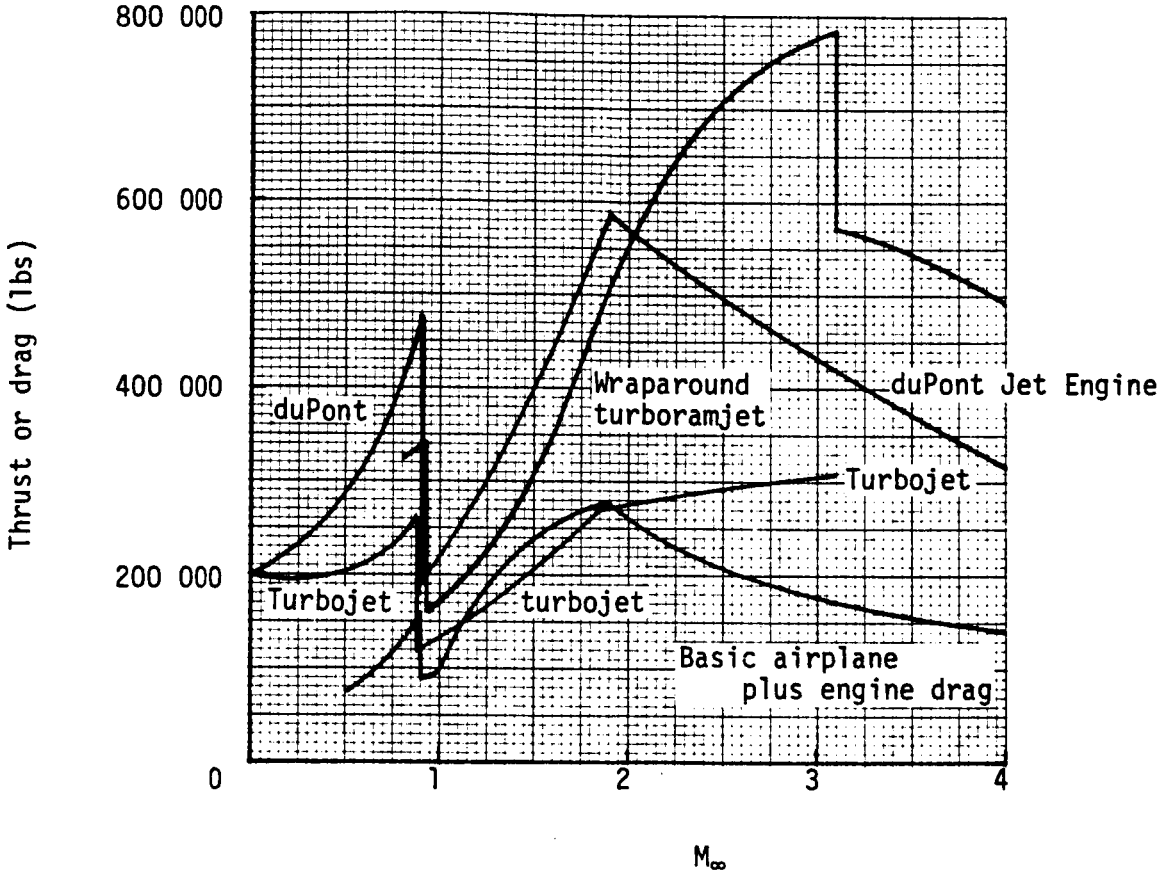

Figure 30. - Thrust of turbojet, wraparound turboramjet and duPont Jet Engine

Comparisons of effective specific impulse are presented in Figures 31 and 32. Fuel consumed during acceleration to Mach 4 is related approximately to the minimum value of this parameter. The duPont Jet Engine is clearly superior to both the SERJ and SCRAMLACE. Both of these engines produce relatively larger static thrust under the sizing rules adopted so that the possibility of improving effective specific impulse by sizing the engines to produce more low-speed thrust does not exist. A proportional increase in low-speed thrust of the three engines would increase the duPont Jet Engine's margin of superiority. On the other hand the position of the turboramjet can be improved by relatively small increases in turbojet size. Figure 33 shows the effective specific impulse at Mach 1.2 and 1.5 as a function of sea-level-static turbojet thrust. If the turbojet were sized large enough, it could have the best fuel consumption of all the engines because it has the highest basic engine specific impulse. However, the weight penalties to improve the thrust are great enough

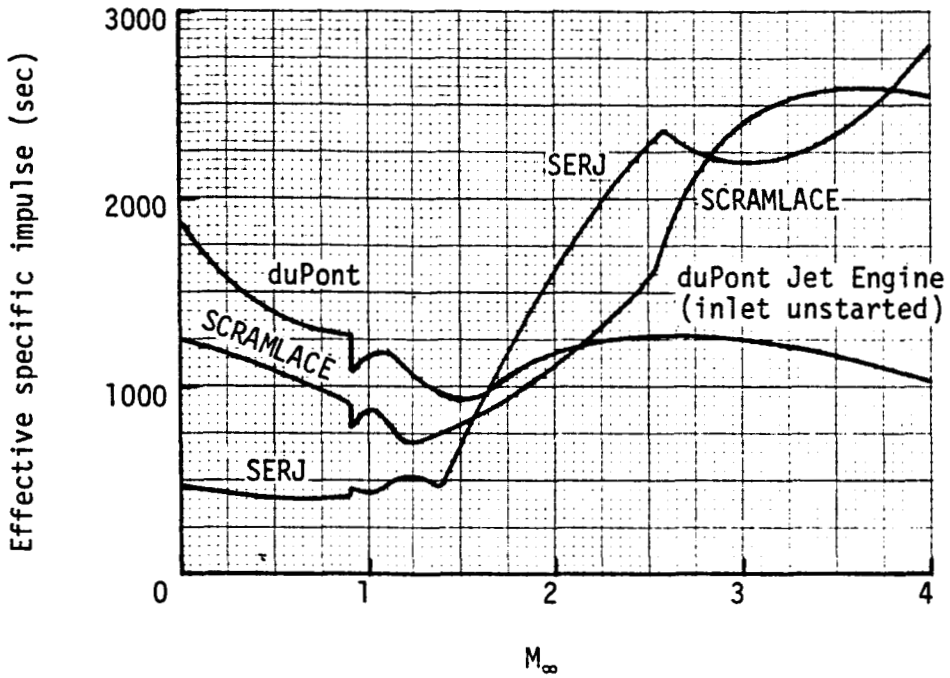

Figure 31. - Effective specific impulse of SERJ, SCRAMLACE and duPont Jet Engine

to limit optimum engine sizes to values that give an effective specific impulse similar to the duPont Jet Engine. Therefore from a fuel consumption standpoint the duPont Jet Engine must be classed as competitive to a wraparound turboramjet but not as clearly superior as it was to SERJ and SCRAMLACE.

In the range from Mach 2 to 4 in Figures 31 and 32, the effective specific impulse of the duPont Jet Engine is presented operating in the ejector mode with an unstarted inlet (normal shock pressure recovery) but not as a pure ramjet with a started inlet. The other engines are assumed to operate with started inlets with Mil Spec pressure recovery (see Figure 21). When the duPont Jet Engine inlet is started, its performance in this speed range is similar to the other engines. The engine pressure ratio increase due either to injection or to rotating turbomachinery has progressively less effect on the engine cycle performance with increasing free stream Mach number. In the case of the duPont Jet Engine used in this example, the fixed nozzle throat area eliminates any significant advantage from air injection with a started inlet. This engine therefore operates as a pure ramjet after the inlet is started as do the SERJ and SCRAMLACE. In order to match the nozzle of the turboramjet, the turbojet is operated to as high a Mach number as possible (approximately 3.1) before transition to the pure ramjet mode.

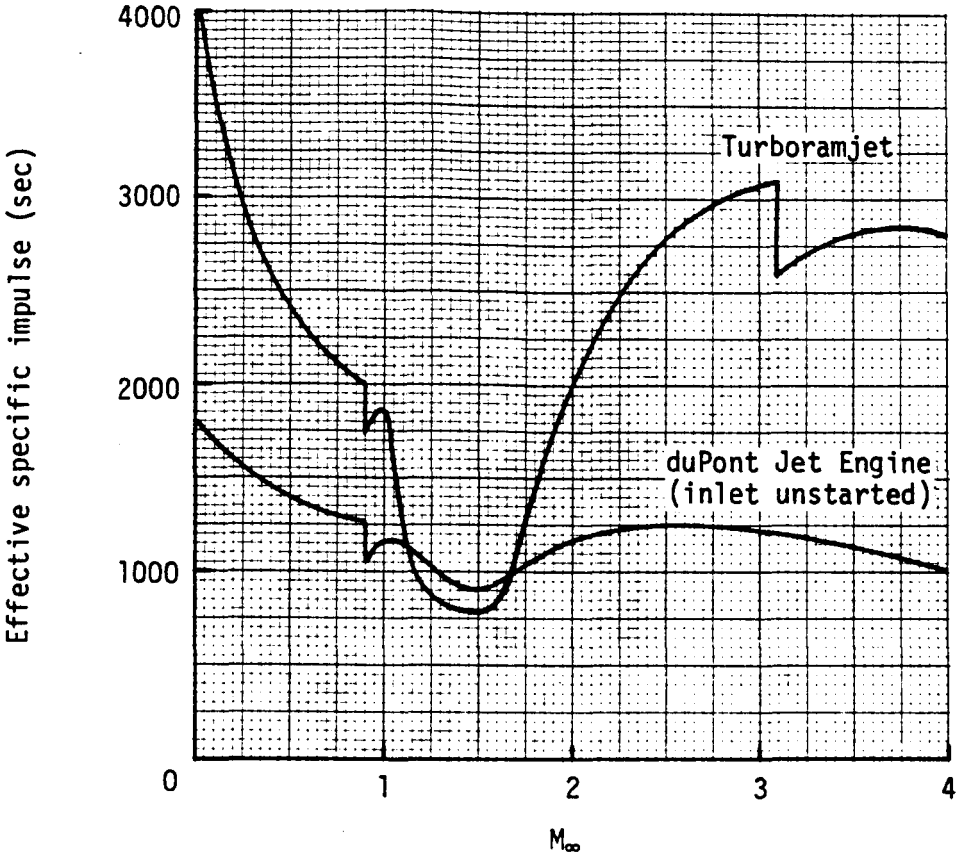

Figure 32. - Effective specific impulse of wraparound turboramjet and duPont Jet Engine

Engine Weights

The weights of the engines are all placed on a comparable basis without adjusting the manufacturers' basic unit weights. If the weights were adjusted to comparable materials and stress allowables, SCRAMLACE would be considerably heavier. All engines are sized to 44.2 square feet of inlet cowl area which corresponds to a 90-inch cowl diameter in the case of an axisymmetric engine. The SERJ and SCRAMLACE are scaled from the class 3 (final) weight proportionately to cowl area to produce a sea-level-static thrust of 128 000 pounds and 111 000 pounds, respectively. Relative to the final class 3 engine sizes, the SERJ is scaled from 70 square feet of inlet cowl area to 44.2 square feet or 63%, and the SCRAMLACE is scaled from 68 square feet to 44.2 square feet or 65%. The turboramjet consists of a 50 000-pound sea-level-static thrust turbojet and a maximum ramjet nozzle throat area equal to the fixed nozzle throat area of the duPont Jet Engine. The weights of the stoichiometric turbojet engine installation and the wraparound turboramjet are assumed to be the same. The major difference between the two engines is in the mode of

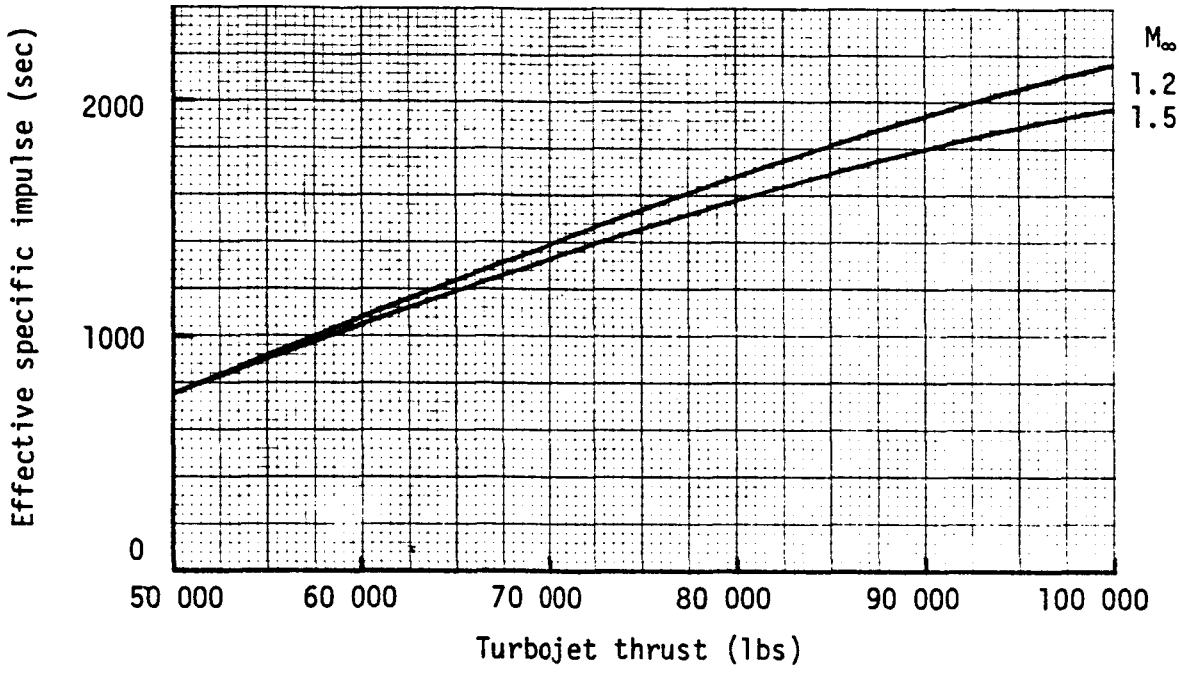

Figure 33. - Turboramjet effective specific impulse versus turbojet size

operation: the stoichiometric turbojet is operated alone and is shut down at the start of ramjet operation; while the wraparound turboramjet features simultaneous operation of the turbojet and ramjet.

The two-dimensional variable geometry inlet used for the SERJ, SCRAMLACE and the turboramjet is assumed to weigh 148 pounds per square foot of cowl area to conform with the Marquardt analysis. This design is based on a maximum internal pressure of 120 pounds per square inch. At this weight ratio, the two-dimensional inlet weighs 6550 pounds. In a comparison between axisymmetric and two-dimensional inlets the Marquardt study predicts that an axisymmetric inlet would weigh 46% less than a comparable two-dimensional inlet. On this basis, a weight of 3540 pounds is used for the axisymmetric version of the turboramjet. The SERJ incorporates a retractable fan and SCRAMLACE a large heat exchanger neither of which is compatible with the use of an axisymmetric inlet.

An allowance is included for a regeneratively-cooled external cowl and a 15% development margin is added to make the weight estimates for these three engines comparable to the estimate for the duPont Jet Engine. Cowling for SCRAMLACE consists of a bottom panel and one-half of a side. The resulting weights are summarized in Table VI, and the weight comparison is presented in Figure 34.

The weight of the duPont Jet Engine pod is about one-half that of the other engines. On the reference airplane used to develop the effective specific impulse, use of the duPont Jet Engine pods results in weight savings of 28 500 pounds and 33 500 pounds for axisymmetric and two-dimensional inlets,

TABLE VI. - ENGINE WEIGHT SUMMARY -
DUPONT JET ENGINE, TURBORAMJET, SCRAMLACE AND SERJ

	90-inch duPont Jet Engine	Turboramjet		SCRAMLACE	SERJ
		axisym-metric inlet	2-dimen-sional inlet	2-dimen-sional inlet	2-dimen-sional inlet
Bare engine	7952	9 400	9 400	8 090	8 100
Variable inlet	†	3 540	6 550	6 550	6 550
Engine cowling	†	1 200	820	590	820
Development margin 15%	1193	2 120	2 520	2 285	2 320
TOTAL PODDED ENGINE	9145	16 260	19 290	17 515	17 790

†Weights attributed to variable inlet and engine cowling included in bare engine weight.

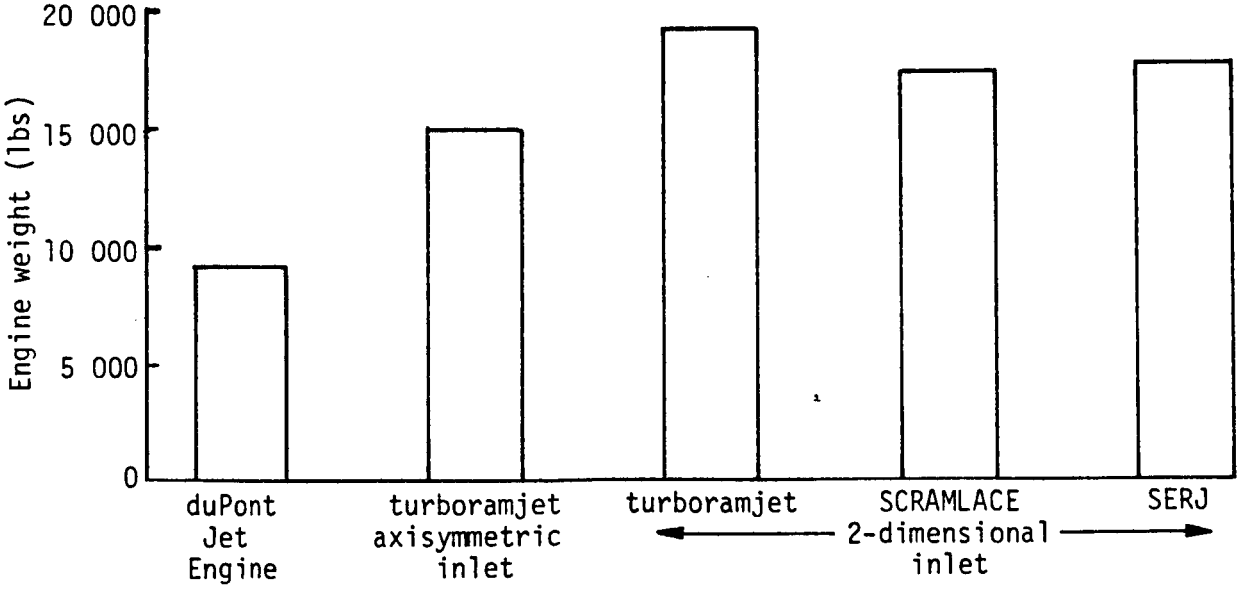

Figure 34. - Engine weight comparison

respectively, installed on the lightest competitive engines. The engine weight savings of 28 500 to 40 000 pounds are about equal to the payload of a single-stage-to-orbit aerospaceplane or to the weight of 140 to 200 passengers in a hypersonic transport. In terms of the two-stage space launch system used as the standard of comparison in the Marquardt studies, the reduction in engine weight is worth 2100 pounds of payload in orbit, an improvement of 10%.

Ramjet Installation

A comparative analysis of three generic types of ramjet installation was made in order to compare the axisymmetric pod embodiment of the duPont Jet Engine to two other possible configurations: a two-dimensional engine with variable inlet contraction ratio and a fixed geometry integrated engine configuration such as the Langley three-dimensional engine. The comparison demonstrates the two-dimensional engine with variable contraction ratio to be the best from an engine-fuel-consumption-for-acceleration standpoint - the pod engine is next, and the three-dimensional integrated engine is the least efficient. From a design-point cruise performance standpoint the two-dimensional variable inlet engine and the two- or three-dimensional fixed geometry engines are nearly equal, and the pod installation is less efficient. The pod is by far the lightest in weight, and the two-dimensional engine with a variable inlet is the heaviest.

The performance as an acceleration engine is presented in Figure 35 as the ratio of thrust minus drag of a pod installation or just the thrust of an integrated engine to the thrust of a fixed geometry integrated engine as a function of free stream Mach number. The term "integrated engine" is defined as an engine whose external surfaces are aligned with the local flow so that

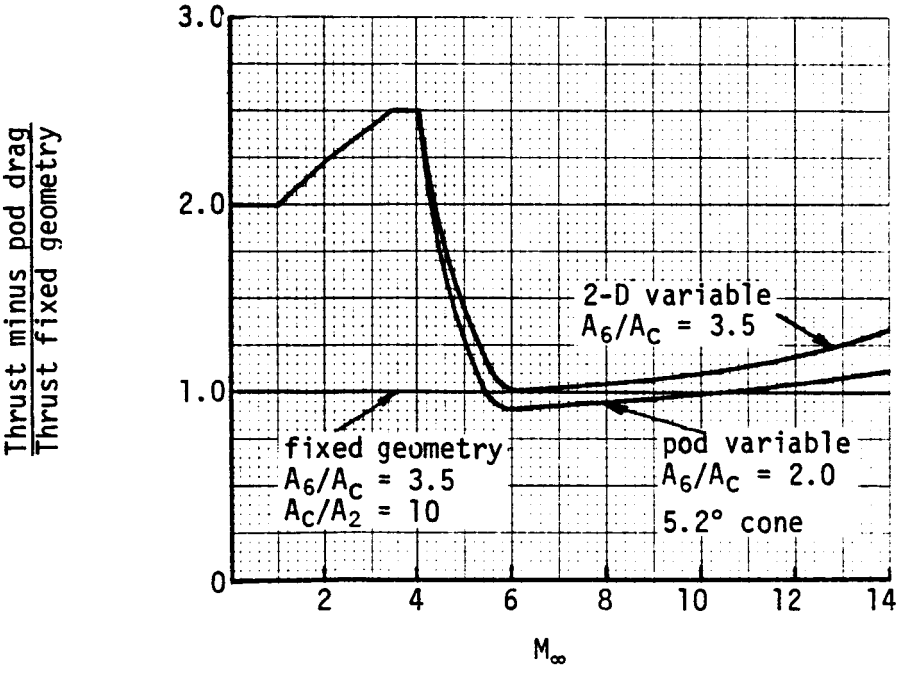

Figure 35. - Relative thrust of ramjet configurations

the only external drag force on the engine is skin friction. This arrangement is schematically compared to a pod arrangement in Figure 36. A pod is integrated into the airplane by considering such additional factors as directional stability, propulsion effects on pitch trim, and favorable interference, but for the purposes of this discussion "integrated" means an installation

Integrated

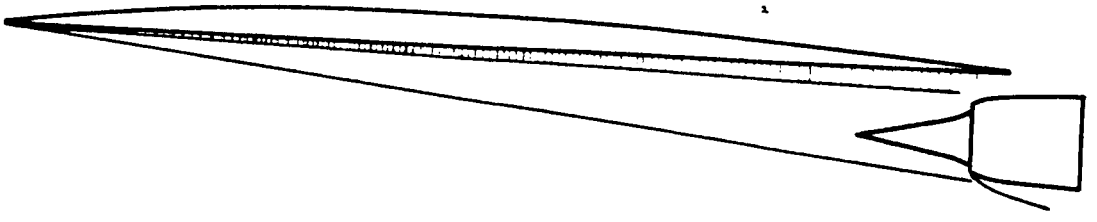

Pod

Figure 36. - Ramjet installations

with no external wave drag. One of the purposes of the integrated engine is to eliminate external wave drag which simultaneously reduces skin friction on the nacelles. Another related purpose is to obtain an engine exit area greater than the inlet cowl area without incurring nacelle wave drag and thereby attaining nozzle expansion ratios that might be impractical with a pod. In so doing the base drag or drag of the rearward sloping portions of the aircraft can be reduced by using some of these surfaces as part of the expansion nozzle.

Two effects are apparent in Figure 35: pod drag limits the ratio of nozzle exit to cowl area to 2.0 for axisymmetric installations, while a value of 3.5 is possible for the integrated installations; and the two-dimensional engine obtains the benefits of variable contraction shown in Figure 37 at the expense of engine weight but without incurring nacelle drag penalties at high speeds. The axisymmetric engine obtains the benefits of variable contraction at the expense of pod drag but with very little weight addition. The benefits of variable contraction outweigh the pod drag penalties over most of the speed range when acceleration performance is being considered. Since the pod is lighter and has better acceleration performance to high Mach numbers, it is clearly a better choice over a fixed geometry engine for an accelerating airplane such as an aerospaceplane.

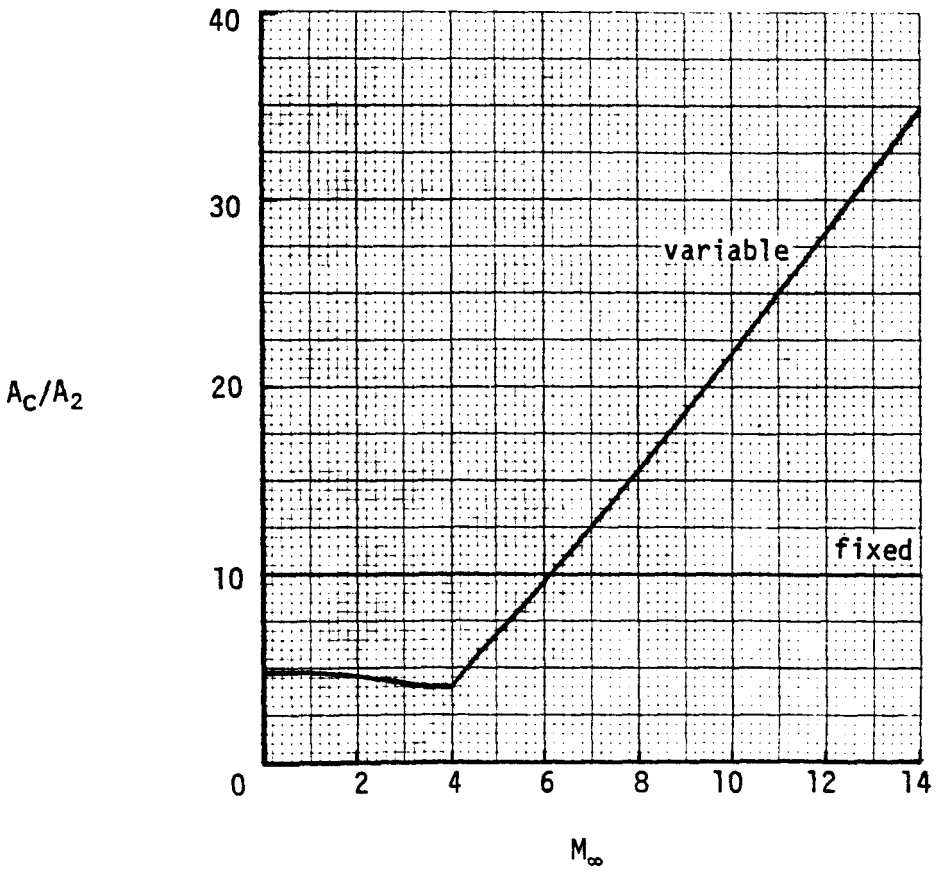

Figure 37. - Inlet contraction ratio versus flight Mach number

The choice between a variable geometry two-dimensional engine and a pod must be made by studying the effect of trading fuel consumption for engine weight in a given mission. The Marquardt study reported in Reference 7 performed such a trade-off for a two-stage space booster and found that a two-dimensional inlet integrated with an axisymmetric engine improved the payload in orbit 1300 pounds out of approximately 20 000 compared with an axisymmetric inlet. The Marquardt study apparently considered only the nacelle drag and weight changes associated with the inlet. The engines used in both cases were axisymmetric ejector ramjets. When the engines considered in Reference 7 are made two-dimensional instead of axisymmetric an additional engine weight penalty of 47 000 pounds is incurred based on the weight summary in Table VII and the engine size corresponding to 275 square feet of cowl area used in Reference 7. This weight penalty results in a loss of 3400 pounds of payload in orbit. Adding 3400 pounds to the -1300-pound penalty assigned to an axisymmetric inlet alone produces 2100 pounds additional payload in orbit from axisymmetric pods compared to a two-dimensional variable-geometry integrated inlet installation.

TABLE VII. - DERIVATION OF TWO-DIMENSIONAL DUPONT JET ENGINE FROM SCRAMLACE DATA†

	duPont Jet axisymmetric weight (lbs)	SCRAMLACE weight (lbs)	duPont Jet 2-dimensional weight (lbs)
Liquid air subsystem	1080	2 790	1 080
Rocket	635	1 590	1 170
Mixer, diffuser, combustor	3115¶	3,540	4 980§
Controls	150	170	150
SUBTOTAL, BARE ENGINE	4980	8 090	7 380
Variable inlet	2310¶	6 550	6 550
Engine cowling	660	590††	590††
Development margin 15%	1195	2 285	2 180
TOTAL, PODDED ENGINE	9145	17 515	16 700

†Engines are adjusted to 44.2 ft^2 of inlet cowl area corresponding to a 90-in cowl diameter duPont Jet Engine.

¶The duPont Jet Engine combines the inlet diffuser and combustor, so the physical boundaries between the inlet and the other items were somewhat arbitrary.

§SCRAMLACE design is scaled to the duPont Jet Engine airflows with all titanium parts changed to nickel base alloys.

††Based on 2 lbs/ft^2 of bottom and two sides of the engine plus 25% for closeout and attaching hardware.

In a single-stage-to-orbit analysis, the trade-off favors reduced weight at the expense of fuel consumption even more heavily than in a two-stage system. In this case the use of podded engines increases the payload by 16 500 pounds compared to use of integrated engines with a variable geometry two-dimensional inlet. The fuel consumed to Mach 14 as a function of thrust/drag at Mach 14 to adjust the weight at rocket ignition is presented in Figure 38. The rocket

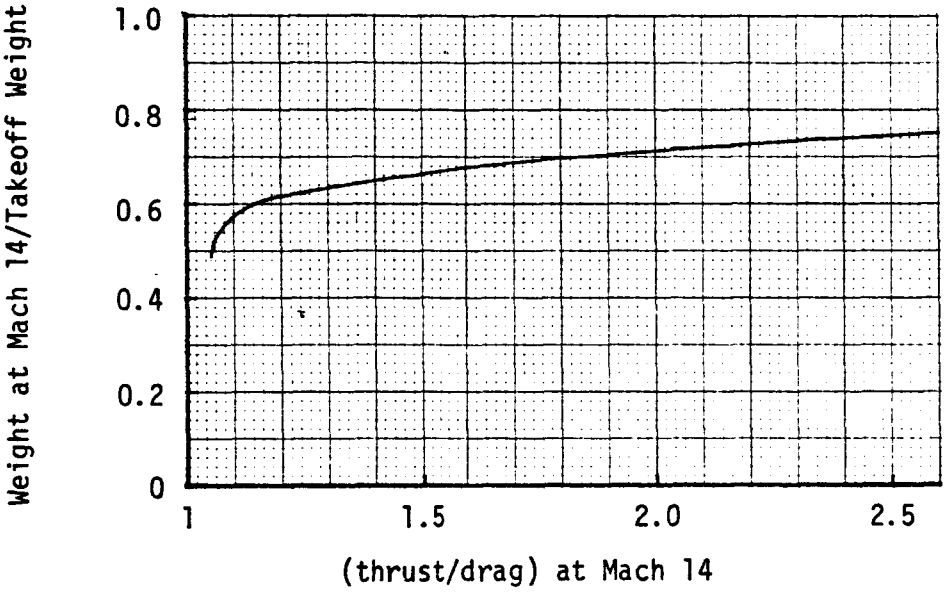

Figure 38. - Weight at Mach 14 versus thrust/drag at Mach 14

mass ratio used from Mach 14 to orbit and return is 2.118. Elimination of pod drag increases the thrust/drag from 1.84 to 2.30 and increases the weight at rocket ignition from 493 000 pounds to 515 000 pounds which in turn increases the zero fuel weight by 10 400 pounds. The increased engine weight required to transform the duPont Jet Engine pod to a rectangular engine with a variable geometry inlet is approximately 30 200 pounds based on a comparison with the SCRAMLACE engine shown in Table VII. The reduction in hydrogen tank weight due to lower airbreathing fuel consumption (estimated at 15% of the difference in fuel to Mach 14) is 3300 pounds. Adding the additional engine weight and subtracting the tankage adjustment and the increase in zero fuel weight gives a net loss of 16 500 pounds of payload. The conclusion is that a podded installation is preferred for both a two-stage space booster and a single-stage aerospaceplane.

Hypersonic cruise presents a different picture for evaluation of engine configurations. Since cruise represents flight at a single Mach number, a fixed geometry engine will be operated at its design-point for a significant period of time, and a large portion of the total fuel used will be burned at this condition. The integrated engines have a performance advantage at cruise over podded engines. The weight savings inherent in fixed geometry will make the

choice between the two integrated engine types favor the fixed geometry if only cruise is considered. If acceleration is considered, however, the importance of variable geometry in enhancing acceleration performance must be traded off against the cruise fuel consumption penalties involved in axisymmetric pod drag which are of the order of 20%. The Marquardt study (Reference 7) places the pod drag at 19% of the airplane drag. To maintain the acceleration thrust of the duPont Jet Engine shown in Figures 29 and 30, a contraction ratio of 5 or less is necessary in a fixed geometry engine. The swept-back struts on the Langley three-dimensional engine may enable it to pass more flow at low speeds and provide the same thrust at a contraction ratio higher than 5. Best performance at Mach 6 is obtained with a contraction ratio of 10 (see Figure 37). Therefore the engines must be up to twice as large if they are to be fixed at the optimum cruise contraction ratio compared with variable contraction. If the contraction were fixed at 5 to maintain the engine size, the performance in cruise would be reduced 13.5% (Reference 7) which represents a reduction in performance approaching the pod drag. Unless the airplane inherently requires a large cowl area in cruise, the pod would be a better choice than the fixed geometry engine with a contraction ratio of 5 because it would have almost equal performance and would be lighter in weight. The swept-back struts used in the Langley three-dimensional engine could potentially increase the throat area during unstarted operation and give the engine more competitive acceleration thrust without an increase in cowl area.

In a typical 4000-mile flight, a 500 000-pound takeoff weight aircraft would cruise for 3200 miles at Mach 6 consuming about 90 000 pounds of fuel with four podded engines and 74 000 pounds with integrated engines. About 75 000 pounds of fuel would be consumed in climb and descent. The difference is about 10% of the total fuel consumed in a typical flight. If the engine package were heavier by 16 000 pounds plus 10% of the payload, the cost per seat mile or per ton mile would remain the same. A typical payload at 4000 nautical miles with four duPont Jet-podded Engines is 84 000 pounds. The breakeven weight difference is 24 400 pounds. From Table VII, the difference in engine weight is 30 200 pounds which is 5800 pounds above the breakeven weight. Therefore, the podded engines are more economical than the variable geometry two-dimensional engines by 10% of fuel cost per seat mile. A fixed geometry engine with swept-back injection struts would represent a competitive solution if its weight could be reduced to be no greater than 24 400 pounds above that of the four podded engines without greatly reducing the optimum cruise contraction ratio.

Differences Between SCRAMLACE and duPont Jet Engine Cycles

The composite cycle that most closely resembles the duPont Jet Engine cycle is the SCRAMLACE. Two essential differences account for the duPont Jet Engine's superior cycle performance. The duPont Jet Engine cycle injects the primary air at 1800°R which is the temperature that gives the maximum inlet pressure ratio as shown in Figure 39. SCRAMLACE injects the primary air at a temperature resulting from stoichiometric combustion which gives less than the optimum pressure ratio as shown by the right-hand portion of the curve

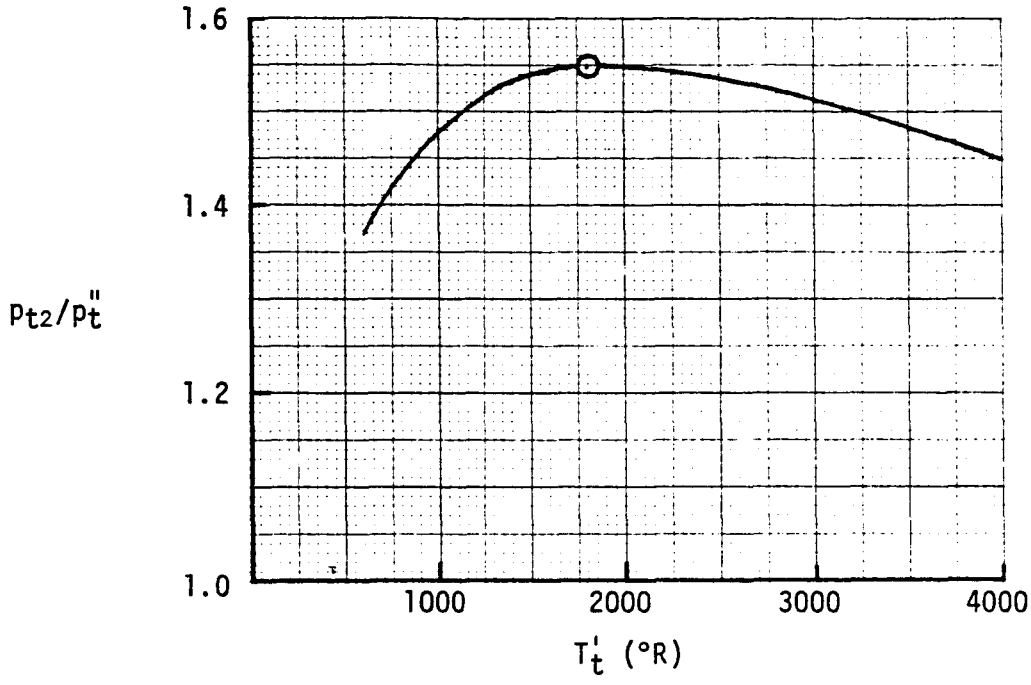

Figure 39. - Inlet pressure ratio versus primary stream total temperature

in Figure 39. The over-all equivalence ratio of SCRAMLACE is considerably higher than the maximum equivalence ratio for which the duPont Jet Engine was designed, which increases thrust at the expense of specific impulse. At takeoff the duPont Jet Engine delivers 50 000 pounds of thrust at an equivalence ratio of 1.65. SCRAMLACE delivers 111 000 pounds at an equivalence ratio of 3.52. The duPont Jet Engine specific impulse at takeoff is 1840 seconds and SCRAMLACE is 1245 seconds.

The lower equivalence ratio of the duPont Jet Engine reduces the heat exchanger airflow and therefore the heat exchanger size. At the same cowl area the duPont Jet Engine has one-fifth the heat exchanger airflow required by SCRAMLACE. At the same takeoff thrust, the duPont Jet Engine would have 44% of the heat exchanger airflow of SCRAMLACE. The SCRAMLACE heat exchanger system weight per unit airflow is about one-half the value developed for the duPont Jet Engine. While part of this difference is accounted for by the antifouling provisions provided by duPont, some of it must reflect a higher degree of optimism with respect to heat exchanger weight used in the SCRAMLACE study. The reduction in heat exchanger flow by four-fifths in the duPont Jet Engine makes the packaging and antifouling of the heat exchanger more practical. Injection of the primary air at 1800°R instead of stoichiometric temperature reduces the duPont Jet Engine injection system complexity and weight compared to the regeneratively-cooled systems employed in SCRAMLACE.

Relative Development Risk

The duPont Jet Engine has lower development risk and considerably lower development costs than the other engines studied. The turboramjet and the SERJ engine both require the development of a turbine engine, and in the sizes contemplated for operational aircraft this represents an extremely expensive program in itself. The SCRAMLACE and the duPont Jet Engine do not require a turbine engine development. The lower heat exchanger airflow and lower primary stream injection temperature make the duPont Jet Engine development less expensive and less risky than SCRAMLACE. The weight and size of the duPont Jet Engine heat exchanger are consistent with present plate-fin heat exchangers. The antifouling technique of cycling a portion of the heat exchanger is current practice in portable LOX plants. The smaller airflow makes this technique practical.

When configurations of the duPont Jet Engine are assessed versus development risk, the axisymmetric pod is far ahead of the two- or three-dimensional engines with respect to time, risk and cost. The axisymmetric engine has the simplest aerodynamic flow field and the engine flow is handled entirely by the engine itself, eliminating extensive development and testing of compression and expansion surfaces which are part of the aircraft. The engine's symmetry eliminates the pitch trim changes with power and speed changes present in the integrated installations. Similarly inlet spillage is symmetrical, eliminating pitch trim changes from this source. The structural concepts and weights for the duPont Jet Engine pod were taken directly from the Hypersonic Research Engine which has been built and tested in the Langley hot structures tunnel. The podded version of the duPont Jet Engine therefore has the least risky design and the most reliable weight of any of the engine cycles studied or of the integrated configurations of the duPont Jet Engine considered for comparison. Because the background on axisymmetric engines is so extensive and because the engine can be developed and tested independently of the airframe, an axisymmetric engine can be developed with a lead time of four to ten years less than an integrated installation.

CONCLUSIONS

The preceding discussions and analyses which constituted the study of an air augmented convertible scramjet engine support the following conclusions:

An air augmented convertible scramjet engine (duPont Jet Engine) can be built which offers an improvement over combined turbojet-ramjet designs and previously known composite cycles because it obtains static and low flight Mach number thrust by using the liquid hydrogen fuel to liquefy intake air which is subsequently injected at high pressure into the inlet to provide flow through the engine and therefore thrust.

The duPont Jet Engine promises a lighter weight than many previously proposed engines using a weight basis consistent with the Hypersonic Research Engine whose flight-weight structure has been successfully tested.

duPont Aerospace Company, Inc.
Torrance, California, April 15, 1972.

APPENDIX

METHODS OF ANALYSIS

The following subsections describe the methods, sources and equations used in developing and implementing the analytical performance model and in analyzing the air liquefaction cycle in the heat exchanger of the duPont Jet Engine.

Analytical Performance Model

The analytical performance model for the duPont Jet Engine was based on equilibrium chemistry of arbitrary reactants. Although the current concept of the engine is restricted to the use of hydrogen-air reactants, the analytical model was designed to accept arbitrary reactants for possible use in predicting theoretical performance for comparison with wind-tunnel tests conducted with vitiated air. The model was designed to predict either design-point or off-design performance. The flow conditions at the inlet throat were based on a one-dimensional analysis of the mixing of the primary and secondary streams in the ramjet inlet. The analyses downstream of the inlet throat were based on classical ramjet techniques with the exception that in the off-design mode three solutions were obtained at the combustor entrance. The three solutions were necessary to predict performance based on subsonic diffusion, shock-in-diffuser or supersonic combustion depending on the flow conditions in the nozzle throat since conditions there can not be known a priori. When the free-stream Mach number became greater than unity, the engine was assumed to be completely submerged in the pressure field behind an oblique shock as shown in Figure 40. The calculation of the pressure field represented the only departure from one-dimensional flow in the analysis. The following paragraphs describe in detail the methods, sources, and equations used in the calculation of chemical equilibria and in the implementation of the analytical performance model of the duPont Jet Engine.

Calculation of chemical equilibria. - The analytical performance model uses the ICRPG† reference program ODE described in Reference 10 to calculate the species concentrations and thermodynamic properties in the four chemical systems present in the duPont Jet Engine. The version of the cited reference program used was that reported in Reference 11 with the exception that the options to calculate the enthalpy potentials and transport properties were removed because of space limitations. The maximum number of species in a chemical system was reduced from 150 to 50 for the same reason.

---

†Interagency Chemical Rocket Propulsion Group.

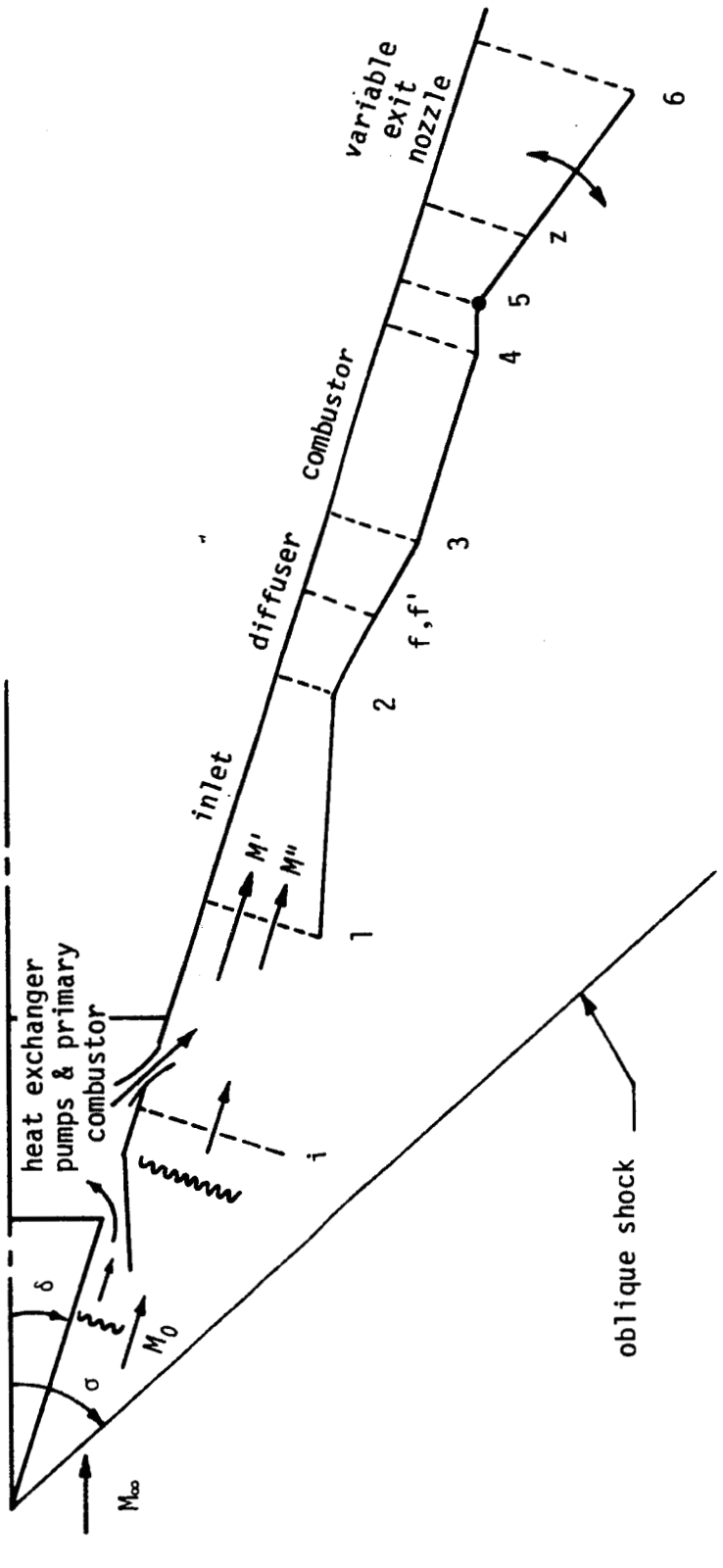

Figure 40. - Schematic of analytical performance model

Appendix

The cited reference program minimizes the Gibbs free energy (see Reference 12) as the condition for chemical equilibrium with the independent variables

$$T = T_0 \tag{1}$$

$$p = p_0 \tag{2}$$

and the composition variables n_j^α, which represent the number of moles of species j in the phase α. The Gibbs free energy can be written as

$$G = G(p, T, n_j^\alpha) \tag{3}$$

Since the Gibbs free energy is an extensive property, equation (3) must be a first degree homogeneous function in n_j^α. This leads to

$$G = \sum_{j,\alpha} \mu_j^\alpha n_j^\alpha \tag{4}$$

where the chemical potential μ_j^α is defined as

$$\partial G/\partial n_j^\alpha \equiv \mu_j^\alpha \tag{5}$$

The conservation of elements in the chemical system (which constitute the constraints on the variations δn_j^α) may be written as

$$\sum_i \left(\sum_{j,\alpha} a_{ij} n_j^\alpha - b_i^0 \right) = 0 \tag{6}$$

where the formula numbers a_{ij} represent the number of atoms of the ith element in the jth species, and the specific formula numbers b_i^0 represent the total number of gram-atoms of element i in the system.

The fundamental function for the variational problem may be written from equations (3) and (6) as

$$g = G + \sum_i \lambda_i \left(\sum_{j,\alpha} a_{ij} n_j^\alpha - b_i^0 \right) \tag{7}$$

where the Lagrangian multipliers λ_i were introduced so that all of the δn_j^α could be considered independently variable. The condition for equilibrium is obtained by setting the first variation of the Functional (7) equal to zero

$$\delta g = \sum_{j,\alpha} (\mu_j^\alpha + \sum_i \lambda_i a_{ij}) \delta n_j^\alpha + \sum_i \left(\sum_{j,\alpha} a_{ij} n_j^\alpha - b_i^0 \right) \delta \lambda_i = 0 \tag{8}$$

Treating the $\delta\lambda_i$ and δn_j^α as independent variations gives

$$\mu_j^\alpha + \sum_i \lambda_i a_{ij} = 0 \tag{9}$$

and also equation (6) which, along with equations (1) and (2), represent a set of nonlinear equations defining a thermodynamic state of the chemical system that can be solved by iterative techniques to obtain the equilibrium compositions of the species and the Lagrangian multipliers.

The use of equations (1) and (2) in forming the Functional (7) implies that the thermodynamic state of the chemical system was specified by an assigned temperature and pressure. This specification will hereafter be referred to as the TP problem. In general, any two equations involving T, p, and n_j^α may be used to define the thermodynamic state. Equation (1) may be replaced by

$$H(T, p, n_j^\alpha) = H_0 \tag{10}$$

(where H in the enthalpy of the products and H_0 is a constant equal to the enthalpy of the reactants) to define the HP problem, or by the entropy function

$$S(T, p, n_j^\alpha) = S_0 \tag{11}$$

to define the SP problem. The problem designations TP, HP, and SP will be used in the following paragraphs to describe the thermodynamic-state calculations.

Freestream conditions. - The calculation of freestream conditions requires the specification of the freestream Mach number (M_∞), and pressure (p_∞). If the altitude (h) and the deviation from standard temperatures (ΔT_∞) are specified, the side calculations

$$p_\infty = f(h, v)$$

and

$$T_\infty = g(h, v) + \Delta T_\infty$$

are made to obtain the state variables. In these equations f represents the altitude function for pressure, g represents the altitude function for temperature, and v represents either geometric or geopotential atmosphere. The TP problem is solved for the equilibrium concentration of the species and the freestream static conditions at the thermodynamic state defined by p_∞ and T_∞.

The freestream total enthalpy is obtained from the energy equation

$$H_{t_\infty} = H_\infty + \frac{M_\infty^2 \, (\gamma_s nRT)_\infty}{2gJ}$$

where n is the reciprocal of the molecular weight, R the gas constant, γ_s the isentropic exponent†, g the acceleration of gravity and J the energy conversion factor. The initial estimate of the freestream total pressure is obtained from the ideal gas relationship

$$p_{t_\infty}^{(1)\P} \simeq p_\infty \left[1 + (\gamma-1) \, M_\infty^2/2\right]^{\gamma/(\gamma-1)}$$

and the SP problem is solved for the freestream total conditions at the thermodynamic state defined by S_∞ and $p_{t_\infty}^{(n)\P}$. Iteration is made on the total pressure $p_{t_\infty}^{(n)}$ until

$$\left|(H_{t_\infty} - H_{t_\infty}^{(n)})/H_{t_\infty}\right| < \varepsilon$$

Pressure field. - The pressure-field calculation requires the specification of either the angle of attack (δ) or the Mach number (M_0). If both parameters are zero, the conditions in the pressure field are identical to those in the freestream. If M_0 is specified, either the total pressure (p_{t_0}) or the static pressure (p_0) must also be specified.

---

†The isentropic exponent is used to calculate the velocity of sound throughout the engine with the exception of the frozen expansions in the nozzle. In this case, the ratio of specific heats is used. The subscript s will be deleted hereafter for convenience.

¶The superscript (1) denotes the initial estimate of the independent variable; the superscript (n) denotes the value of the independent variable after the nth iteration.

When $\delta > 0$ and $M_0 > 1$, the initial estimate of the shock angle (σ) is obtained from the middle root of the cubic equation

$$y^3 + by^2 + cy + d = 0$$

where

$$y = \sin^2\sigma$$

$$b = -(M_\infty^2 + 2)/M_\infty^2 - \gamma \sin^2\delta$$

$$c = (2M_\infty^2 + 1)/M_\infty^4 + [(\gamma+1)^2/4 + (\gamma-1)/M_\infty^2] \sin^2\delta$$

$$d = -(\cos^2\delta)/M_\infty^4$$

and

$$\sigma^{(1)} \simeq \sin^{-1}\sqrt{y(2)}$$

From the details of the oblique shock system shown in Figure 41 the continuity, momentum, and energy equations across the shock may be written as

$$\rho_\infty V_{\infty n} = \rho_0 V_{0n}$$

$$V_{\infty t} = V_{0t}$$

$$p_0 + \rho_0 V_{0n} = p_\infty + \rho_\infty V_{\infty n}^2$$

and

$$H_{t_0} = H_{t_\infty}$$

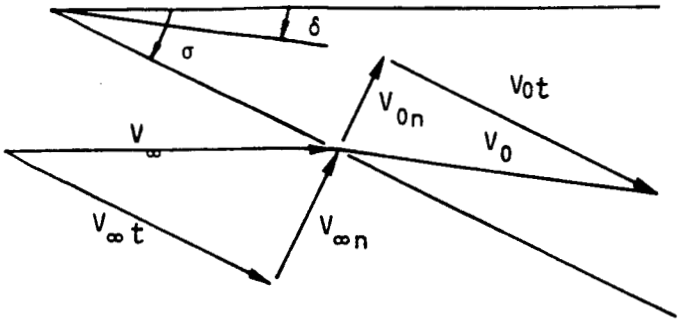

Figure 41. - Oblique shock system

From these equations and the initial estimate of the shock angle, the continuity, momentum, energy and state equations may be written

$$(W/A)_0^{(n)} = (W/A)_\infty \sin \sigma^{(n)}/[\sin (\sigma^{(n)} - \delta)] \tag{12}$$

$$p_0^{(n)} = p_\infty + (W/A)_\infty (V_\infty/g) \sin^2 \sigma^{(n)}[1 - \tan(\sigma^{(n)} - \delta)/\tan \sigma^{(n)}] \tag{13}$$

$$V_0^{(n)} = V_\infty \cos \sigma^{(n)}/[\cos(\sigma^{(n)} - \delta)] \tag{14}$$

$$H_0^{(n)} = H_{t0} - V_0^{2(n)}/2gj \tag{15}$$

$$(W/A)_0^{(n')} = g p_0^{(n)} V_0^{(n)}/n_0^{(n)} R T_0^{(n)} \tag{16}$$

where n_0 is the reciprocal of the molecular weight. The HP problem can now be solved for the static conditions in the pressure field at the thermodynamic state defined by $p_0^{(n)}$ and $H_0^{(n)}$. Iteration is made on $\sigma^{(n)}$ repeating the calculations in equations (12) through (16) and solving the HP problem until

$$|[(W/A)_0^{(n)} - (W/A)_0^{(n')}]/(W/A)_0^{(n)}| < \varepsilon$$

The initial estimate for the total pressure is obtained from the ideal gas relationship and the total conditions in the pressure field are determined by solving the SP problem with the state variables $p_{t0}^{(n)}$ and S_0. Iteration is made on $p_{t0}^{(n)}$ until

$$|(H_{t0} - H_{t0}^{(n)})/H_{t0}| < \varepsilon$$

If M_0 and p_{t0} are specified, the HP problem is solved for the total conditions in the pressure field using the state variables p_{t0} and H_{t0}. The initial estimate for the static pressure is obtained from the ideal gas relationship and the SP problem is solved for the static conditions in the pressure field using the state variables $p_0^{(n)}$ and S_0. Iteration is made on $p^{(n)}$ until

$$|(M_0 - M_0^{(n)})/M_0| < \varepsilon$$

When M_0 and p_0 are specified, obtain the first approximation for entropy from

$$S_0^{(1)} = S_\infty,$$

and solve the SP problem with the state variables p_0 and $S_0^{(n)}$ to obtain $M_0^{(n)}$. Iterate on $S_0^{(n)}$ until

$$|(M_0 - M_0^{(n)})/M_0| < \varepsilon$$

The procedure for obtaining total conditions is identical to the $\delta > 0$ case, above.

When $M_0 > 1$, the flow is passed through a normal shock before entering the primary and secondary inlets as shown in Figure 40. In the following formulation, the conditions downstream of the normal shock are denoted by the subscript 0 - those upstream by the absence of a subscript.

The continuity, momentum and energy equations may be written as

$$(W/A)_0 = (W/A)$$

$$Ivac_0 = Ivac$$

and

$$H_{t0} = H_t$$

where

$$W/A = g\ p\ V/n\ R\ T$$

and

$$Ivac = V/g + p/(W/A)$$

The initial estimates of static and total pressures downstream of the normal shock may be obtained from the ideal-gas relationships

$$M_0^{*2} \simeq 1/M^{*2} \simeq [1 + (\gamma-1)M^2/2]/[(\gamma+1)M^2/2]$$

$$M_0^2 \simeq 2M_0^{*2}/[(\gamma+1) - (\gamma-1)M_0^{*2}]$$

$$p^{(1)} \simeq p[1 + 2\gamma(M_0^2 - 1)/(\gamma+1)]$$

$$p_{t0}^{(1)} \simeq p_0^{(1)}[1 + (\gamma-1)M_0^2/2]^{\gamma/(\gamma-1)}$$

The total conditions downstream of the normal shock may be obtained by solving the HP problem with the state variables $p_{t0}^{(n)}$ and H_{t0}. Then the SP problem may be solved with the state variables $p_0^{(n)}$ and $S_0^{(n)}$ to obtain the static

conditions. Iterative procedures may be used with $p_{t_0}^{(n)}$ and $p_0^{(n)}$ repeating the HP and SP calculations until

$$|(Ivac_0 - Ivac_0^{(n)})/Ivac_0| < \varepsilon$$

and

$$|[(W/A)_0 - (W/A)_0^{(n)}]/(W/A)_0| < \varepsilon$$

Ejector. - The ejector consists of the primary and secondary flow systems as shown in Figure 40. Air enters the primary inlet at flow conditions behind the normal shock in the pressure field. The primary flow is induced by the volume change of the air as it is cooled, condensed and pumped from the heat exchanger. The primary air is pumped to a high pressure in the liquid phase, combusted with sufficient hydrogen to raise the temperature of the primary stream to about 1800°R, and injected at a high velocity through a supersonic nozzle ahead of the internal compression surfaces of the secondary inlet where it induces a secondary airflow. In the accommodation region between the injection station (i) and station 1, the primary and secondary streams adjust to uniform pressure, the processes are assumed to be isentropic, and shear forces between the streams and the walls are assumed to be zero. Mixing occurs downstream of station 1 and is assumed to be complete at station 2 - the inlet throat. The flow processes between stations 1 and 2 are non-isentropic due to mixing, to finite shear forces and heat transfer between the streams and the walls and to the degradation of the primary stream momentum at station 1 by the velocity coefficient, C_V', and the injection angle, β'. The off-design analysis of the ejector will be discussed in the following paragraphs. The design-point analysis may be deduced from the material presented. In general, an off-design analysis determines the flow parameters and performance in a fixed-geometry engine while a design-point analysis determines the engine geometry from specified flow parameters.

Primary air system: The independent variables in the primary air system are the total pressure, p_t', and the equivalence ratio, ϕ', which are determined to match the dependent variables - flow per unit area in the primary nozzle throat, $(W/A)_*'$, and the primary stream total temperature, T_t', respectively. The flow in the primary stream is determined by the total fuel flow in the engine, W_{ft}, the total temperature of the primary air at the entrance to the heat exchanger, T_{t_∞}, and the quantity of hydrogen, W_f', required to attain the total temperature in the primary combustor. As discussed on pages 19 and 20, above, when the pressure dependence was eliminated, the condensation ratio

could be expressed as a linear function of the total temperature in the free stream as shown in Figure 6. Hence

$$r = -0.001589404\ T_{t_\infty} + 7.0198676 \qquad (17)$$

where

$$r \equiv W_a'/W_{ft}$$

and W_a' is the mass flow of primary air liquefied in the heat exchanger. The energy levels in the primary combustor are taken to be those of the hydrogen and air at the exit of the heat exchanger. The energy added to the air from the pump work was not considered since it was subsequently removed as pump work. The energy levels were determined by an analysis of the air liquefaction cycle and are tabulated in Tables VIII and IX for air and hydrogen, respectively. There would be a small variation in the energy levels of air and hydrogen as a function of freestream Mach number and altitude had the pressure dependence on the air liquefaction cycle been retained.

TABLE VIII

ENERGY LEVEL OF AIR

Species	Weight (%)	Enthalpy (CAL/gm-mole)	T (°K)
N	75.57	-1531.2	78
O	23.15	-1522.7	78
AR	1.28	-1093.7	78

TABLE IX

ENERGY LEVEL OF HYDROGEN

M_∞	h (ft)	Enthalpy (CAL/gm-mole)	T (°K)
0.0	0	-879	164
0.5	36 000	-982	147
1.0	36 000	-933	155
1.5	36 000	-825	173
2.0	36 000	-704	193
2.5	36 000	-547	217
3.0	36 000	-386	241
3.5	36 000	-237	263
4.0	36 000	-116	281

The engine geometry and over-all equivalence ratio, ϕ_t, are the specified parameters in the off-design analysis. Initial values of the total fuel flow, W_{ft}, and the equivalence ratio, ϕ', and total pressure, p_t', in the primary combustor are assumed. The condensation ratio, r, is obtained from Equation (17) and the entrainment ratio of secondary to primary airflows, μ, is calculated from

$$\mu \equiv W''/W_a' = 1/(r\ \phi_t\ \phi^*) - 1$$

where ϕ^* is the stoichiometric mixture ratio,

$$W_a' = rW_{ft}^{(n)}$$

and

$$W'' = \mu W_a'$$

The total enthalpy of the reactants in the primary combustor are calculated from the energy equation

$$H_t'^{(n)} = [(O/F)^{(n)} H_{ta} + H_{tf}]/[1 + (O/F)^{(n)}]$$

where the oxidant-to-fuel ratio is defined by

$$(O/F)^{(n)} = 1/\phi'^{(n)}/\phi^*$$

The conditions in the primary combustor are obtained by using successive values of the independent variables ϕ' and p_t' until the dependent variables T_t' and $(W/A)_*'$ are matched as described in the following four steps.

(1) The HP problem is solved with the state variables $p_t'^{(n)}$ and $H_t'^{(n)}$ to obtain $T_t'^{(n)}$. Iteration is made on $\phi'^{(n)}$ until

$$|(T_t' - T_t'^{(n)})/T_t'| < \varepsilon$$

(2) The flow is expanded to sonic conditions by solving the SP problem with the state variables $S'^{(n)}$ and

$$p_*'^{(1)} = p_t'^{(n)}[2/(\gamma+1)]^{\gamma/(\gamma-1)}$$

to obtain $M_*^{'(n)}$. Iteration is made on $p_*^{'(n)}$ until

$$|M_*^{'(n)} - 1| < \varepsilon$$

(3) The dependent variable, $(W/A)_*^{'}$, is calculated from the continuity equation

$$(W/A)_*^{'} = W_a^{'}(1 + \phi'\phi^*)/A_*^{'}$$

to solve for the independent variable, $p_t^{'}$, and the current value of the dependent variable is obtained from

$$(W/A)_*^{'(n)} = g\ p_*^{'(n)} V_*^{'(n)}/n^{(n)} R\ T_*^{'(n)}$$

where $V_*^{'(n)}$ is the sonic velocity.

(4) Iteration is made on $p_t^{'(n)}$ repeating steps (1) through (3), above, until

$$|[(W/A)_*^{'} - (W/A)_*^{'(n)}]/(W/A)_*^{'}| < \varepsilon$$

Finally, the total entrainment ratio, μ_t, primary fuel flow, $W_f^{'}$, and total primary flow, $W^{'}$, are obtained from

$$\mu_t = (O/F)\ \mu\ /(1 + O/F)$$

$$W_f^{'} = W_a^{'}/(O/F)$$

and

$$W^{'} = W_a^{'} + W_f^{'}$$

Accommodation of primary and secondary streams: In the accommodation region between the injection station (i) and station 1 (see Figure 40), the primary and secondary streams are expanded isentropically to a uniform static pressure which satisfies the flow area at station 1. In the event that the combined

primary and secondary flows can not pass station 1, the total fuel flow, W_{ft}, is reduced until the combined flows are maximized. The procedure is described in detail in the following three steps.

(1) An initial value of p_1 is chosen such that the secondary stream remains subsonic. That is

$$p''_* < p_1^{(n)} < p_{t0} \tag{18}$$

(2) The SP problem is solved for both primary and secondary streams with the state variables $p_1^{(n)}$, S' and S_0 to obtain $(W/A)'^{(n)}_1$, $(W/A)''^{(n)}_1$ and

$$A_1^{(n)} = W'/(W/A)'^{(n)}_1 + W''/(W/A)''^{(n)}_1$$

Iteration is made on $p_1^{(n)}$ subject to the constraint (18) until

$$|(A_1 - A_1^{(n)})/A_1| < \varepsilon \tag{19}$$

(3) If the combined flows can not pass station 1, reduce the total fuel flow, $W_{ft}^{(m)}$, and repeat the primary air system calculations. Iteration is made on $W_{ft}^{(m)}$ and $p_1^{(n)}$ until the constraint (19) is satisfied with the additional constraint

$$\partial\{(W/A)'_1/[1 + \mu_t(W/A)'_1/(W/A)''_1]\}/\partial p_1 = 0$$

to maximize the flow through A_1.

Mixing of the primary and secondary streams: A general one-dimensional analysis was applied to the mixing of the primary and secondary streams between station 1 where they were assumed to have adjusted to a uniform pressure and station 2 where mixing was assumed to be complete. The reactants in the primary and secondary chemical systems were merged to form the chemical system at the end of mixing. All reactants in the secondary system were converted to oxidants and, if the number of elements present was less than six, the reactants were combined into a single pseudo-reactant by using the specific formula numbers of the elements. The pseudo-reactant has a molecular weight of unity and an assigned enthalpy equal to that of the free stream. The oxidant-to-fuel ratio of the mixed streams was determined from

$$(O/F)_2 = (W'' + W'_a)/W'_f$$

and the equivalence ratio from

$$\phi_2 = 1/[(O/F)_2\ \phi_2^*]$$

The following equations apply to both prescribed pressure and prescribed area mixing between stations 1 and 2.

momentum equation

$$W_2\ V_2/g + p_2\ A_2 = W_1''\ V_1''/g + W_1'\ V_1'\ C_V'\cos\beta' + p_1\ A_1 + (p_1 + p_2)(A_2 - A_1)/2$$

$$- C_f\ A_W[(W_1'\ V_1'\ C_V'\cos\beta' + W_1''\ V_1'')/2gA_1 + (W/A)_2\ V_2/2g]/2$$

where C_f is the skin friction coefficient, A_W the wall surface area, and the pressure integral on the wall is approximated by the average of the pressures at stations 1 and 2. Combining terms in the momentum equation and solving for the velocity at station 2 yields

$$V_2 = \{(1 - C_f\ A_W/4A_1)(W''\ V'' + W'\ V'\ C_V'\cos\beta')/W_2$$

$$+ g(p_1 - p_2)[(A_1/W_2) + 1/(W/A)_2]/2\}/[1 + C_f\ A_W(W/A)_2/4W_2] \qquad (20)$$

energy equations

$$H_{t2} = (H_t' + \mu_t\ H_{t0})/(1 + \mu_t) + Q_{12}/W_2 \qquad (21)$$

and

$$H_2 = H_{t2} - V_2^2/2g\ j \qquad (22)$$

where Q_{12} is the heat loss (-) or gain (+) through the walls between stations 1 and 2.

continuity equations

$$W_2 = W_1' + W_1'' \tag{23}$$

and

$$W_2 = g\,\rho_2\,V_2\,A_2 \tag{24}$$

equation of state

$$p_2/\rho_2 = n_2\,R\,T_2 \tag{25}$$

second law

$$S_2 > (S' + \mu_t\,S_0)/(1 + \mu_t) \tag{26}$$

Equations (24) and (25) may be combined to yield

$$(W/A)_2 = g\,p_2\,V_2/n_2\,R\,T_2 \tag{27}$$

Equations (20), (21), (22), (23), (27) and two equations implicit in the HP problem represent a system of seven equations in the eight unknowns V_2, H_{t2}, H_2, p_2, W_2, A_2, n_2 and T_2 so that if either p_2 or A_2 is specified, a solution to the mixing problem is possible.

When performing design-point performance analyses, the wall surface area between stations 1 and 2 is not generally known. In this case, the length, ℓ, of the mixing tube may be specified in the number, N_d, of hydraulic diameters, D_h, so that

$$\ell = N_d D_h$$

where

$$D_h = 4\,R_h = 2(R_0 - R_i)_1$$

in terms of the unknown inner and outer radii of an annular mixing tube at station 1. The wall surface area may be approximated by

$$A_w \simeq 4\ N_d\ \pi\ (R_0^2 - R_i^2) = 4\ N_d\ A_1 \tag{28}$$

for prescribed pressure mixing, and exactly by

$$A_w = 2\ N_d\ A_1(1 + A_2/A_1) \tag{29}$$

for prescribed area mixing. These equations are also valid for cylindrical mixing tubes.

prescribed pressure mixing

The flow area at station 2 is assumed equal to that at station 1, the static enthalpy is obtained from Equations (20), (21) and (22), the HP problem is solved with the state variables p_2 and $H_2^{(n)}$, and $(W/A)_2^{(n)}$ is obtained from Equation (27). The current values of $(W/A)_2^{(n)}$ are substituted successively into Equation (20) and the above calculations are repeated until

$$|[(W/A)_2^{(n+1)} - (W/A)_2^{(n)}]/(W/A)_2^{(n+1)}| < \varepsilon$$

A single solution - sonic, subsonic, or supersonic - is always obtained for prescribed pressure mixing. If the solution is supersonic and does not violate the second law, the flow is passed through a normal shock. In all valid solutions, the Kantrowitz area is obtained and assigned to the inlet throat at station 2.

prescribed area mixing

An initial value is assumed for the static pressure at station 2, the static enthalpy is obtained from Equations (20), (21) and (22), the HP problem is solved with the state variables $p_2^{(n)}$ and $H_2^{(n)}$, and $(W/A)_2^{(n)}$ is obtained from Equation (27). Iteration is made on $p_2^{(n)}$ until

$$|[(W/A)_2 - (W/A)_2^{(n)}]/(W/A)_2| < \varepsilon \tag{30}$$

The two roots of the preceding system of equations when used with prescribed area mixing correspond to conditions on either side of a normal shock; however, the root corresponding to the subsonic (or sonic) solution is always obtained in the current analysis. In the event that the flow can not pass through the

prescribed area at station 2, the total fuel flow, W_{ft}, is reduced and the calculations for the primary air system, the accommodation region (station 1) and prescribed area mixing (station 2) are repeated. The equations in the three systems are iterated with the independent variables $p_2^{(n)}$ and $W_{ft}^{(m)}$ until the constraint (30) is satisfied and

$$|M_2^{(n)} - 1| < \varepsilon$$

Diffuser. - The analysis of the diffuser in the performance model is identical to that in Reference 11 for obtaining design-point performance. In the case of off-design performance when the flow at the inlet throat at station 2 is sonic, the three solutions representing subsonic diffusion, supersonic diffusion and supersonic diffusion with normal shock are obtained at the combustor entrance (station 3). The continuity, energy and momentum equations in the diffuser may be written as

$$W_3 = W_2(1 + BLF_{23})$$

$$H_{t3} = H_{t2} + Q_{23}/W_3$$

and

$$Ivac_3 = [W_2 Ivac_2 + \int_2^3 pdA - \bar{q}_{23} A_{w23} C_{f23}]/W_3 \qquad (31)$$

where BLF_{23} is the percentage bleed (±) and $\bar{q}_{23}$ is the average dynamic pressure in the diffuser. The problem in using Equation (31) arises in the evaluation of the pressure integral since it is impossible to know the pressure variation between stations 2 and 3 with the dissipative terms (heat loss and friction) present in the energy and momentum equations. This problem can be resolved by dividing the diffuser into several sections, expanding (or diffusing) the flow isentropically through the successive sections while introducing a portion of the dissipative terms at constant area following each isentropic expansion. In the limit, this procedure should produce quite accurate results. The method will be described in the following paragraphs by (1) expanding the flow isentropically from station 2 to f (see Figure 40), (2) introducing all of the losses at constant area (station f'), and (3) expanding the flow isentropically to station 3.

The area ratio at station f is taken to be the mean between stations 2 and 3.

$$A_f/A_2 = (1 + A_3/A_2)/2$$

and the mass flow per unit area may be written as

$$(W/A)_f = (W/A)_2 \, A_2/A_f$$

The initial estimate of p_f is obtained from the following real-gas relationships

$$M_f \simeq f(A_f/A_2, M_2, \gamma)$$

$$p_f^{(1)} \simeq p_{t2}[1 + (\gamma-1)M_f^2/2]^{-\gamma/(\gamma-1)}$$

The static conditions are obtained by solving the SP problem with the state variables $p_f^{(n)}$ and S_2. Iteration is made on $p_f^{(n)}$ until

$$|[1 - (W/A)_f^{(n)}/(W/A)_f]| < \varepsilon$$

and the following parameters are calculated

$$Ivac_f = V_f/g + p_f/(W/A)_f$$

$$q_f = \gamma p_f M_f^2/2$$

The vacuum specific impulse and total enthalpy are corrected for friction and energy loss as follows:

$$A_{W23} = (A_{W23}/A_C) \, A_C$$

$$\tau_{23} = q_f \, C_{f23}$$

$$F_{f'} = Ivac_f \, W_3 - \tau_{23} \, A_{W23}$$

$$Ivac_{f'} = F_{f'}/W_3$$

$$(W/A)_{f'} = (W/A)_f$$

$$H_{tf'} = H_{t3}$$

The initial estimates of total and static pressures are obtained from

$$p_{tf'}^{(1)} \simeq 0.8\ p_{tf}$$

$$p_{f'}^{(1)} \simeq p_{tf'}^{(1)}[1 + (\gamma-1)M_{f'}^2/2]^{-\gamma/(\gamma-1)}$$

and the HP problem is solved with the state variables $p_{tf'}^{(n)}$ and $H_{tf'}$ to obtain the total conditions. Then the SP problem is solved with $p_{f'}^{(n)}$ and $S_{f'}$ to obtain the static conditions. Iteration is made on $p_{tf'}^{(n)}$ and $p_{f'}^{(n)}$ until

$$|1 - Ivac_{f'}^{(n)}/Ivac_{f'}| < \varepsilon$$

and

$$|1 - (W/A)_{f'}^{(n)}/(W/A)_{f'}| < \varepsilon$$

Finally the flow is expanded isentropically from station f' to station 3 where

$$p_{t3} = p_{tf'}$$

$$(W/A)_3 = (W/A)_2(A_2/A_3)(1 + BLF_{23})$$

and

$$S_3 = S_{f'}$$

The initial estimate of p_3 is obtained from the ideal-gas relationships, and the SP problem is solved with the state variables $p_3^{(n)}$ and S_3 to obtain the static conditions at the diffuser exit. Iteration is made on $p_3^{(n)}$ until

$$|1 - (W/A)_3^{(n)}/(W/A)_3| < \varepsilon$$

The above analysis is valid for both subsonic and supersonic diffusion. A third solution is obtained by diffusing supersonically and passing the flow through a normal shock at station 3.

Combustor. - All reactants present at the entrance to the combustor are changed to oxidants. The weight fractions of fuels, WF_o, and oxidants, WF_f, are changed to WF'_o as follows:

$$WF'_{o,i} = (O/F)_2 WF_{o,i}/[1 + (O/F)_2] \ , \ i = 1, N_o$$

$$WF'_{o,i+N_o} = WF_{f,i}/[1 + (O/F)_2] \ , \ i = 1, N_f$$

and

$$N'_o = N_o + N_f$$

where $(O/F)_2$ is the oxidant-to-fuel ratio, N_o the number of oxidants, and N_f the number of fuels in the mixed stream. If oxidants are injected in the combustor to simulate an igniter, they are input as oxidants with mass units (lbm/sec) instead of weight fractions. The new weight fractions of the oxidants are calculated as follows:

$$W_{o,i} = WF'_{o,i} W_3, \ i = 1, N'_o$$

$$W_{o,i+N'_o} = W_{o,i}(j), \ i = 1, N_o(j)$$

$$W_3 = W_3 + \sum_{i=1}^{N_o(j)} W_{o,i}(j)$$

$$N'_o = N'_o + N_o(j)$$

$$WF'_{o,i} = W_{o,i}/W_3, \ i = 1, N'_o$$

where $W_{o,i}(j)$ denotes the mass flow of the injected oxidant i, and $N_o(j)$ the number of injected oxidants. The oxidant-to-fuel ratio of the reactants in the combustor is

$$O/F = W_3/(W_{ft} - W'_f)$$

where W_f' was the fuel added in the primary combustor. The equivalence ratio in the combustor is obtained from

$$\phi_c = 1/[(O/F)\phi_c^*]$$

which may differ from the over-all equivalence ratio ϕ_t because the fuel injected in the primary combustor was changed to an oxidant at the entrance of the combustor. This change is reflected in both the oxidant-to-fuel ratio, O/F, and the stoichiometric mixture ratio, ϕ_c^*. Chemical or mixing efficiencies may be simulated in the combustor by the concept of an inert element, or molecule, which has the identical properties of a fuel but which is not permitted to react with any other species.

The one-dimensional analysis that follows applies to either subsonic or supersonic combustion.

momentum equation

$$W_4V_4/g + p_4A_4 = W_3V_3/g + p_3A_3 + (p_3 + p_4)(A_4 - A_3)/2$$

$$- [(W/A)_4V_4/2g + (W/A)_3V_3/2g]C_fA_W/2 + (W_4 - W_3)Ivac_f \cos \beta_f \qquad (32)$$

where $Ivac_f$ is the vacuum specific impulse of the injected fuel and β_f is the fuel injection angle. Combining terms and solving for the combustor exit velocity in Equation (32) yields

$$V_4 = [(1 - C_fA_W/4\ A_3)W_3V_3 + g(p_3 - p_4)(A_4 + A_3)/2$$

$$+ g(W_4 - W_3)Ivac_f \cos \beta_f]/W_4(1 + C_fA_W/4\ A_4) \qquad (33)$$

energy equations

$$H_{t4} = [(O/F)_4H_{to4} + H_{tf4}]/[1 + (O/F)_4] + Q_{14}/W_4 \qquad (34)$$

and

$$H_4 = H_{t4} - V_4^2/2g\ j \qquad (35)$$

where H_{to4} is the total specific enthalpy of oxidants and H_{tf4} the total specific enthalpy of fuels in the combustor, and Q_{14} is the cumulative heat loss (-) or gain (+) per unit time through the engine walls between station 1 and the exit of the combustor.

continuity equations

$$W_4 = W_3 + W_{ft} - W_f' \tag{36}$$

and

$$W_4 = g\ \rho_4 V_4 A_4 \tag{37}$$

equation of state

$$p_4/\rho_4 = n_4 R\ T_4 \tag{38}$$

Equations (37) and (38) may be combined as

$$(W/A)_4 = g\ p_4 V_4 / n_4 R\ T_4 \tag{39}$$

Equations (33), (34), (35), (36), (39) and two equations implicit in the HP problem represent a system of seven equations in the seven unknowns V_4, H_{t4}, H_4, p_4, W_4, n_4 and T_4 so that solution of the combustion problem is possible. One of the two roots of the above system of equations represents subsonic combustion, the other supersonic combustion.

An initial estimate of the static pressure, p_4, at the exit of the combustor is chosen and Equations (33), (34) and (35) are solved from that condition at station 3 representing subsonic diffusion to obtain $H_4^{(n)}$. The HP problem is solved with the state variables $p_4^{(n)}$ and $H_4^{(n)}$, and $(W/A)_4^{(n)}$ is obtained from Equation (39). The system of equations is iterated with successive values of $p_4^{(n)}$ until

$$\left| 1 - (W/A)_4^{(n)} / (W/A)_4 \right| < \varepsilon$$

The flow is then compressed isentropically to obtain the total conditions at the combustor exit. An initial estimate for the total pressure is obtained from the ideal-gas relationship, and the SP problem is solved with the state

variables $p_{t_4}^{(n)}$ and S_4 to obtain $H_{t_4}^{(n)}$. The SP problem is iterated using successive values of $p_{t_4}^{(n)}$ until

$$| 1 - H_{t_4}^{(n)}/H_{t_4} | < \varepsilon$$

If the total pressure at the exit of the combustor is less than the static pressure in the pressure field, a solution does not exist for the specified engine and flight conditions. This condition was encountered in the simulation of the duPont Jet Engine at sea-level-static conditions when very small values of equivalence ratio were prescribed to simulate engine starting. A solution could always be obtained under these circumstances by stroking the inlet spike forward to increase the inlet-contraction ratio and decrease the total flow through the engine. The net effect of this geometry change was to decrease the Mach number at the entrance of the combustor thereby decreasing the total pressure loss during combustion.

Nozzle throat. - If the flow at the combustor exit is supersonic, the nozzle throat calculation is omitted. The conditions in the nozzle throat are obtained by isentropic expansion of the flow at the combustor exit to sonic conditions at station 5. An initial estimate of the static pressure is obtained from the ideal-gas relationship, and the SP problem is solved with the state variables $p_5^{(n)}$ and S_4. The SP problem is iterated with successive values of $p_5^{(n)}$ until

$$| M_5^{(n)} - 1 | < \varepsilon$$

The area at which the flow is choked is obtained from

$$A_5^* = W_4/(W/A)_5^*$$

and the characteristic velocity from

$$C^* = g\, p_{t_4}/(W/A)_5^* \qquad (40)$$

Engine control. - The method used for controlling the duPont Jet Engine depends on whether the sonic throat area, A_5^*, is greater or less than the actual throat area, A_5. A flowchart of the control scheme is shown in Figure 42 and is described in the following paragraphs.

If $A_5^* > A_5$ the flow will not pass through the throat. If, in addition, the combustor entrance conditions were based on subsonic diffusion, the total pressure at the combustor exit will have attained its maximum possible value.

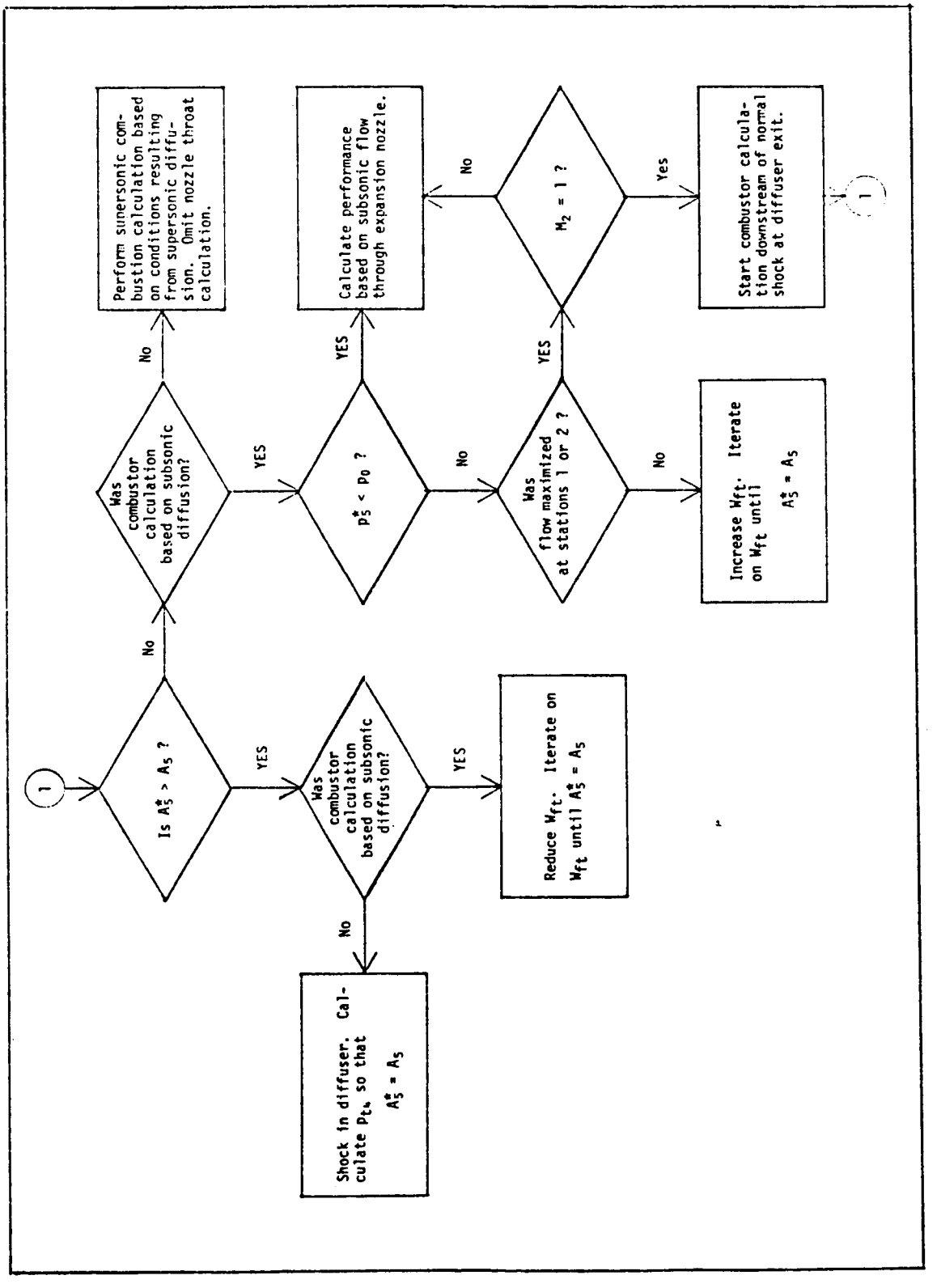

Figure 42. - Flowchart of engine control - analytical performance model

Therefore, the only control feature available is the over-all fuel flow, W_{ft}. In this instance W_{ft} must be reduced. Conditions in the primary air system, accommodation and mixing stations, diffuser, combustor and nozzle throat are reevaluated with successive values of W_{ft} until

$$A_5^* = A_5$$

When $A_5^* < A_5$ with subsonic diffusion, the flow in the nozzle throat is subsonic. Either the over-all fuel flow may be increased or the combustor exit total pressure may be decreased by placing a normal shock in the diffuser in order to produce sonic flow in the nozzle throat. First, a test is made on p_5^*. If p_5^* is less than the static pressure, p_0, in the pressure field, sonic flow in the nozzle throat is never possible†, and the engine performance is based on subsonic flow through the expansion nozzle. When $p_5^* > p_0$ and the flow had not been maximized at either station 1 or 2, the over-all fuel flow may be increased to produce sonic flow in the nozzle throat. Iteration on W_{ft} in this instance is the same as that described above. If the flow was maximized at station 1 ($M_2 \neq 1$), performance is calculated based on subsonic flow through the expansion nozzle. If the flow was maximized at station 2 ($M_2 = 1$), the combustor calculation is repeated from conditions downstream of the normal shock at the diffuser exit, A_5^* is recalculated and the flowchart in Figure 42 is reentered at the symbol 1. When $A_5^* > A_5$, it is implied that a normal shock exists between station 2 and 3 in the diffuser, and the total pressure at the combustor exit is determined so that $A_5^* = A_5$. The initial estimates of total and static pressures are obtained from

$$p_{t_4}^{(1)} \approx C^*(W/A)_5/g$$

and

$$p_5^{(1)} \approx p_{t_4}^{(1)}[2/(\gamma + 1)]^{\gamma/(\gamma-1)}$$

and the HP problem is solved with the state variables $p_{t_4}^{(n)}$ and H_{t_4} to obtain $S_4^{(n)}$. The SP problem is solved with the state variables $p_5^{(n)}$ and $S_4^{(n)}$ to obtain $(W/A)_5^{(n)}$ and $M_5^{(n)}$. The HP and SP problems are solved with successive values of $p_{t_4}^{(n)}$ and $p_5^{(n)}$ until

$$| M_5^{(n)} - 1 | < \varepsilon$$

†This assumes that the inlet spike position had been optimized.

and

$$| 1 - (W/A)_5^{(n)}/(W/A)_5 | < \epsilon$$

When $A_5^* < A_5$ with the normal shock at the diffuser exit, it is implied that subsonic combustion can not be sustained. The combustor exit conditions are reevaluated based on supersonic combustion, and the nozzle throat calculation is omitted.

The control of the duPont Jet Engine by varying the total fuel flow and/or equivalence ratio is most easily understood by discussing the relationship of the fuel flow with ejector performance. The effect of primary total pressure on ejector pressure ratio for prescribed area mixing is shown qualitatively in Figure 43 for a fixed geometry engine. The curved lines AB, CE, and FH represent the ejector performance for fixed values of primary stream total pressure, p_t', and fuel flow, $\dot{W}_{ft}$, with the secondary flow Mach number, M", varying from zero on the extreme left to its maximum (subsonic) value on the locus of maximum theoretical entrainment ratios, BH. The primary stream total pressure and the fuel flow increase along vertical lines while the over-all equivalence ratio, ϕ_t, remains constant along vertical lines and increases as the entrainment ratio approaches zero. The sum of the primary and secondary flows increases with increasing values of both the abscissa and ordinate.

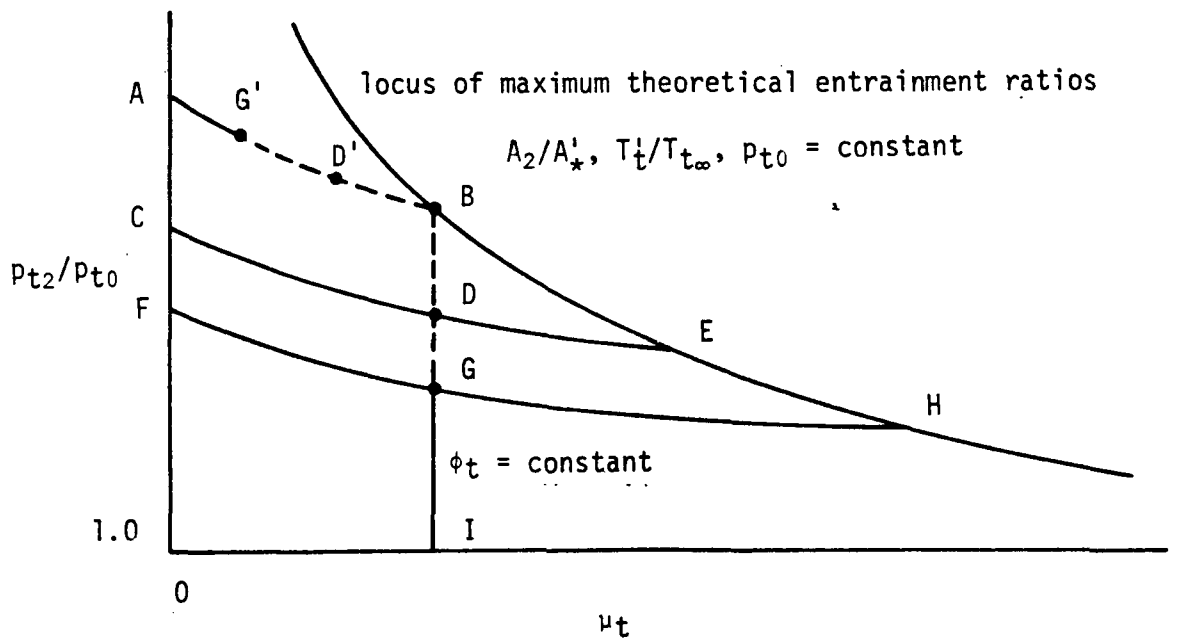

Figure 43. - Qualitative results from prescribed area mixing analysis

Solution B in Figure 43 assumes that the flow at station 1 (see Figure 40) was maximized by determining maximum fuel flow and secondary Mach number corresponding to a desired value of equivalence ratio as described in the discussion in the ejector subsection above. If subsequent analyses showed that the total flow corresponding to the solution at point B would pass through the inlet and nozzle throats at stations 2 and 5, respectively, this point would represent the ejector performance for the prescribed conditions. On the other hand, when the total flow at B can not pass the inlet throat, either of the solutions at points D' of D could be attained. Holding the fuel flow constant while decreasing the secondary flow (increasing the equivalence ratio), the solution at D' would be required to produce sonic flow in the inlet throat. In practice, the engine would automatically adjust to the solution at D' provided that the fuel flow remained constant. However, the analytical performance model was designed to determine engine performance based on fixed equivalence ratios so that the solution at D is attained by reducing the fuel flow to produce sonic flow in the inlet throat while holding the entrainment and equivalence ratios constant. In the event that the total flow corresponding to the solutions at D or D' can not pass the nozzle throat, either of the solutions at points G or G' may be attained as described above to produce sonic flow at station 5.

Expansion nozzle. - The analytical performance model considers the expansion nozzle to be continually adjustable so that the flow may be expanded to the static pressure, p_0, in the pressure field at all engine operating conditions. The flow is expanded (or diffused) isentropically to p_0 based on frozen and/or shifting equilibrium. The species concentrations may be frozen at any point in the expansion process.

The mass flow per unit area at nozzle station z at which the species concentrations are to be frozen is obtained from

$$(W/A)_z = (W/A)_5/(A_z/A_5)$$

The initial estimate of the static pressure is obtained from the ideal-gas relationships, and the SP problem is solved with the state variables $p_z^{(n)}$ and S_4 to obtain the static conditions at station z. The SP problem is iterated with successive values of $p_z^{(n)}$ until

$$| 1 - (W/A)_z^{(n)}/(W/A)_z | < \varepsilon$$

The flow is then expanded isentropically to the nozzle exit by solving the SP problem with the state variables p_0 and S_4, and the nozzle exit area is obtained from

$$A_6 = W_4/(W/A)_6$$

Performance. - The engine performance is calculated at both gage and zero pressure datum.

Gage pressure datum:

$$\text{INLET TOTAL MOMENTUM} = W_0 V_0/g$$

$$\text{GROSS THRUST} = W_4 V_6 C_V/g$$

$$\text{ADDITIVE DRAG} = \int_{A_0}^{A_C} (p - p_0)dA$$

Zero pressure datum:

$$\text{INLET TOTAL MOMENTUM} = W_0 V_0/g + p_0 A_0$$

$$\text{GROSS THRUST} = W_4 V_6 C_V/g + p_0 A_6$$

$$\text{ADDITIVE DRAG} = \int_{A_0}^{A_C} (p - p_0)dA + p_0(A_C - A_0)$$

Engine performance:

$$\text{NET THRUST} = \text{GROSS THRUST} - \text{INLET TOTAL MOMENTUM} - \text{ADDITIVE DRAG}$$

$$I_{sp} = \text{NET THRUST}/W_{ft}$$

$$C_t = \text{NET THRUST}/q_0 A_C$$

Typical Heat Exchanger Analysis

A typical heat exchanger calculation at sea-level-static conditions is reproduced below.

Basic equations. - The heat absorbed by the hydrogen must equal the heat absorbed from the air to cool and liquefy it. The heat exchanger is analyzed in two parts: a precooler and a condenser. The precooler cools the air from free-stream total conditions to the temperature at which the oxygen will liquefy at the pressure in the condenser. The condenser liquefies both the oxygen and the nitrogen.

For the precooler:

$$[H_a(\text{freestream-total}) - H_a(\text{precooler-out})]W'_a/W_{H_2}$$

$$= H_{H_2}(\text{precooler-out}) - H_{H_2}(\text{condenser-out})$$

For the condenser:

$$0.24(W'_a/W_{H_2})[H_{O_2}(\text{saturated-vapor}) - H_{O_2}(\text{at-liquid-nitrogen-temperature})]$$

$$+ 0.76(W'_a/W_{H_2})[H_{N_2}(\text{saturated-vapor}) - H_{N_2}(\text{liquid})]$$

$$= H_{H_2}(\text{condenser-out}) - H_{H_2}(\text{pump-out})$$

The specific enthalpy of the hydrogen leaving the condenser is determined by the necessary temperature difference between the air and hydrogen at this point. This point is usually called the pinch point because the difference between the air and the hydrogen is a minimum at this point in the heat exchanger. The allowable temperature difference is defined by the heat exchanger effectiveness:

$$\varepsilon = [T_a(\text{precooler-in}) - T_a(\text{precooler-out})]$$

$$/[T_a(\text{precooler-in}) - T_{H_2}(\text{condenser-out})]$$

or since

$$T_a(\text{precooler-in}) \equiv T_{t_\infty}$$

and

$$T_a(\text{precooler-out}) = T_{O_2}(\text{saturated})$$

the hydrogen temperature may be obtained from

$$T_{H_2}(\text{condenser-out}) = [T_{O_2}(\text{saturated})]/\varepsilon - [(1-\varepsilon)/\varepsilon]T_{t_\infty}$$

The effectiveness in turn is a function of the heat exchanger geometry and surface area, but is nearly constant for a given heat exchanger. The number of thermal units, NTU, represents the surface area and its effectiveness. The value corresponding to the duPont Jet Engine heat exchanger is 5.5. The heat exchanger effectiveness was determined from Reference 4 to be equal to 0.97 for the cross-counterflow arrangement used.

Computations. - The basic equations were solved for W_a/W_{H_2} using the thermodynamic data in References 13 through 17. The hydrogen para-to-ortho conversion data were taken from Reference 13. A case for sea-level-static conditions is solved below as an example:

Free-stream total temperature	519°R.
Free-stream total pressure	14.7 psi
Heat exchanger pressure drop	20%
Hydrogen pump outlet at 700 psi with 70% impeller efficiency	-66 Btu/lb
Condenser pressure	11.75 psi
Temperature for O_2 liquefaction	158.3°R.
Temperature for N_2 liquefaction	135.7°R.

Using the effectiveness equation:

$$T_{H_2}(\text{condenser-out}) = 158.3/0.97 - 0.03 \times 519/0.97$$

$$T_{H_2}(\text{condenser-out}) = 147.0°\text{R.}$$

$$H_{O_2}(\text{saturated at } 158.3) = 33.7 \text{ Btu/lb}$$

$$H_{O_2}(\text{liquid at } 135.7°\text{R.}) = -68.3 \text{ Btu/lb}$$

$$H_{H_2} \text{ at } 147°R. = 497.0 \text{ Btu/lb}$$

$$[0.24\ (33.7 + 68.3) + 0.76\ (103.3 - 10.7)]W_a/W_{H_2} = 497 + 66$$

$$W_a/W_{H_2} = 5.94$$

From the precooler equation:

$$5.94\ (124.0 - 37.7) = H_{H_2}(\text{precooler-out}) - 497$$

$$H_{H_2}(\text{precooler-out}) = 1{,}009 \text{ Btu/lb}$$

$$T_{H_2}(\text{precooler-out}) = 270°$$

The data presented in Figure 6 were calculated in the same manner as the example above.

REFERENCES

1. Keenan, J. H.; Neuman, E. P.; and Lustwerk, F.: An investigation of ejector design by analysis and experiment. Jou Appl Mech Vol 17(3). September 1950. And Jou Appl Mech Vol 18(1). March 1951. p. 117.

2. Surendraiah, M.; and Rao, D. M.: Performance of a two-dimensional centre-jet ejector. Nat. Aero. Lab TN-AE-18-63. Bangalore, India. July 1963.

3. Hickman, K. E.; Gilbert, G. B.; and Carey, J. H.: Analytical and experimental investigation of high entrainment jet pumps. NASA CR-1602. July 1970.

4. Kays, W. M.; and London, A. L.: Compact heat exchangers, 2d ed. McGraw-Hill Book Company. New York. 1964.

5. Harry, A. J.; and Hindin, S. G.: Investigation of the para-ortho conversion of hydrogen. Englehard Industries, Inc. Technical report AFAPL-TR-65-59. July 1965. Contract AF 33(657)-11125.

6. Buchmann, O. A.: Structures and cooling development. Hypersonic Research Engine Project - Phase IIA. Third interim technical data report - 3 August through 2 November, 1967 - Item 55-7.03, NAS1-6666. AiResearch Mfg. Co. Report 67-2833. 1967.

7. A study of composite propulsion systems for advanced launch vehicle applications (U). Volumes 2 and 3 (parts 1 and 2, of main technical report - composite engine study) dated September, 1966 and Volume 2 (extension phase of main technical report) dated April, 1967. Prepared for NASA under contract NAS7-377 by the Marquardt Corporation (CONFIDENTIAL - TITLE UNCLASSIFIED).

8. Ellison, James C.: Investigation of the aerodynamic characteristics of a hypersonic transport model at Mach numbers to 6. NASA TN D-6191. April 1971.

9. Spalding, D. B.; and Chi, S. W.: The drag of a compressible turbulent boundary layer on a smooth flat plate with and without heat transfer. Jou Fluid Mech Vol 18. October 1966. pp. 117-143.

10. Gordon, Sanford; and McBride, Bonnie J.: One-dimensional equilibrium. (a preliminary report, c. 1968)

REFERENCES (concluded)

11. Gaede, A. E.: Computer Program Description; Subsonic or Supersonic Combustion Ramjet Performance Based on Equilibrium Chemistry of Arbitrary Reactants. AiResearch Mfg. Co. Report AP-70-6776, Los Angeles, Ca., December 1970.

12. Zeleznik, Frank J.; and Gordon, Sanford: Calculation of complex chemical equilibria. Ind. Eng. Chem., vol 60, no. 6, June 1968, pp. 27-57.

13. Farkas, Adelbert: Orthohydrogen, parahydrogen and heavy hydrogen. Cambridge University Press. 1935. p. 14.

14. NBS Monograph 94. Thermodynamic properties of parahydrogen to 180°R.

15. NBS Technical Note 130. Thermodynamic properties of parahydrogen from 180°R to 540°R.

16. NBS Technical Note 129. Thermodynamic properties of nitrogen to 540°R.

17. Stewart, R.: The thermodynamic properties of oxygen. Doctoral thesis, University of Iowa. 1966.